Åbo Akademi University

Eva von Haartman

Design and Evaluation of Nanoparticle-Based Delivery Systems: Towards Cancer Theranostics

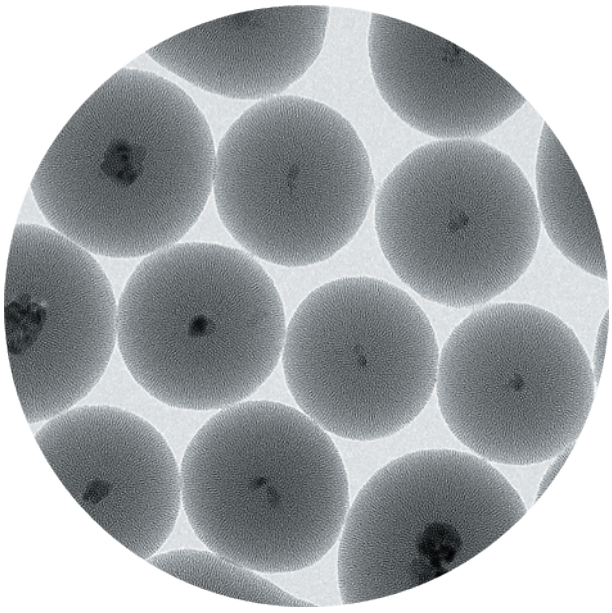

Cover figure: Core@shell structures of nanodiamonds coated with mesoporous silica.

DESIGN AND EVALUATION OF NANOPARTICLE-BASED DELIVERY SYSTEMS: TOWARDS CANCER THERANOSTICS

EVA VON HAARTMAN

Pharmaceutical Sciences Laboratory
Faculty of Science and Engineering
Åbo Akademi University
Turku, Finland, 2017

From

Pharmaceutical Sciences Laboratory
Faculty of Science and Engineering
Åbo Akademi University
FI-20520 Turku, Finland

Supervisor

Professor Jessica Rosenholm
Pharmaceutical Sciences Laboratory
Faculty of Science and Engineering
Åbo Akademi University, Turku, Finland

Co-supervisor

Professor Catharina de Lange Davies
Biophysics and Medical Technology
Department of Physics
Norwegian University of Science and Technology, Trondheim, Norway

Reviewers

Adjunct Professor Hélder A. Santos
Division of Pharmaceutical Chemistry and Technology
Faculty of Pharmacy
University of Helsinki, Helsinki, Finland

and

Professor Twan Lammers
Department of Nanomedicine and Theranostics
Institute for Experimental Molecular Imaging
RWTH Aachen University Clinic, Aachen, Germany

Dissertation opponent

Professor Lennart Bergström
Department of Materials and Environmental Chemistry
Stockholm University, Stockholm, Sweden

ISBN 978-952-12-3507-8 (printed version)
ISBN 978-952-12-3508-5 (digital version)
Painosalama Oy – Turku, Finland 2017

"Whenever a theory appears to you as the only possible one,
take this as a sign that you have neither understood the theory
nor the problem, which it was intended to solve."

— Karl Popper

ABSTRACT

The design, characterization and applicability of nanoparticle (NP)-based delivery systems intended for cancer theranostics, are presented in this thesis. Mesoporous silica nanoparticles (MSNs) have been widely established as biocompatible and efficient carriers of hydrophobic molecules, such as drugs for *in vitro* and *in vivo* tumor targeting. Although their intracellular delivery and cargo release have been demonstrated, knowledge of the underlying drug release mechanisms still remain unclear. For future control and prediction of these parameters, which from a clinical perspective are imperative to all drug delivery systems (DDSs), the release of hydrophobic cargo from MSNs is studied. In simple aqueous solvents, cargo release is strongly associated with nanocarrier degradation, whereas in media mimicking intracellular conditions, where lipids or hydrophobic structures are present, the physicochemical properties of the cargo molecule itself and its interactions with the surrounding medium are the release-governing parameters. For comparison, the relationship between intracellular cargo release and degradation of poly(alkylcyanoacrylate) (PACA) nanocarriers is also investigated, for which the release is found to be dependent on the biodegradation of the carrier. The influence of NP monomer composition on intracellular delivery and the role of different endocytosis pathways are also assessed.

This thesis moreover presents a novel multifunctional composite NP for combined optical imaging, tracking and drug delivery. The used approaches include creation and optimization of core-shell nanostructures of photoluminescent (PL) nanodiamonds (NDs) encapsulated within mesoporous silica shells that allow tuning of the composite NP size and loading of hydrophobic cargo molecules. Through subsequent surface engineering, efficient passive uptake by endocytosis, followed by intracellular release of cargo, is achieved and displayed by optical fluorescence imaging. The approaches presented in this thesis are highly interdisciplinary, placed at the meeting point between chemistry, physics, engineering, biotechnology and pharmaceutical sciences, and provide a basis for the rational design and evaluation of NP-based DDSs, intended for cancer theranostics, mainly by intravenous (IV) administration.

SAMMANFATTNING

I den här avhandlingen presenteras utveckling, karaktärisering och tillämpning av nanopartikelbaserade bärarsystem för cancerteranostik. Mesoporösa kiseldioxidnanopartiklar är allmänt etablerade som biokompatibla och effektiva bärare av hydrofoba molekyler, så som läkemedel för *in vitro*- och *in vivo*-målinriktning av cancer. Trots att deras intracellulära leverans och därpå följande läkemedelsfrisättning har uppvisats, är kunskapen kring de verksamma mekanismerna för läkemedelsfrisättningen fortfarande bristande. För framtida kontroll och förutsägelse av dessa parametrar, vilket ur ett kliniskt perspektiv är ytterst viktigt, studeras frigörningen av hydrofoba molekyler från de ovannämnda partiklarna under olika betingelser. I enkla vattenlösningar är frisättningen starkt kopplad till nedbrytningen av bäraren, medan den i komplexa vattenlösningar, som innehåller lipider eller hydrofoba strukturer, styrs främst av molekylens fysikalisk-kemiska egenskaper och dess växelverkan med den omgivande lösningen. Som jämförelse, studeras även frisättningen av hydrofoba molekyler från organiska poly(alkylcyanoakrylat) nanopartiklar i förhållande till partiklarnas nedbrytning. Ytterligare evalueras inflytandet av partiklarnas monomersammansättning och olika endocytotiska mekanismer på partiklarnas intracellulära upptag.

Avhandlingen presenterar också nya multifunktionella nanokompositer som lämpar sig för optisk avbildning och som läkemedelsbärare. De tillämpade metoderna inkluderar utveckling och optimering av nanostrukturer, bestående av en fotoluminescent nanodiamantkärna inkapslad i ett mesoporöst kiseldioxidskal, vars tjocklek kan varieras för att reglera partikelstorleken. Samtidigt fungerar kiseldioxidskalet som ett läkemedelsbärande matrix. Genom funktionalisering av partikelytan kan ett effektivt, passivt, intracellulärt partikelupptag, följt av läkemedelsfrisättning, uppnås och åskådliggöras med hjälp av optisk fluorescensmikroskopi. De nya ansatserna inom nanomaterialutveckling som förs fram i den här avhandlingen implementerar såväl kemiska och fysikaliska som ingenjörstekniska, farmakologiska och bioteknologiska koncept. Resultaten erbjuder en bas för systematisk design och evaluering av nanopartikelbaserade läkemedelsbärarsystem avsedda för cancerteranostik, huvudsakligen via intravenös administrering.

LIST OF ORIGINAL PUBLICATIONS

I. von Haartman, E.; Lindberg, D.; Prabhakar, N.; Rosenholm, J. M. On the intracellular release mechanism of hydrophobic cargo and its relation to the biodegradation behavior of mesoporous silica nanocarriers. *Eur. J. Pharm. Sci.* **2016**, *95*, 17-27.

II. Sulheim, E.; Baghirov, B.; von Haartman, E.; Bøe, A.; Åslund, A. K. O.; Mørch, Y.; de Lange Davies, C. Cellular uptake and intracellular degradation of poly(alkyl cyanoacrylate) nanoparticles. *J Nanobiotechnology* **2016**, *14* (1). doi:10.1186/s12951-015-0156-7.

III. von Haartman, E., Jiang, H., Khomich, A. A., Zhang, J., Dolenko, T. A., Ruokolainen, J., Gu, H., Shenderova, O. A., Vlasov, I. I., Rosenholm, J. M. Core-shell designs of photoluminescent nanodiamonds with porous silica coatings for bioimaging and drug delivery I: fabrication. *J. Mater. Chem. B* **2013**, *1* (18), 2358-2366.

IV. Prabhakar, N.; Näreoja, T.; von Haartman, E.; Koho, S.; Şen Karaman, D.; Hänninen, P.; Dolenko, T.; Vlasov, I. I.; Sahlgren, C.; Rosenholm, J. M. Core-shell designs of photoluminescent nanodiamonds with porous silica coatings for bioimaging and drug delivery II: application *Nanoscale* **2013**, *5* (9), 3713-3722.

LIST OF SUPPORTING PUBLICATIONS

I Åslund, A.; Sulheim, E.; Snipstad, S.; von Haartman, E.; Baghirov, H.; Starr, N.; Løvmo, M.; Lelú, S.; Scurr, D.; de Lange Davies, C.; Schmid, R.; Mørch, Ý. Quantification and qualitative effects of different PEGylations on PBCA nanoparticles. *Mol. Pharm.* **2017**. doi: 10.1021/acs.molpharmaceut.6b01085

II Snipstad, S.; Hak, S.; Baghirov, H.; Sulheim, E.; Mørch, Ý.; Lelú, S.; von Haartman, E.; Bäck, M.; Peter, K.; Nilsson, R.; Klymchenko, A. S.; de Lange Davies, C.; Åslund, A. K. O. Labeling Nanoparticles: Dye Leakage and Altered Cellular Uptake. *Cytometry A* **2016**. doi: 10.1002/cyto.a.22853.

III Rosenholm, J.M.; Gulin-Sarfraz, T.; Mamaeva, V.; Niemi, R.; Özliseli, E.; Desai, D.; Antfolk, D.; von Haartman, E.; Lindberg, D.; Prabhakar, N.; Näreoja, T.; Sahlgren, C. Prolonged Dye Release from Mesoporous Silica-Based Imaging Probes Facilitates Long-Term Optical Tracking of Cell Populations In Vivo. *Small* **2016**, *12* (12), 1578-1592.

IV Kankaanpää, P.; Tiitta, S.; Bergman, L.; Puranen, A.-B.; von Haartman, E.; Lindén, M.; Heino, J. Cellular recognition and micropinocytosis-like internalization of nanoparticles targeted to integrin α2β1. *Nanoscale* **2015**, *7* (42), 17889-17901.

V Prabhakar, N.; Näreoja, T.; von Haartman, E.; Şen Karaman, D.; Burikov, S. A.; Dolenko, T. A.; Deguchi, T.; Mamaeva, V.; Hänninen, P. E.; Vlasov, I. I.; Shenderova, O. A.; Rosenholm, J. M. Functionalization of graphene oxide nanostructures improves photoluminescence and facilitates their use as optical probes in preclinical imaging. *Nanoscale* **2015**, *7* (23), 10410-10420.

VI Neukirch, L. P.; von Haartman, E.; Rosenholm, J. M.; Vamivakas, A. N. Multi-dimensional single-spin nano-optomechanics with a levitated nanodiamond. *Nat. Photonics* **2015**, *9* (10), 653-657.

VII Wittig, R.; Rosenholm, J.; von Haartman, E.; Hemming, J.; Genze, F.; Bergman, L.; Simmet, T.; Lindén, M.; Sahlgren, C. Active targeting of mesoporous silica drug carriers enhances γ-secretase inhibitor efficacy in an in vivo model for breast cancer. *Nanomedicine* **2013**, *9* (7)**,** 971-987.

CONTRIBUTION OF THE AUTHOR

I The author is responsible for all experimental work in this publication, except for the preparation of cell lysate and optical imaging performed by Neeraj Prabhakar, SEM imaging by Linus Silvander and HPLC measurements by Jarl Hemming.

II The author has established the protocol for cellular uptake of nanoparticles in PC3 cells, comprising flow cytometry and confocal microscopy imaging. Einar Sulheim and Habib Baghirov are responsible for the main part of the experimental work and writing of this publication. The nanoparticles were synthesized by Ýrr Mørch.

III The author is responsible for the synthesis, development and chemical surface-modification of core-shell nanoparticles as well as their physicochemical characterization, except for SEM performed by Linus Silvander, TEM by Hua Jiang and PL measurements by Andrei Komich, Sergey Burikov, Tatiana Dolenko and Igor Vlasov. The nanodiamonds were produced by Olga Shenderova.

IV The author is responsible for the synthesis, development and chemical surface-modification of core-shell nanoparticles as well as their physicochemical characterization, except for TEM performed by Hua Jiang, optical imaging by Neeraj Prabhakar and Tuomas Näreoja, and PL measurements by Tatiana Dolenko, Denis Vlasov, Victor Ralchenko and Igor Vlasov. The nanodiamonds were produced by Satoru Hosimi.

SYMBOLS AND ABBREVIATIONS

APTS	3-aminopropyltriethoxysilane
APTMS	3-aminopropyltrimethoxysilane
BBB	blood-brain barrier
BET	Brunauer-Emmett-Teller theory for surface area determination
BJH	Barrett-Joyner-Halenda method for deriving mesopore sizes
CavME	caveolin-mediated endocytosis
CLSM	confocal laser scanning microscopy
CMC	critical micelle concentration
CME	clathrin-mediated endocytosis
CPT	camptothecin
CTAB	cetyltrimethylammonium bromide
CTACl	cetyltrimethylammonium chloride
CVD	chemical vapor deposition
EDS	X-ray energy-dispersive spectroscopy
EELS	electron energy-loss spectroscopy
EPR	enhanced permeability and retention
DAPI	4′,6-diamidino-2-phenylindole, blue fluorescent nucleic acid stain
DAPT	N-[N-(3,5-Difluorophenacetyl)-L-alanyl]-S-phenylglycine t-butyl ester, γ-secretase inhibitor drug
DDS	drug delivery system
DiI	1,1'-Dioctadecyl-3,3,3',3'-tetramethylindocarbocyanine perchlorate, lipophilic dye (also $DiIC_{18}$)
DLS	dynamic light scattering
DLVO	Derjaguin, Landau, Verwey, Overbeek theory of interaction between charged surfaces in a liquid medium
DMEM	Dulbecco's modified Eagle's medium
DMF	dimethyl formamide
DMSO	dimethyl sulfoxide
DNA	deoxyribonucleic acid
DND	detonation nanodiamond
DSC	differential scanning calorimetry
EDS	energy dispersive spectra
FCM	flow cytometry
FDA	U.S. Food and Drug Administration
FITC	fluorescein isothiocyanates
FLIM	fluorescence lifetime imaging
FRAP	fluorescence recovery after photobleaching

FRET	Förster resonance energy transfer
FSC	forward scattering
γ	surface tension
GC	gas chromatography
GRAS	generally regarded as safe
GSI	gammasecretase inhibitor
HeLa	human cervical cancer cell line
HEPES	4-(2-hydroxyethyl)-1-piperazineethanesulfonic acid
HPHT	high-pressure high-temperature
HPLC	high-performance liquid chromatography
HRTEM	high-resolution transmission electron microscopy
HUVEC	human umbilical vein endothelial cells
IEP	isoelectric point
IV	intravenous
IUPAC	International Union of Pure and Applied Chemistry
K	Kelvin, temperature scale
λ	wavelength
LDV	laser Doppler velocimetry
log P	oil/water partition coefficient on a logarithmic scale
M41S	a class of mesoporous nanomaterials first introduced by Mobil Oil Company
MB	microbubble
MCM-41	Mobil Composition of Matter No.41; mesoporous materials with a 2-dimensional hexagonal structure
MDA-MB-231	human breast cancer cell line
MPS	mononuclear phagocyte system
MRI	magnetic resonance imaging
MSN	mesoporous silica nanoparticle
ND	nanodiamond
NNI	US National Nanotechnology Initiative
NP	nanoparticle
NR668	modified nile red hydrophobic fluorescent dye
NV	nitrogen vacancy
ONP	organic nanoparticle
PACA	poly(alkylcyanoacrylate)
PANI	polyaniline
PBCA	poly(butylcyanoacrylate)
PC3	prostate cancer cell line
PdI	polydispersity index
PEG	poly(ethylene glycol)

PEI	poly(ethylene imine)
PET	positron emission tomography
p-HTAM	pentamer hydrogen thiophene acetic acid methyl ester
pK_a	acid dissociation constant (K_a) on a logarithmic scale
PL	photoluminescence/photoluminescent
PLA	polylactic acid
PLGA	polylactic-co-glycolic acid
POCA	poly(octylcyanoacrylate)
PSD	particle size distribution
PVP	poly(vinylpyrrolidone)
PZC	point of zero charge
Q^n	terminology used for indicating the number of bridging bonds *n* (-O-Si) tied to the central Si atom
RBE5	brain endothelial cell line
RES	reticuloendothelial system
RT	room temperature
SAXS	small-angle X-ray scattering
SDA	structure-directing agent
SEM	scanning electron microscopy
SSC	sideway scattering
STED	Stimulated emission depletion
TEM	transmission electron microscopy
TEOS	tetraethyl orthosilicate
TGA	thermogravimetric analysis
TMOS	tetramethyl orthosilicate
US	ultrasound
XRD	X-ray diffraction
ZPL	zero-phonon line
ζ	zeta potential

TABLE OF CONTENTS

INTRODUCTION

Nanomedicine describes the development and application of nanoscale materials and devices, i.e. nanotechnology, to solve problems related to medicine, including diagnosis, disease prevention and treatment.[1–4] In this highly interdisciplinary field, the benefits of science and engineering, physics, materials chemistry, cellular and molecular biology, pharmacology and medicine all come together. Advances within these fields have enabled the production of new fascinating, and even "smart" nanomaterials, in parallel with characterization by an array of sophisticated techniques.[5,6] As the dimensions of a material enter the nanoscale, profound changes in reactivity and electrical, conductive, optical, physical, mechanical, magnetic, and surface properties may occur as a result of the high surface-to-volume ratio.[5] These unique nanoeffects are the basis of the novel applications of nanomaterials. Although the definition of nanomaterials as proposed by the US National Nanotechnology Initiative (NNI) is limited to an upper size of 100 nm,[7] it is ultimately the change in physical and biological properties, not the exact size, that defines the utility of the material. The useful size range of nanomedicines is therefore, more commonly considered to span from a few nanometers up to 1000 nm in diameter, which coincides with the size range of most biomolecules.

During the last three decades, a wide array of nanocarrier-based DDSs has been designed for targeting various pathological conditions, such as fungal infections, anemia, various autoimmune, immunodeficiency and neuro-degenerative diseases and numerous different forms of cancer (e.g. breast, gastric, pancreatic, lymphoma, etc.).[8] Such DDSs include inorganic metallic, ceramic, semiconductor, and carbon NPs as well as organic structures, such as dendrimers, micelles, liposomes, and polymeric NPs, and various combinations of these.[9,10] Their *in vivo* administration routes include oral, pulmonary, subcutaneous and intravenous administration, only to name a few. The rationale behind using nanocarrier-based DDSs is to minimize drug degradation and loss, decrease harmful side-effects, improve the pharmacokinetics and increase the bioavailability of the drug via efficient delivery followed by sustained, controlled or targeted release at the desired site of action.[11–13] Especially cancer therapy may thereby greatly benefit from DDSs, as many anticancer drugs are both highly toxic and poorly water-soluble, which create huge challenges for their effective and safe administration by conventional drug formulations. Achieving proper drug targeting represents perhaps the most challenging goal for DDSs, as it requires the DDS to stay intact, while carrying the drug, preferentially without any premature release, across numerous physiological barriers that separate the administration site

from the target site. Additionally, an ideal drug carrier would also biodegrade and be excreted within a reasonable period after drug release, in order to avoid adverse effects associated with cellular or organ accumulation.

Owing to their superior controllable structural and morphological parameters, combined with flexible functionalization regimes, amorphous MSNs, derived through sol-gel processing of silica (SiO_2),[14] have emerged as promising candidates for *in vitro* and *in vivo* diagnostics and intracellular delivery of, especially, poorly water-soluble drugs for cancer treatment.[15–18] *In vivo*, MSNs have been shown suitable for cancer targeting through intravenous, local as well as oral administration.[19] The high versatility of the MSN platform in terms of particle and pore surface functionalization, furthermore offers a multitude of opportunities for creating both targeted and stimuli-responsive release systems through conjugation with various targeting ligands or pore capping agents, respectively. Among various organic nanostructures presented, PACA NPs have emerged as appealing candidates for drug delivery applications due to their high versatility, excellent functionalization possibilities, biocompatibility and controllable degradation rate.[20,21] Compared to many other biodegradable polymers, their good *in vitro* stability and fast *in vivo* enzymatic degradation offer many advantages for drug delivery applications. Biodegradable PACA NPs have, for instance, shown promise as drug carriers both to solid tumors and across the blood-brain barrier (BBB).[22]

At the same time as the supply of new diagnostic and therapeutic substances and particles has grown, new and improved *in situ* imaging techniques have revolutionized the area of biological and medical sciences by allowing highly detailed studies of biological systems. This has enabled more accurate detection of tumors as well as monitoring of cancer progression and treatments. Especially fluorescence microscopy has proven to be a fast and reliable method for studying cellular structures and events both *in vitro* and *in vivo*.[23] Organic fluorescent dyes are typically used as diagnostic agents despite drawbacks, such as photobleaching and cytotoxicity. Hence, there is a demand for bright, stable, and non-toxic fluorescent probes. One promising candidate for meeting these demands is photoluminescent ND,[24,25] which is non-cytotoxic, has excellent mechanical properties and displays bright and stable fluorescence.[26] NDs do, however, typically have quite irregular surface structures and a large variability of surface groups. This may cause problems in terms of dispersibility, which is a prerequisite for the biological applicability of any NP. This problem can be circumvented by creating core-shell structures comprising a ND core with a porous silica coating, thus increasing the amount of biologically active agents that can be incorporated into the particles and creating a homogeneous and easily modifiable particle surface. Encapsulation

of various inorganic nanostructures within the silica matrix to create such core-shell composite NPs has recently gained attention as an effective way of exploiting, and possibly even enhancing the benefits of several nanomaterial classes by combining them in one multifunctional probe.[27]

Creating novel multifunctional nanocomposite materials comprising both diagnostic and therapeutic functions, known as "theranostics" may have a great impact on the biomedical and pharmaceutical fields.[15,28] However, in order to have a real clinical relevance it requires that new materials be developed with a clear focus on addressing unmet clinical needs, which are directly coupled to the disease and patient-specific requirements. Understanding of how critical parameters, such as particle size, charge and surface functionalization influence material toxicity, biodistribution, pharamacokinetics, clearance and interactions with the immune system, cellular structures and functions, is of crucial importance for evaluating the true value of the DDS.[23] As the true essence of nanomedicine lies in its multidisciplinarity, close cooperation between chemists, materials scientists, biologists and clinicians is needed in order to develop, assess and effectively translate these nanomaterials into the clinic.

REVIEW OF THE LITERATURE

1 Design of nanomaterials

Nanotechnology is a multidisciplinary field, in which tools and techniques originating from physics, chemistry, biology and engineering meet to study and control the design, synthesis, characterization and application of materials with at least one dimension on the nanometer scale.[29,30] The main and collective goal of nanotechnology can be described as obtaining new devices and technologies with enhanced functional characteristics as compared to existing conventional technologies. Nanomaterials (examples in *Figure 1*) can be divided into classes based on their spatial dimensions: zero-dimensional nanostructures include various NPs (metal, metal oxide, carbon-based, liposomes, polymers, core-shell composites), one-dimensional nanostructures comprise nanowires, -rods and -tubes and two-dimensional nanostructures refer to different thin films and surface coatings that can be produced through a variety of vapor deposition techniques.[31] These materials have applications in a wide range of fields including photonics, sensing, imaging, therapeutics, biomedicine, adsorption, energy conversion, catalysis, food industry, etc.[30,32] The concept of nanomaterials is typically defined by an upper size limit of 100 nm. In the field of medical science and human health care, however, the useful size range of nanomedicines is more commonly accepted as a few nanometers up to 1000 nm.

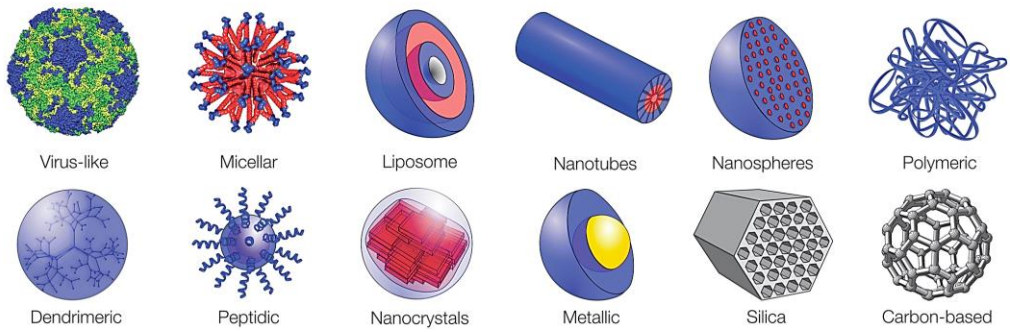

Figure 1. *Schematics of different nanostructures. Modified from Ageitos et al. (2016).*[33]

At large owing to the significant increase in availability of new production and manipulation methods as well as physicochemical and biological characterization tools, the field of nanotechnology has undergone an explosive growth during the past three decades.[5,6] Without doubt one of the greatest beneficiaries of this development is the biomedical industry,[34] where

nanomaterials find applications in imaging and diagnostics, drug development, drug and gene delivery, and even personalized medicine.[1,35] The implementation of nanotechnology in the field of medical sciences and diagnostics is called nanomedicine and can be defined as the monitoring, repair, construction and control of biological systems at the molecular level with the help of engineered nanomaterials and devices.[1,2,36] Nanomaterials that can be used as nanomedicines include e.g. proteins, polymers, dendrimers, micelles, liposomes, emulsions, nanoparticles and nanocapsules. As most nanomedicines are constructed to have the same dimensions as a variety of biomolecules, they can be engineered to cross cellular barriers and interact with biological components, such as specific cells or tissue, mimic the behavior of various biomolecules, such as proteins, lipids, nucleic acids and supramolecular structures of these components, act as carriers of a vast array of chemical substances and perform a number of complicated tasks in a biological environment.[5] Hence, by integrating fundamental chemistry and physics with materials science and biotechnology we have been able to create the highly interdisciplinary field of nanotechnology, that can serve as a powerful tool for creating new smart and advanced materials with the purpose of studying and unlocking the secrets to numerous complicated biological processes (*Figure 2*).

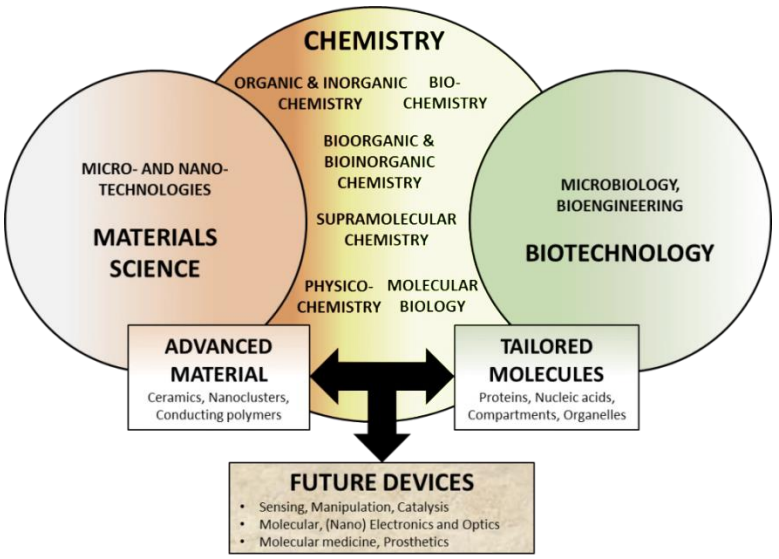

Figure 2. *Chemistry acts as the basis for the development of both materials science and biotechnology. Integration of these fields have allowed huge progress in the development of advanced materials and devices and tailored biomolecules. Adapted from Niemeyer (2001).*[5]

1.1 Effects on the nanoscale

The structure and properties of nanomaterials differ significantly both from those of single atoms and molecules, and from those of bulk materials. Nanomaterials can therefore be perceived as a link between single molecules and infinite bulk systems. NPs are typically classified as materials with at least one dimension ≤100 nm.[9] This classification, though somewhat arbitrary, is widely established in scientific literature and at large covers the size range, in which certain nanospecific properties of a material become size-dependent and different from those of the corresponding bulk material. The size, at which nanomaterials display different properties to the bulk material, varies and is material-dependent. When the size of the material components enters the nanoscale, a number of new phenomena arise. The size directly affects the physical interactions of the system, which become dominated by short-range forces, such as van der Waals attractive and electrostatic forces as the gravitational forces become negligible. Additionally, the high surface-to-volume ratio of nanosized materials may provide the material with a vast range of new physicochemical properties; thermodynamic, electronic, spectroscopic, electro-magnetic, optical or chemical properties can arise as a result of the increased number of surface atoms.[37–40] Some of these size-dependent nanoscale effects have long been exploited for various applications; the optical absorption of gold NPs has been used in the dyeing of glass already in late Greco-Roman times.[41] More recent applications include exploiting the photoactivity (optical transparency and adsorption) of TiO_2 and ZnO NPs in UV-protective sunscreens,[41] and utilizing the light emission of semiconductor materials for biolabeling purposes.[42,43]

While the high relative surface area of nanomaterials and their consequently enhanced chemical reactivity is the exact property, which is being exploited in many nanotechnological applications, it might potentially also include environmental and health risks. Cytotoxicity caused by nanostructures through interaction with biological systems is referred to as nanotoxicology, and examines the effect of physical and chemical material properties, such as particle size, shape, aggregation, surface chemistry and composition, on the induction of toxic responses in biological systems.[44] The size of NPs lies in the same range as biomolecules, biological barriers and cellular components, which is why they have the potential to cross physiological membranes and be taken up in cells and tissues,[45] with potentially harmful consequences. This trait can, however, also be used beneficially in the fields of nanomedicine and nanobiotechnology to successfully deliver and trace e.g. various therapeutics, fluorescent markers, transfection agents or biosensors in living cells.[45–50]

The transport efficiency of materials over cellular membranes is strongly size-dependent and decreases with increased particle size.[51,52] However, particle-induced cytotoxicity has also been reported as inversely size-dependent,[53] which indicates that smaller is not necessarily always better from a biological point of view. Amorphous silica NPs are generally considered as biocompatible and non-cytotoxic[54–56] both *in vitro* and *in vivo*,[57] although a few publications have reported some toxicological effects for silica particles smaller than 200 nm.[58] In consideration of size-dependent intracellular uptake and toxicological effects the useful range of nanomedicines in practice falls into the range 5-250 nm, as they moreover show similarities in physiological and anatomical impact.[59] For any NP, cytotoxicity is dependent, in addition to particle size, also on surface functionalization, dose, exposure and administration route. Hence, these aspects all need to be taken into account when developing new nanomaterials for biological applications.

1.2 Synthetic approaches

Various NPs with controlled dimensions from one to several hundred nanometers and narrow size distributions can be prepared in large quantities by relatively simple methods. There are two main strategies for the fabrication of nanomaterials: the top-down and bottom-up approaches (*Figure 3*), both with their own advantages and disadvantages. The top-down approach includes manufacturing methods where the final nanosized product is obtained by splinting larger bulk materials into smaller components. Often these techniques include detrition and milling. In addition, micropatterning techniques, such as photolithography and inkjet printing appertain to this group. Lithography can be considered a hybrid approach as some lithographic techniques, such as etching and photolithography, are considered top-down techniques, while nanolithography, nanomanipulation, the growth of thin films and new unconventional pattering techniques, such as self-organization and self-folding, are classified as bottom-up techniques.[31,60] The largest disadvantage of top-down techniques is that they typically produce materials with surface imperfections and structural defects.[61] Since the size and shape of NPs in great measure affect their catalytic, adsorptive, adhesive, optical and magnetic properties as well as chemical reactivity, such morphological defects can potentially have harmful effects on the physicochemical properties of the material.

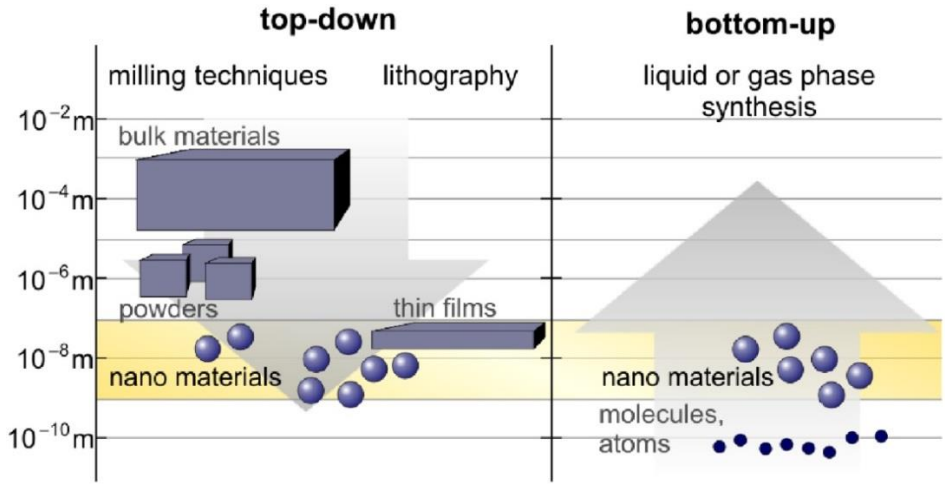

Figure 3. *Nanomaterials can be produced by top-down or bottom-up techniques.*[62]

Nobel physicist Richard Feynman can be said to have brought on the huge interest for the development of bottom-up strategies, as he, in his famous lecture "There's plenty of room at the bottom" from 1959, put forth the idea of being able to control the manufacturing of materials at the atomic level.[63] Bottom-up techniques make use of the self-assembly of atoms or molecules to form larger supramolecular structures, organized molecular films and NPs using a vast range of techniques.[64] Bottom-up approaches generally offer good control of both structural and chemical features of the synthesized material, which constitutes the most fundamental aspect of nanomaterial fabrication.

The most common group of bottom-up approaches, which can be used for producing both organic and inorganic NPs are liquid-phase techniques. Liquid-phase techniques, in general, allow effective size, shape and surface functionality control as well as prevention of particle aggregation, since structure-directing agents, stabilizers and various other organic molecules can be incorporated into the material during synthesis. Liquid-phase techniques can be divided into thermodynamic equilibrium approaches and kinetic approaches. The former requires generation of solution supersaturation of growth species, followed by nucleation and growth, and includes techniques such as e.g. molecular self-assembly and sol-gel processing. Various metal oxide NPs are typically synthesized through sol-gel processing,[65–67] of which colloidal silica is probably the most widely studied material.[14] Sol-gel processing is furthermore used in the synthesis of various core-shell nanostructures.[68–70]

Kinetic approaches require either limitation of the amount of precursor available for particle growth or confinement of the reaction to a limited space. Two commonly used kinetic approaches are the synthesis of NPs inside

micelles or by microemulsion.[31] Microemulsion-based methods are fairly simple and inexpensive and are therefore commonly used for the production of a vast array of NPs. A microemulsion is a thermodynamically stable dispersion of two immiscible or partly miscible liquids with an added emulsifier or surfactant acting as the stabilizer.[71] The emulsion can be a water-in-oil, oil-in-water or water-in-supercritical fluid emulsion. Especially water-in-oil emulsions that appear when water is homogeneously dispersed in organic media, have attracted a lot of attention due to their application in the synthesis of metallic[72,73] semiconductor,[74] and different polymeric NPs[75]. Among the polymeric NPs, polyaniline (PANI),[76,77] polylactic acid (PLA),[78] polylactic-co-glycolic acid (PLGA),[78,79] and PACA[80,81] NPs are all commonly used as nanocarriers in biomedical applications. Co-polymers with hydrophilic and flexible properties, such as poly(ethylene glycol) (PEG), are typically introduced for the purpose of providing stealth properties to the NPs.[82]

2 Ordered mesoporous silica

2.1 Sol-gel synthesis of porous inorganic materials

The sol-gel process is a widely used technique for producing metal oxides by the bottom-up approach. Starting from a chemical solution (sol), which acts as a precursor for an integrated network (gel) of particles or polymers, NPs can easily be produced through a single-step procedure (*Figure 4*).[14] Inorganic salts or metal alkoxides are typically used as silica precursors, which undergo stepwise hydrolysis and condensation during the polymerization process, gradually changing the structure of the sol and ultimately forming a colloid. A wide range of nanomaterials, including amorphous MSNs with varying properties can be synthesized by this low-temperature method.[83]

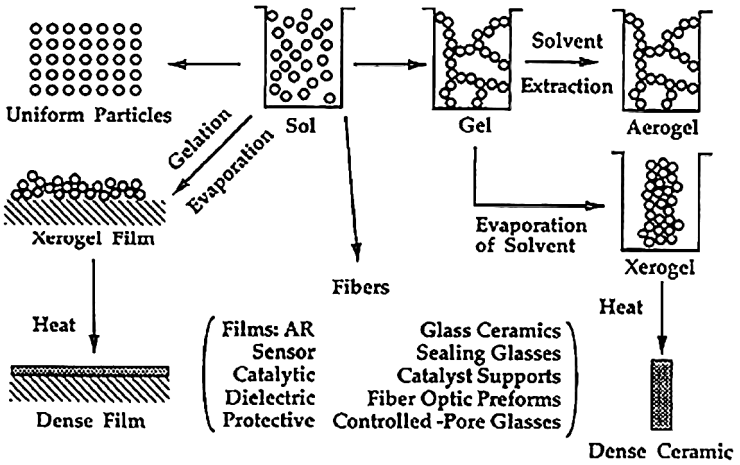

Figure 4. *Overview of the sol-gel process.*[14]

In 1968 Stöber *et al.* reported the formation of monodisperse non-porous silica nano- and microparticles, with diameters ranging from 50 nm to 2 μm, by the means of hydrolysis and subsequent condensation of silicates in alkaline alcoholic solutions.[84] At alkaline conditions, the solubility of silica increases and the silica species are negatively charged. When highly diluted reaction conditions are simultaneously employed to avoid inter-particle aggregation, the sol-gel processing can proceed by *Ostwald ripening*, which allows for a well-controlled nucleation and growth pattern that, ideally, starts with a short initial burst of nucleation and is followed by a uniform growth, creating particles with a spherical homogeneous structure. Through regulation of the synthesis parameters in terms of type and concentration of alcohol, ammonia, water and silica precursors, the size and morphological structure of the final product can be altered. In addition to the original Stöber synthesis, many modified versions

of the synthesis have also to date been presented for the production of porous silica NPs[85–87] and silica coatings on different core materials.[88–91]

In 1992 scientists at Mobil Oil Research managed to successfully synthesize a new family of periodically ordered aluminosilicate mesoporous materials called the M41S class of materials.[92,93] The original members of the M41S family, illustrated in *Figure 5*, are Mobil Composition of Matter No. 41, MCM-41 with a two-dimensional hexagonal pore structure, MCM-48 with a three-dimensional cubic pore structure and MCM-50 with a pillared lamellar structure.[94]

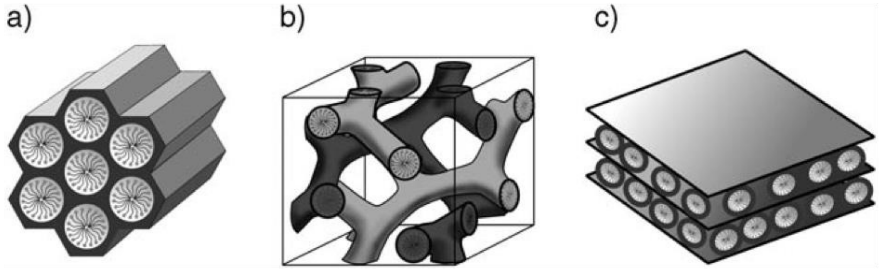

Figure 5. *Schematic presentation of the structures of the M41S family of mesoporous ordered materials: a) MCM-41 (hexagonal), b) MCM-48 (cubic), and c) MCM-50 (lamellar).*[94]

These materials can be synthesized using supramolecular surfactant aggregates as structure-directing agents (SDA), around which the inorganic silicate or aluminosilicate species is allowed to polymerize, forming a mesoscopically ordered hybrid organic-inorganic material. Subsequent removal of the organic SDA by chemical extraction or thermal calcination reveals the final product: an inorganic material with an ordered porous structure. The principal for the synthesis of M41S materials is basically the same as that of zeolite molecular sieves, which relies on the co-operative self-assembly of the silica and surfactant species.[95] However, by using supramolecular surfactant structures instead of single molecules as SDA, materials with larger pore sizes (1.5-10 nm) can be manufactured, compared to the pore size of zeolites, which is typically restricted to 1.5 nm.[95,96]

Since the discovery of the M41S family of materials, several modifications of the synthesis have been proposed to produce especially MCM-41 type MSNs. Grün *et al.* introduced a modification of the Stöber synthesis, in which the formation of submicrometer-sized MCM-41 type particles was catalyzed by alkaline conditions using alcohol as a co-solvent and quaternary ammonium salts as SDA.[97] Nooney *et al.* showed that the size of the particles could also be fine-tuned by varying the silicate/surfactant ratio of the synthesis solution.[98] Cai *et al.* furthermore noted the importance of using dilute synthesis

conditions and low surfactant concentrations in order to achieve a more controlled nucleation and growth pattern and thereby a more well-defined particle morphology.[99,100] In addition to intrinsic silica NPs, a number of silica composite NPs have also been synthesized through the sol-gel route; core-shell NPs employing silica-coatings around various core materials,[46,101–103] as well as silica hollow spheres have been introduced.[104,105] As size is an ever-critical property of all materials intended for biomedical applications, a great deal of focus has also been directed towards establishing effective ways to control both the particle and the pore size of the synthesized materials. While a large pore volume can host a considerable amount of therapeutic guest molecules, a certain particle size may potentially impede or enhance the cellular uptake of the material, thus also affecting the overall bioavailability of the therapeutic agents.

2.2 Polymerization of silica

On the fundamental level, the polymerization of silica proceeds through three steps: nucleation, growth and aggregation. Sols and gels can be produced through hydrolysis and condensation reactions of an inorganic or organic alkoxide precursor. When an organic silicon alkoxide, $Si(OR)_4$, is used as the precursor molecule, polymerization through hydrolysis and condensation proceeds via the following reactions, where R indicates an alkyl group:[106]

$$\equiv Si - OR + H_2O \rightleftharpoons \equiv Si - OH + ROH$$
Hydrolysis
Esterification

$$\equiv Si - OR + HO - Si \rightleftharpoons \equiv Si - O - Si + ROH$$
Alcohol condensation
Alcoholysis

$$\equiv Si - OH + HO - Si \rightleftharpoons \equiv Si - O - Si + H_2O$$
Water condensation
Hydrolysis

Hydrolysis and condensation usually occur simultaneously. As condensation proceeds, the amount of free hydroxyl groups decrease when the number of Si-O-Si bonds is maximized. As a result, ring structures are formed giving rise to three-dimensional particles that act as nuclei. These particles grow through *Ostwald ripening*, which is a pH- and temperature-dependent process, through which particles grow in size, while simultaneously decreasing in number due to dissolution of smaller more unstable particles into monomeric silica that subsequently reprecipitates on larger particles.[107]

A number of parameters, such as reaction temperature, pH, type of solvent, catalyst (acid/base) and silica precursor govern the polymerization reaction kinetics. Because water and alkoxides are immiscible, an alcohol is normally used as co-solvent to homogenize the solution, although gels can be produced also in the absence of alcohol, as alcohol is created as a byproduct of hydrolysis. The hydrophilicity of the silica precursor also gradually increases when it is hydrolyzed, which helps homogenize the system. Acids are typically used to catalyze gel formation while bases, typically ammonia or sodium hydroxide, are used in particle syntheses. The acidic or basic strength as well as the H_2O/Si molar ratio, called the *r*-value, also influence the extension of hydrolysis. Hydrolysis under acidic conditions, where the H_2O/Si ratio is low, proceeds fast and produces weakly branched, polymeric sols. Hydrolysis under basic conditions, where the H_2O/Si ratio is high, oppositely, proceeds slower and produces highly condensed, particulate sols. Theoretically, an *r*-value of 2 should be enough to achieve complete hydrolysis and condensation, since more water is produced during condensation. However, in practice not even an excess of water leads to completion of the reaction, but instead a number of intermediate silicate species are generated.

An overview of the silica polymerization process is shown in *Figure 6*, according to which polymerization at acidic conditions and alkaline salt-containing conditions occurs through aggregation of small particles to form gels.[14] The aggregation can be reversed by raising the pH of the solution. At alkaline salt-free conditions, particle growth occurs through *Ostwald ripening*, which leads to a decrease in number of particles due to the highly pH- and temperature-dependent solubility of silica,[106] which causes smaller particles to dissolve into monomeric silica that subsequently redeposits on larger particles.

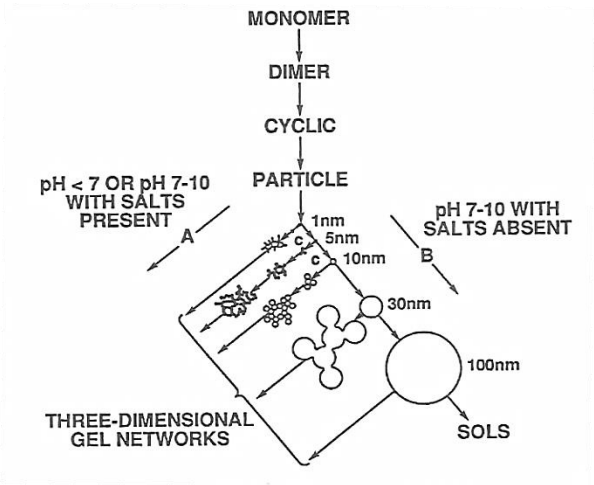

Figure 6. *Polymerization process of silica.*[14]

Silica polymerization occurs through different mechanisms depending on the pH of the reaction solution and can be divided into three different domains: pH <2, pH 2-7 and pH >7. pH 2 serves as the lower boundary, since both the point of zero charge (PZC), where the net surface charge of the molecule equals zero, and the isoelectric point (IEP), where the electrophoretic mobility equals zero, are in the pH range 1-3 for silica. Below pH 2, where the silicate species are positively charged, the gel times are relatively long and the polymerization rate is proportional to the concentration of hydrogen ions [H^+]. Near the IEP, where the electrostatic repulsion between particles is very low, particle growth and aggregation occur simultaneously. Between pH 2 and pH 7 the condensation rate is presumably proportional to the concentration of hydroxyl ions [OH^-] and pH 7 serves as another boundary, above which the solubility of silica increases fast. Above pH 7, at increasingly high pH, all condensed silica species are negatively charged and the interparticle repulsion allows for particle growth mainly by addition of monomers to more highly condensed species, without aggregation or gelation. The primary particles thus grow through *Ostwald ripening*, the final size of the particles ultimately depending on both the silica solubility and the reaction temperature.

2.3 Mechanism of formation of mesoporous silica

Mesoporous materials are defined by the International Union of Pure and Applied Chemistry (IUPAC) as having pores in the size range 2-50 nm.[108] The probably most well-known classes of periodic mesoporous silicas are the MCM-41, MCM-48 and MCM-50 solids, which belong to the M41S family of periodically ordered mesoporous silicas developed by Mobil Oil Company.[92,93] These materials have pore diameters in the approximate range 2-10 nm and exhibit well-defined pore structures, narrow pore size distributions and large specific surface areas. By creating supramolecular aggregates of ionic surfactants, such as e.g. cetyltrimethylammonium bromide (CTAB) or cetyltrimethylammonium chloride (CTACl) as SDA, these materials can be produced under basic conditions. Three different mechanisms have been proposed for the synthesis of M41S materials: liquid-crystal templating, self-assembly and cooperative self-assembly. [94,109] In true liquid-crystal templating, illustrated in *Figure 7a,* the surfactant concentration is high enough to catalyze the formation of a lyotropic liquid-crystalline phase without the presence of a silica precursor, typically tetraethyl- (TEOS) or tetramethylortosilicate (TMOS). In cooperative liquid-crystal templating (*Figure 7b*) self-assembly of the SDA and the inorganic silicate species can occur even at very low concentrations of SDA.

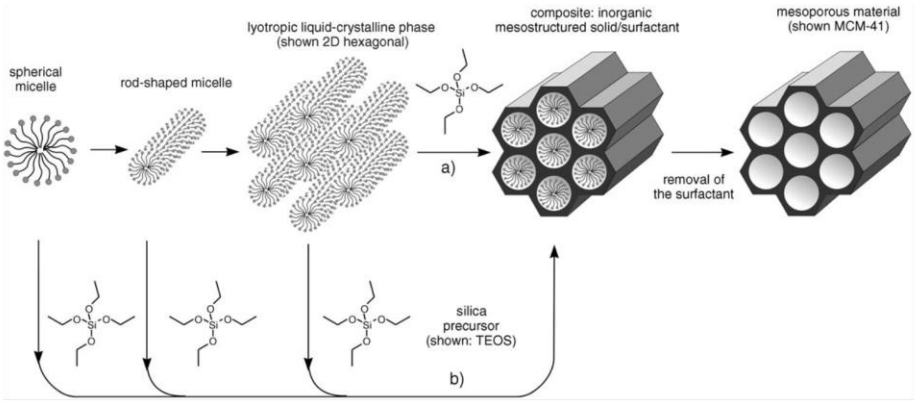

Figure 7. *Formation of mesoporous materials by structure-directing agents through a) true liquid-crystal template mechanism and b) cooperative liquid-crystal mechanism.*[94]

Based on the nature of the SDA and silicate species as well as the acid/base characteristics of the reaction medium, the surfactant/silicate assembly can proceed through a number of different pathways illustrated in *Figure 8*,[94] as originally proposed by Huo *et al.*[110,111] The synthetic pathway a) is termed S^+I^- (S: surfactant, I: inorganic species) and the reaction proceeds in alkaline conditions with cationic quaternary ammonium surfactants as SDA. This pathway represents the interactions that occur during the assembly of M41S-type mesoporous silicas, among them MCM-41 materials, which are in primary focus in this thesis. Reaction b) (pathway $S^+X^-I^+$) takes place under acidic conditions where the silica species are positively charged and therefore requires a mediator ion X^- (usually a halide) to create an interaction with the cationic surfactant.[112] Reactions c)-d) represent cases where negatively charged surfactants are used in alkaline or acidic conditions. Pathways a)-d) represent different electrostatic interactions while e)-f) arise due to hydrogen bonding in the presence of uncharged silica species and neutral or nonionic surfactants.

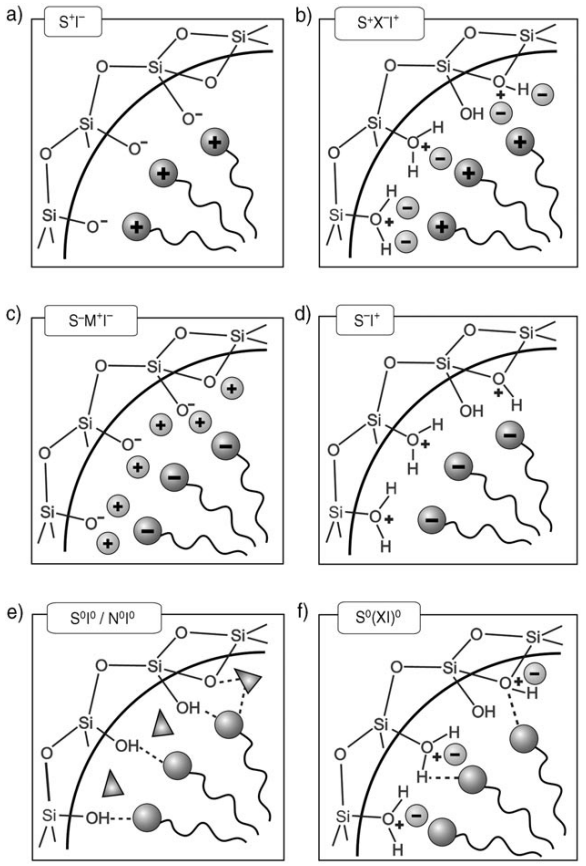

Figure 8. *Interaction between the inorganic species and the head group of the surfactant in syntheses carried out in acidic, basic or neutral media.*[94]

Surfactants are typically amphiphilic molecules that contain a hydrophilic head group and a hydrophobic tail group. Due to the hydrophobic nature of the tail groups, surfactants tend to aggregate to form micelles in hydrophilic environments when the surfactant concentration reaches the so called critical micelle concentration (CMC).[113] The shape of the micelles, and thereby the resulting mesophase architecture of the synthesized material can be estimated based on the packing parameter, g, of the surfactant molecules. The surfactant packing is related to the volume, V, and length, l, of the hydrophobic surfactant chains, and to the effective area, a_0, of the hydrophilic surfactant head groups at the interface through the equation $g=V/la_0$.[112,114,115] The packing parameter increases when starting from a highly curved micellar structure of spherical micelles ($g<1/3$), through hexagonal ($g=1/3-1/2$), through cubic ($g=2/3-3/4$) to lamellar ($g=1/2-1$). The size, charge and shape of the surfactant molecules largely govern the interactions at the surfactant/silicate interface, where there is a continuously ongoing charge-matching between the hydrophilic surfactant

head groups and the charged silanols.[116] These charge-matching interactions as well as the packing of the alkyl chains affect the final packing of the surfactant molecules. Charge-matching is sensitive to pH, cosurfactants and counterions while organic chain-packing is influenced by the length of the alkyl-chain, synthesis temperature and organic additives.[112,117] Increased alkyl-chain length leads to increased water repulsion, resulting in larger pores. These two above-mentioned interactions principally determine the size and shape of the resulting surfactant micelles, thus determining the mesophase morphology (pore size and shape) of the final product.[118] There are also ways of manipulating the pore size with pore-swelling agents[119,120] or through post-synthesis hydrothermal treatments,[121,122] which have been found to successfully increase both the pore size and pore wall thickness of mesoporous silica materials.[122,123]

2.3.1 MCM-41 mesoporous silica nanoparticles

Owing to their many unique physicochemical traits, MCM-41 type mesoporous silica-based NPs, have during the last decades emerged as promising and versatile probes for different biomedical applications. Firstly, amorphous silica is generically accepted as biocompatible, biodegradable and non-toxic in biological systems and has by the United States Food and Drug Administration (FDA) been classified as "generally regarded as safe" (GRAS).[57,124,125] Secondly, preparation of the particles in an easy one-pot synthesis under alkaline conditions allows tuning of the particle (20 nm-2 um) and pore (2-10 nm) size, and selective functionalization of the silica surface with a variety of organic functional groups.[126] Highly monodisperse particles with large specific surface areas (900-1500 cm^2 g^{-1}), large pore volumes (0.5-1.5 cm^3 g^{-1}) and narrow pore size distributions can be synthesized. These properties play important roles in the context of effective subsequent functionalization of both the inner and outer surface of the particles,[54] with different functional groups, fluorescent molecules for imaging and tracking purposes (**Supporting Publication III)**, high payloads of therapeutic molecules, and targeting ligands such as peptides, proteins or antibodies (see *Figure 9*).[127]

Dilute synthesis conditions in terms of surfactant and silicate concentration, are generally needed in order to maintain good dispersion stability throughout the nucleation and growth process. Mixtures of the cationic quaternary ammonium salt CTAB and the silicon alkoxide TEOS are common in the production of MCM-41 materials,[112,116] and generally lead to silica frameworks comprising large pores and highly ordered hexagonal pore structures. Since the silicon alkoxide species and water are immiscible because of differences in polarity large amounts of alcohol is typically used as a cosolvent to help homogenize the synthesis solution.[128] By shifting the polarity

of the solution, by changing the water/alcohol volume ratio or by changing the surfactant/silicon alkoxide ratio, the particle size can be fine-tuned.

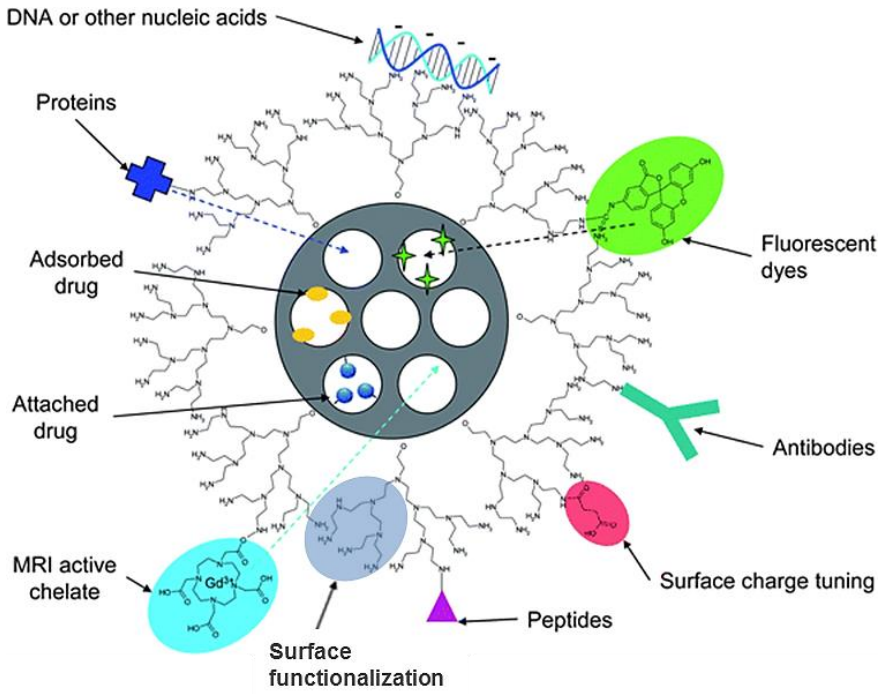

Figure 9. *Surface functionalization and cargo loading possibilities of MSNs. Modified from Rosenholm et al. (2010).*[129]

2.3.2 Novel core-shell nanoparticles

As the fields of biomedical imaging and nanomedicine are rapidly evolving, a demand for novel multifunctional materials, capable of serving both as bright and stable imaging probes and as carriers of therapeutic and targeting agents, have also arisen. This demand has sparked the development of numerous new composite materials, among them core-shell NPs,[28] in which e.g. metals,[130–132] metal oxides,[49,91,133] and carbon-based nanostructures[130,134] are incased within metal oxide,[130,133,49,91] sulfide,[43,131] selenide,[50,132] polymer[133,135,136] or carbon[137] shells to combine the advantages of several material classes within one nanosized probe.

2.3.2.1 Nanodiamonds as labels for fluorescence imaging

Nanodiamonds belong to the family on carbon nanomaterials that includes also carbon nanotubes and -wires, carbon dots, graphene- and graphite-based NPs, and fullerenes.[39,138–140] A broad size-range of ND particles can be produced, either by top-down or bottom-up approaches. The former involves grinding of larger microsized particles produced by different high-temperature high-

pressure (HPHT) techniques,[25,141] while the latter constitutes detonation of high-energy carbon-containing explosives that generates so called detonation nanodiamond (DND),[142,143] and chemical vapor deposition (CVD)[144,145]. Before the final product is obtained, the synthesized NDs generally undergo several purification steps that may include sonication, filtration, ion-exchange, different acid treatments to remove graphitic and organic impurities from the surface and peroxide treatments for removal of metals, followed by washing, fractioning, and drying procedures.[146–148] *Figure 10* displays typical surface functional group compositions of DND after oxidation and reduction treatments. Synthetic ND is currently used in a broad range of applications, such as polishing, lubrication, photonics (**Supporting Publication VI**), biophysics, biotechnology, and nanomedicine[149–151]. The vast range of applications owe to their extraordinary material characteristics, including chemical inertness, hardness, biocompatibility, high refractive index, photostability and facile surface-functionalization.[149,152–154] Despite their many advantageous characteristics, the synthesized NDs are typically irregularly shaped and fairly polydisperse with heterogeneous surface chemistries and structures.[24] These traits can be especially unfavorable when trying to achieve controlled and efficient surface functionalization.

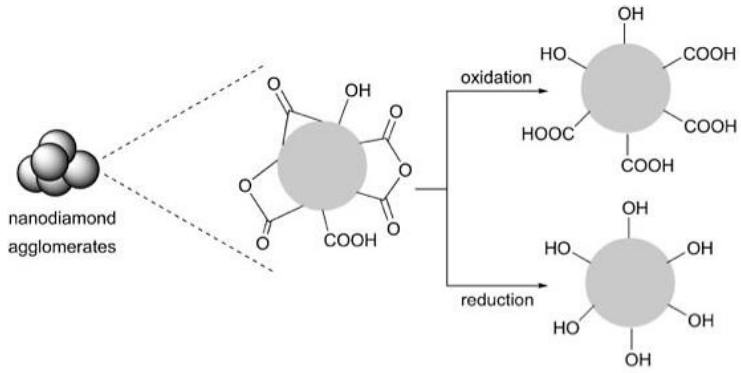

Figure 10. *Functional groups on pristine detonation nanodiamond and effects of oxidation or reduction treatments.*[155]

Quite recently, the use of NDs as imageable and traceable probes for *in vitro* and *in vivo* biomedical applications has gained specific interest due to the possibility to introduce PL centers into the diamond crystal structure,[156] combined with reported low toxicity *in vitro* in a number of cell types[152,157–159] as well as *in vivo* in mice and rats upon intravenous,[160] intraperitoneal,[161] or pulmonary[162] administration. The processing of PL color centers involves introduction of foreign atoms into the diamond crystal structure during ND

synthesis and, hence, substituting carbon atoms in the diamond crystal lattice for nitrogen,[163] nickel[164] or silicon[165] atoms. Adjacent vacancies can thereafter be formed by means of irradiation with electrons,[166] protons,[156] or He^{+24} ions. Subsequent annealing in vacuum, at high temperature conditions (600-800°C) causes diffusion of the vacancies to sites close to the foreign atoms, which induces formation of the PL vacancy centers.[146,152]

The most widely studied color centers in NDs intended for bioimaging applications are the nitrogen vacancy (NV) centers that emit PL in the red and near-infrared region of the light spectrum. The NV centers can occur in neutral (NV^0) or negatively charged (NV^-) states and exhibit zero-phonon lines (ZPL) at 575 nm and 638 nm (*Figure 11*), respectively, with wide phonon bands of lower energy.[156,166,167] Especially the negatively charged (NV^-) vacancy center is of particular interest, since its emission falls into the spectrum suitable for bioimaging with different fluorescence microscopy techniques, including also super-resolution microscopy.[168,169] The vacancy center is excited at ~560 nm and the emission can typically be collected at 650-730 nm,[147,163] which furthermore makes it easy to distinguish from the autofluorescence of cells that falls into the range 350-550 nm. Furthermore the NV^- color center shows remarkable photostability with no signs of photobleaching even when subjected to high-power excitation.[102,152,168,170] The structural defects of the typically very heterogeneous ND surface are additional sources of luminescence, whose intensity per volume is known to increase with decreasing diamond particle size,[171] contrary to the PL intensity of the color centers, which is not particle volume-dependent. However, the photostability of the PL centers has been shown to strongly depend on diamond crystal size, morphology and the location of the nitrogen impurity.[172,173]

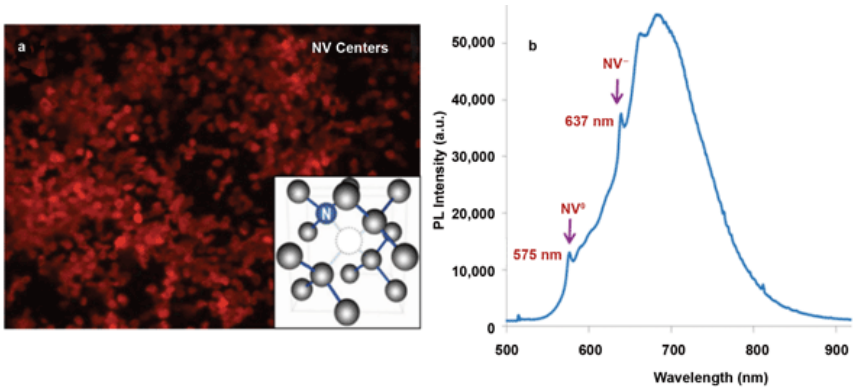

Figure 11. *a) Fluorescence microscopy image of fluorescent ND particles containing NV centers. Inset shows the diamond crystal structure at the NV center. b) PL emission spectra of 100 nm ND particles containing NV centers. Excitation: $\lambda = 532$ nm.*[174]

2.3.2.2 Coating of core structures with MCM-41 mesoporous silica

Encapsulation of various inorganic NPs within either non-porous or mesoporous silica shells through controlled sol-gel reactions, is widely used for the purpose of preserving the structure and unique properties of the NPs, for exerting particle size and shape control, and especially in the case of mesoporous silica, as a way of imparting better drug carrying and delivery capabilities onto the core@shell composite NPs.[175,47,176,177,91,130,27] In 2003, Graf *et al.* presented a general method for coating various colloidal particles with silica.[103] This two-step method comprises an initial stabilization step by adsorption of poly(vinyl-pyrrolidone) (PVP) onto the particles followed by a phase-transfer into alkaline ethanol solution where the silica shell is grown by additions of TEOS. Kim *et al.* (2006) and later also Gorelikov and Matsuura (2008) reported a simplified general procedure for the coating of hydrophobic inorganic NPs with MCM-41 mesoporous silica shells in aqueous media,[46,89] based on the well-known Stöber method.[84] This procedure proved successful in generating high yields of uniform mesoporous silica coatings without employing an intermediate polymer layer onto the core NPs prior to silica shell growth, but instead using only CTAB both as a particle-stabilizing surfactant as well as a phase-transfer and mesopore structure-directing agent.[46]

The seeded growth mechanism and resulting morphology and shell thickness of

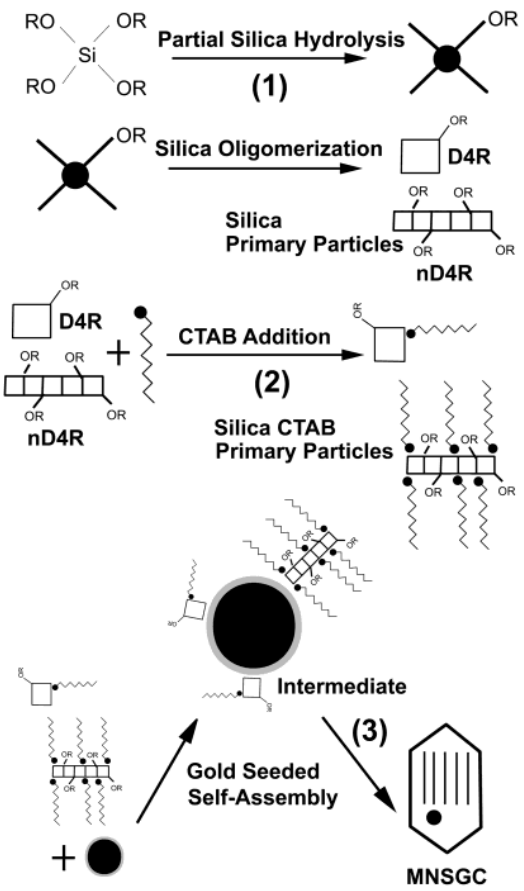

Figure 12. *Three-step mechanism for the formation of core-shell gold-silica MNSGC particles: (1) hydrolysis of monomeric silicon esters and condensation into oligomers; (2) formation of silica/CTAB primary particles; and (3) mesopore growth via either aggregation of primary particles or deposition of monomeric silica and CTAB molecules.*[174]

the composite NPs are strongly affected by the nature of the silica source, seed concentration, CTAB/silica ratio and solvent composition. These factors therefore need to be carefully optimized in order to achieve successful coating of any given core NP. Nooney *et al.* proposed a three-step self-assembly mechanism for the mesoporous silica shell-growth on gold NPs, precoated with a thin layer of non-porous silica, involving initial silica oligomerization followed by formation of silica/CTAB primary particles and finally aggregation of primary particles or deposition of monomeric silica and CTAB onto the NP seeds (*Figure 12*).[178] The hydrolysis rate of the alkoxysilane, which decreases with increased alkyl chain length,[179] was found to be of crucial importance for the coating process. Faster hydrolysis leads to higher initial concentrations of silica oligomers in solution,[106] which increases the probability of silica self-nucleation. A slower hydrolysis rate, which produces lower initial silica oligomer concentrations, by contrast increases the probability of silica oligomer collision with NP seeds, consequently leading to the seeded growth of a mesoporous silica layer. Nooney *et al.* also concluded that high CTAB/silica ratios reduced flocculation of gold seeds but simultaneously increased the probability of silica self-nucleation. Furthermore, by changing the polarity of the solvent the authors were able to generate particles with either spherical or faceted morphologies. Kim *et al.* were further able to control the silica coating thickness on iron oxide NPs by varying the number of seeds in the solution.[47] Another common approach for increasing the silica coating thickness is the addition of TEOS to the NP dispersion in several consecutive steps.[89,180] Complete removal of CTAB from the particle surface prior to the addition of silica precursor was, however, as previously established by Liz-Marzán *et al.* and Pastoriza-Santos *et al.*, found necessary in order to prevent nucleation of new silica particles.[181,182]

Core-shell NPs of hydrophilic cores coated with mesoporous silica could certainly also be of great interest, especially for a number of biomedical applications. In principal, coating of hydrophilic cores could be considered preferable over hydrophobic cores, as there is no need for stabilization or pre-coating prior to the polymerization of silica at aqueous conditions. Nonetheless, the manufacturing of such nano-composites poses a great challenge, because successful mesoporous coating requires meticulous and laborious control over the reaction environment, in terms of charge-matching interactions between the surfactant and silicate species, and finally also the core particles, acting as nucleation sites. These interactions are, *per se*, dependent on a number of parameters discussed earlier in chapters 2.2 and 2.3. The seeded growth mechanism of NPs is furthermore influenced by the precursor hydrolysis rate and possibly also interparticle distance between the seeds, as proposed by

Chou and Chen (2008).[183] There are, thus, inarguably, a multitude of parameters that need to be controlled in order to achieve successful mesoporous coating of hydrophilic core structures. The development of a simple general approach for the direct synthesis of such nanocomposites would hence be extremely valuable. In **Publication III** and **IV** we develop a simple one-step procedure carried out in aqueous medium, with the crucial addition of ethanol as co-solvent,[184] for the successful coating of hydrophilic nanosized cores with mesoporous silica shells, resulting in improved aqueous dispersibility and cargo-carrying capacity as well as facilitated surface-functionalization of the composite NP system.[102,170]

2.4 Removal of structure-directing agent

When the synthesis of a new material is complete, the templating molecules need to be removed from the material to obtain the final porous structure. Removal of the structure-directing agent usually also affects the pore size and structure of the material since it is typically carried out under elevated temperatures. Efficient surfactant removal is of high importance, as even small amounts of remaining surfactant may interfere with subsequent functionalization steps or cause toxicity in biological enviroments.[185]

Template removal can be carried out through different techniques, the two most common being calcination and solvent extraction. Calcination involves heating of the material, under nitrogen, oxygen or airflow and serves as an efficient technique to remove any organic template molecules that are present on the inner or outer surface of the material. This aspect needs also to be considered when working with core-shell NPs comprising carbonaceous cores in order not to harm the core material. For synthetically produced nanodiamond, for instance, we have found that the NDs undergo combustion already at T~770-970 K (unpublished results). Extractive methods might therefore be more favorable for these types of particles. Slow heating rates, around 1 K/minute, and heating temperatures up to 823 K are typically used during calcination. After reaching the maximum heating temperature, the heating is normally continued over 4-8 hours at a constant temperature. The calcination treatment causes further condensation of the material, which results both in a decreased number of surface silanols and a slight decrease in pore size.[185–187]

In addition to calcination, the SDA can also be removed by chemical means, through solvent extraction, often combined with mechanical agitation, such as shaking or ultrasonication on a water bath. Different means of extraction are applied depending on the acid/base characteristics, in which the material was synthesized. In the case of mesoporous materials synthesized in

acidic media ($S^+X^-I^+$ route), the surfactant molecules and halide ions (X^-) form S^+X^- ion pairs that interact weakly with the neutral or slightly positive silica network and can therefore easily be removed even by distilled water at elevated temperature (~343 K) conditions.[188] The extraction of surfactant from materials synthesized in alkaline media (S^+I^- route), such as MCM-41 type mesoporous silica, is more demanding due to the strong electrostatic interactions that develop between the cationic surfactant head group and negatively charged silicate species. Extraction can be carried out in acid, alcohol or neutral salt solutions, ammonium acetate or nitrate or mixtures of the above-mentioned. In any case, ion exchange is required to remove the surfactant species.[187,189] Efficient surfactant removal is typically achieved by extraction in acidic ethanol, but requires several repetitions to ensure complete removal of all organic residues.[190]

3 Silica surface chemistry and engineering

Particle size and surface properties largely define the performance of nanomaterials intended for biomedical applications, as they influence both the colloidal stability and biological behavior of the material. For particles within the colloidal size range, surface interactions become dominant due to their extremely high surface-to-volume ratio. These materials may display a number of new chemical and physical characteristics, such as magnetic, optical, electric, adsorptive or catalytic properties that their corresponding bulk material lacks.

3.1 Dispersion stability

In addition to the outer surface area, MSNs also have an extremely large inner (pore) surface area that remarkably expands their ability to react and interact with ions, atoms and molecules in their surrounding environment.[190] Colloidal stability can be improved either by electrostatic or steric stabilization through proper silica surface-functionalization. The stability of the colloidal dispersion is dependent on NP size, surface chemistry and the characteristics of the surrounding media. It is, thus, a sum of a number of simultaneously interacting forces, such as van der Waals (attractive), electrostatic repulsion and steric stability forces, together determining the stability of the particle dispersion.[191] According to the Derjaguin, Landau, Verwey and Overbeek (DLVO) theory, colloidal particles interact only through van der Waals forces and electrostatic forces.[192] Based on this assumption, a stable dispersion is obtained if the energy of the repulsive forces is stronger than that of the attractive forces. Solvent interactions are also present but considered to be of minor importance for the resulting force balance. The electrostatic stability of the particle is most often described by the zeta (ζ) potential, for which a value $-30\ \text{mV} \geq \zeta \geq +30\ \text{mV}$ is typically required to achieve good stability.[193]

Maintaining aqueous dispersion stability is of the utmost importance when synthesizing NPs for different biological applications. The pH and ionic strength of the medium may cause dissociation or ionization of surface groups or adsorption of ionic species onto the charged surface, which affect the stability of the dispersion. Especially at physiological conditions, where electrolyte concentrations are typically high, this sets a challenge for attaining sufficient dispersion stability by electrostatic means.[194,195] Silica surface functionalization with polymers or biomolecules, such as enzymes, proteins or antibodies, also generally requires aqueous conditions. Irreversible particle aggregation during and in between functionalization steps should, hence, be prevented to assure successful surface-modification, and the particles should also be able to withstand degradation both during functionalization in aqueous

media, and finally at physiological conditions. The stability of a particle dispersion is affected by the net surface charge of all functional groups present on the particle surface and on their linking-chemistry at the prevailing conditions, in terms of pH, temperature and electrolyte strength.

3.2 Surface chemistry of silica

The surface of silica NPs is covered by hydroxyl, or silanol (≡Si-OH), and siloxane (≡Si-O-Si≡) groups that directly affect the nature of the silica surface by providing it with varying degrees of hydrophilic or hydrophobic properties. The more silanols present, the higher the hydrophilicity of the surface.[196] As both the PZC and IEP of silica lies in the pH range 1-3, the surface silanols are deprotonated over most of the pH range,[14] providing the silica particle with a net negative surface charge. The protonation and deprotonation of the surface silanols hereby also determine the surface charge and, thus, the colloidal stability of the NPs.

Figure 13 illustrates the different silica species, termed Q^n, found on the NP surface, *n* standing for the number of bridging oxygens present.[197] The silanols have varying acidic strength depending on the number of hydroxyl groups connected to the silicon atom.[106] The most commonly occurring surface silanol species, the Q^3 isolated silanol (≡Si-OH),[198] has a reported pK_a value between 2 and 4.5, while the pK_a value of 8.5 for the first deprotonation step of the Q^2 geminal silanol (=Si-$(OH)_2$) is considerably higher.[199,200] The net negative charge at physiological conditions (pH 7.4) can, thus be ascribed mainly to the deprotonation of Q^3 silanols. On the silica surface, Q^4 siloxane species with oxygen atoms on the surface, can also be found. Furthermore, there is structurally bound water (internal silanols) inside the silica matrix. The silica surface composition can be altered by thermal treatment of the material. Physisorbed water molecules can be removed from the silica surface by heating, the required temperature depending on the structural characteristics of the material. While room temperature may be enough for achieving complete desorption of water from the surface of nonporous

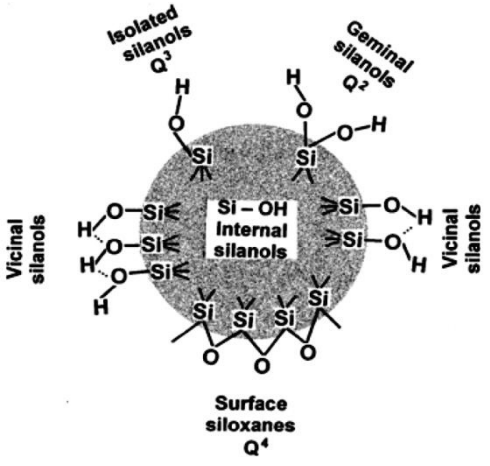

Figure 13. *Types of silanol groups and siloxane bridges on the surface of amorphous silica and internal silanols. Q^4, surface siloxanes; Q^3, single silanols; Q^2, geminal silanols.*[197]

silica, temperatures as high as 473 K might be required for mesoporous silica due to the presence of the nanometer-sized pores.[197] Surface silanols can, however, start condensating already at lower temperatures, in order to liberate additional water. Iler thereby concluded in his monograph,[14] that the only safe way to remove excessive water molecules from the surface of mesoporous silica without altering the surface hydroxyl composition is to dry the material in vacuum at room temperature. Calcination at high temperatures causes further condensation of the silica network, decreasing the number of surface silanols, both on the outer surface and on the pore walls of the material. This leads to a decrease in hydrophilicity and further to improved hydrolytic stability of the NPs. The surface of silica can also be rehydroxylated through acid hydrolysis[201] or by boiling the calcined particles in water.[202] The surface chemistry of silica, thus, directly reflects the thermal history of the material.

3.3 Solubility of silica in aqueous environments

The surface structure and chemistry of intrinsic silica NPs also govern their hydrolytic stability. The solubility of silica is known to be highly pH-dependent,[14,106,203] which is a direct consequence of the acid/base characteristics of the surface silanols. The Q^2 silanols have a lower degree of condensation, and are therefore considered to be more reactive, than the Q^3 silanol species.[204] As a result, the Q^2 silanols also dissolve faster and, hence, play an decisive role in the solubility of silica NPs. Especially the Q^2 silanols located inside the pores are thought to have a significant effect on the interfacial chemistry and degradation of mesoporous silica at, and above, physiological pH, as several studies suggest that the degradation of intrinsic MSNs occurs initially from the inside of the particles, by bulk degradation (*Figure 14*).[205–207] Surface polarity influences the hydrolytic stability as strong hydrogen bonding between surface hydroxyl groups and water molecules can occur in aqueous environments, resulting in rapid diffusion of water into the pores. This causes dissociation of Si-O-Si bonds, which consequently consumes the pore structure.

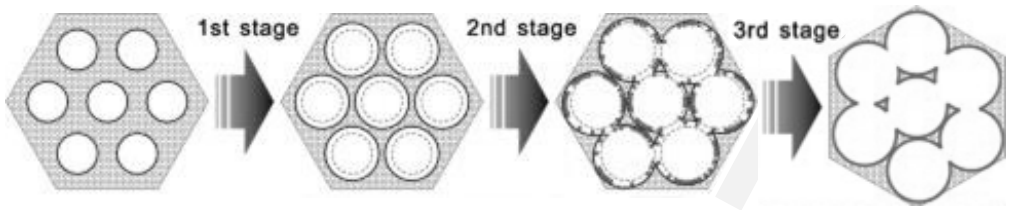

Figure 14. *Schematic illustration of the degradation of hexagonally ordered mesoporous silica from the inside. Modified from He et al. (2010).*[205]

Factors, such as thermal history, surfactant-removal method, particle size and shape, and surface functionalization have also been shown to affect degradation behavior.[206,208–211] Surface-functionalization with organic molecules is often performed in order to increase the hydrophobicity and hydrolytic stability of the particles. However, as the chemical nature and concentration of all surface-bound functional groups contribute to the aqueous behavior of the NPs, different functional groups might either improve or impair the hydrolytic stability of the particles. Amine groups that are commonly either as-synthesized or grafted onto the particle post-synthesis to facilitate subsequent surface-functionalization, have been discovered to boost the degradation rate of silica at neutral and alkaline conditions,[212] as was also observed in **Publication I**. In aqueous environment, proton transfer from hydroxyl groups of the residing surface silanols to the amine groups is promoted. Highly water-soluble intermediate zwitterionic species are thus created on the silica surface,[213] which enhances the hydrolysis of ≡Si-O-Si≡ bonds.[212,214]

Several molecules used for fluorescent labeling of NPs, such as e.g. fluorescein isothiocyanate (FITC), have pK_a values close to the physiological pH 7.4. With a pK_a of 6.9, the FITC molecule occurs primarily in its protonated state at physiological pH and does therefore not notably affect particle charge or stability. Furthermore, since isothiocyanates react to form very strong thiourea bonds with amines, FITC does not react with the surface silanols.[215] The hydrolytic stability of a NP is, however, affected by a number of other, simultaneously active physical and chemical factors that each needs to be taken into account in order to maintain proper hydrolytic stability throughout the complete design and modification process of the nanomaterial.

3.4 Functionalization of the silica surface

The surface properties of MSNs can be considered as their basis of functionality. Therefore, combining the advantages of this porous inorganic material with various functional organic molecules to create multifunctional hybrid inorganic-organic materials is extremely attractive from a materials science point of view. A variety of functional groups, polymers, biomolecules and drugs can be incorporated into the silica matrix, introduced onto the outer surface and/or inner surface (pore walls) of the material, either through covalent attachment, electrostatic adsorption, or by taking advantage of hydrophobic interactions, in order to make the particles suitable for different diagnostic, therapeutic, or combined (theranostic) applications.[216] The linking-chemistry in nature is often based on interactions between amines and carboxylic acids, which makes the introduction of these functional groups onto the silica surface especially interesting.[217,218]

3.4.1 Co-condensation of functional silanes

The easiest way of modifying the silica surface with functional groups is through co-condensation of the silica source with an organosilane precursor. Since its introduction by Burkett *et al.* in 1996, the approach has been used for functionalizing porous silica materials with alkyl,[219,220] mercapto,[220–222] amino,[221,223–225] cyano,[223–225] phenyl,[220] thiol,[220,226] and numerous other functional groups.[227] A small portion of the tetraalkoxysilane [$Si(OR)_4$], used as silica source, is typically substituted with a trialkoxysilane precursor [R'-$Si(OR)_3$], containing the desired functional groups. Because co-condensation can be performed as a one-step synthesis, it typically generates fairly homogeneous surface distributions of functional groups,[228] whose surface density is furthermore quite easy to control by varying the amount of organosilane and the time point (see *Figure 15*), at which it is added.[229] One disadvantage of the procedure is that some of the functional groups might end up embedded inside the silica matrix, instead of on the surface of the material, thus rendering them inaccessible as reactive surface sites. The primary disadvantage of co-condensation is, however, that it usually produces materials with lower mesoscopic order than those produced through post-grafting approaches. High concentrations of alkoxyorganosilane may result in completely disordered pore structures, or induce self-condensation of the alkoxyorgano-silane species at the cost of co-condensation with the silica precursor.[94] Another critical aspect concerning co-condensed materials is that structure-directing agents have to be removed by extraction, since calcination at elevated temperatures would destroy the organic functional moieties.

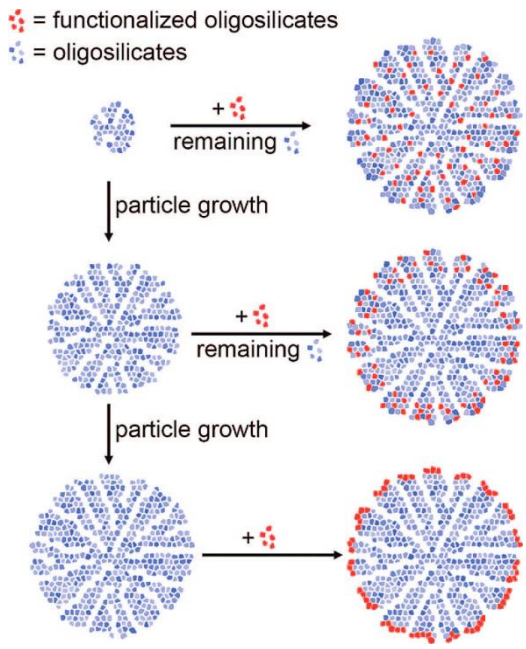

***Figure 15**. Distribution of functional groups depending on addition time of the organosilane in situ.*[229]

3.4.2 Post-synthesis grafting with silanes

High concentrations of various surface functional groups can be grafted onto the silica surface primarily by reacting organosilanes with the free silanol groups on the surface of the material. Although the method rarely affects the

pore structure, the organic molecules can concentrate at the pore openings and, thus, impair the diffusion of molecules into the pores.[230] If the pore diameter of the material is very small or the organic functional groups relatively large the pores may become partially or even completely blocked. Consequently, the surface functional groups will concentrate to the outer surface of the material, leading to an inhomogeneous surface distribution. A more uneven distribution of surface functional groups than in co-condensed materials is common also partly as a consequence of low reactivity of the surface silanols[231] but also due to physisorbed water molecules that are often present on the silica surface and can easily induce self-condensation of the organosilane.[55,232] Completely anhydrous reaction conditions during surface-functionalization are therefore to be preferred. The distribution of functional groups at these conditions depends solely on the accessibility and reactivity of the free surface silanols. The co-condensation and post-grafting approaches are illustrated in *Figure 16*.

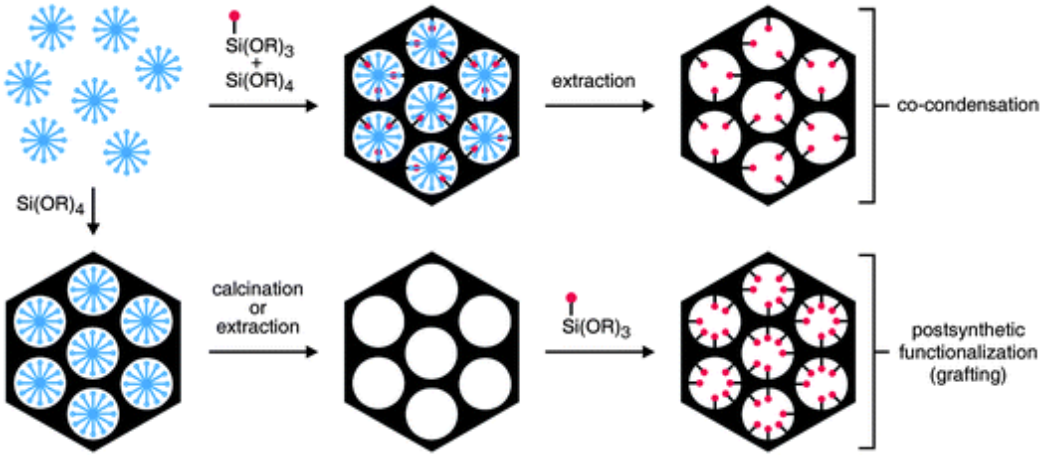

Figure 16. *Schematic illustration of the co-condensation process (above) and post-synthesis grafting (below).*[233]

3.4.3 Surface-grafting with poly(ethylene imine)

Due to its high positive charge density over a wide pH range and thereto related favorable characteristics of deoxyribonucleid acid (DNA) protection, cell binding, cellular uptake and endosomal escape, the polycation poly(ethyleneimine) (PEI) has successful been used as a versatile non-viral vector for gene delivery and transfection.[234,235] In addition, PEI can also be grafted onto the surface of either intrinsic or pre-grafted silica through hyperbranching polymerization of aziridine at acidic conditions (*Figure 17*),[231,236] which allows for a high density of amine groups to be grafted onto the silica surface, and further for the density to be varied by changing the aziridine/silica ratio. The amine groups can serve as effective hooks for facile subsequent

surface-functionalization, and effectively improve the dispersion stability of silica NPs at physiological conditions by providing them with a high positive charge, originating from the protonation of amine groups at these conditions.[193,224] The high positive surface charge provided by PEI promotes NP contact with the negatively charged cell membrane, thus, enhancing the intracellular uptake of silica NPs compared to corresponding unfunctionalized particles.[224,237] Controversially, while a certain high molecular weight PEI is needed for efficient cellular uptake, its use also involves risks concerning toxicity, since too high a density of cationic surface charges may cause physical membrane damage and increased cytotoxicity associated with enhanced intracellular calcium flux.[238,239] PEI has also been reported to promote endosomal escape by destabilizing lysosomal membranes,[240,241] referred to as the "proton sponge effect".[242] This is a most desirable effect, as it can help drugs and nanocarriers escape degradation or exocytosis through the endo-lysosomal pathway and, thus, increase the probability of them reaching their target sites,[243] many of which are situated in the cytosol.[243–245] Although the exact mechanism for this phenomenon still remains unclear, the most generally accepted explanation, though heavily debated,[246,247] relates to the high buffering capacity of polyamines, which is thought to result in an increased lysosomal pH.[242,244,245,248] Another proposed mechanism is that the positively charged polymer branches of PEI may interact with and, hence, disrupt the endosomal membrane.[249] Although reporting no change in lysosomal pH as a result of PEI uptake, Benjaminsen *et al.* recently concluded that due to the high proton binding ability of PEI, an exaggerated proton pump activity and influx of protons, in order to maintain the proton gradient across the lysosomal membrane, is reasonable to expect,[250] implicating that the proton sponge hypothesis may actually be correct. As influx of protons consequently leads to influx of chloride ions to maintain charge neutrality, PEI-functionalized particles may, thereby, cause endosomal escape, but possibly also intracellular toxicity through osmotic swelling and rupture of the lysosomal membrane.[250,251] In order to achieve efficient cellular uptake without evoking toxic responses it is therefore crucial to control both the PEI polymer length and density.[252]

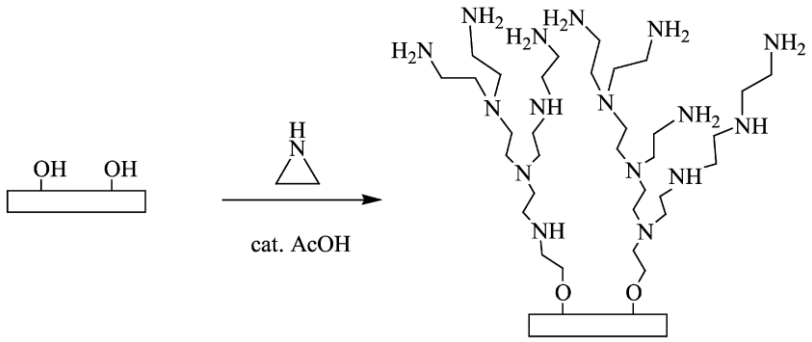

***Figure 17**. Schematic representation of the PEI-functionalization by hyperbranching polymerization of aziridine onto a solid surface.*[231]

3.4.4 Electrostatic adsorption

Electrostatic adsorption relies on the interaction between two oppositely charged substances. A variety of chemical substances, such as ions, drugs, surfactants, polymers and biomolecules can be electrostatically adsorbed onto the silica surface (*Figure 18*).[253,254] Especially different polymers and polymer complexes can be used for improving both the hydrolytic and dispersion stability of NPs by acting as an electrostatic or steric hinder.[210,211] The surface distribution of the polymer depends on the interactions between the particle surface and the polymer itself, but also on the polymer chain-length and solvent interactions. Naturally, the stabilizing effect depends strongly on the degree of polymer coverage on the nanocarrier and the thickness of the polymer layer.[211] While an adequate amount of adsorbed polymer may efficiently stabilize a colloidal dispersion, too high a density of the polymer layer may, conversely, restrain the mobility of the polymer chains and, thus, impair dispersion stability.

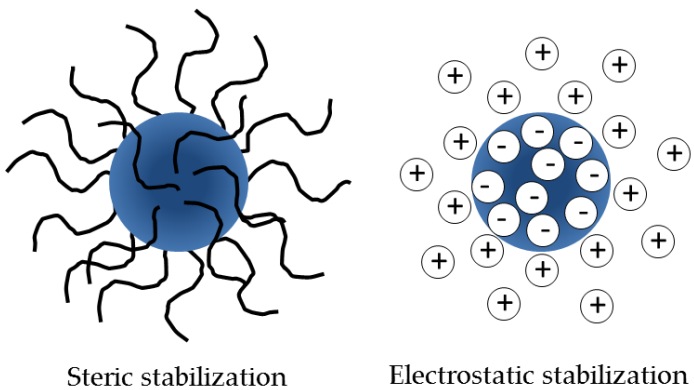

***Figure 18.** NP dispersion stability can be achieved via steric or electrostatic stabilization with polymers.*

Polyethylene glycol (PEG) is a hydrophilic, nonionic polymer, which is non-toxic and non-immunogenic and therefore commonly used for providing steric stabilization to various NPs intended for bioapplications.[255,256] PEG is also known to reduce non-specific adsorption of proteins or opsonins onto the surface of NPs,[47,257] which is important in order for the particles to escape recognition and clearance by cells of the immune system. PEGylation has been shown to, thereby, significantly prolong the circulation time of nanocarriers,[256,258] also observed in **Supporting Publication I**, making them readily suitable for instance as drug carriers for *in vivo* passive targeting of tumors. However, the very presence of PEG may also limit the drug delivery efficiency by preventing interactions between the nanocarrier and the cell surface.[259,260] It should, moreover, be kept in mind that the PEGylation stealth effect depends strongly both on the length and density of the PEG chains as well as on the nature of the proteins that it is interacting with, and that PEGylation merely decreases protein adsorption, not prevents it entirely.

Due to its hydrophilic nature, PEG will eventually detach from the particle in an aqueous environment if not covalently grafted onto the particle surface.[261] A way of circumventing this scenario and simultaneously improving the hydrolytic stability of PEG is to covalently attach it to another polymer with higher hydrolytic stability, thus, creating a co-polymer complex that can subsequently be adsorbed onto the particle surface.[258,262] A good example of where the advantageous characteristics of two polymers have been exploited in combination is the PEI-PEG co-polymer complexes prepared by Sen Karaman *et al.*[262] The PEI part of the polymer, which is faced towards the particle surface, serves the function of providing it with a high positive charge, which is known to both stabilize the particles electrostatically in a physiological environment and promote interaction with and uptake by negatively charged cells. The uncharged PEG-chains, facing into the surrounding liquid, may potentially conceal the high cationic surface charge sufficiently to lower the cytotoxicity of PEI and reduce unspecific protein interactions and recognition by the body's own immune cells by enhancing the steric stability of the NPs, consequently prolonging their circulation time for *in vivo* passive targeting applications.[47,263] Creating such co-polymers with the right PEI/PEG ratio may therefore enable exploitation of several advantageous properties of both polymers, while suppressing their adverse effects, potentially proving very beneficial when modifying the surface of NPs intended for biological applications (**Publication IV & Supporting Publication V**).

4 Organic nanoparticles

Organic nanoparticles (ONPs) can be characterized as solid particles composed of organic compounds, typically lipids or polymers, in the size range 10-1000 nm in diameter.[264] A range of different ONPs (*Figure 19*), including micelles, liposomes, dendrimers, lipid and polymeric NPs, and nanogels,[265–267] find applications in a wide spectrum of industrial areas such as electronics, photonics, sensing, medicine and biotechnology.[268] Although these types of NPs have gained much less attention than inorganic NPs, they have been intensively studied over the past two decades, especially as carriers of poorly water-soluble drugs and compounds for biomedical applications.[2,269] The most common preparation methods are either emulsification-based[270] or involves precipitation of organic compounds in solution, the latter including nanoprecipitation, self-assembly and nanogelation.[271] However, newer approaches, such as spray-drying[272], super-critical fluid[273] and piezoelectrical[274] technologies also exist.

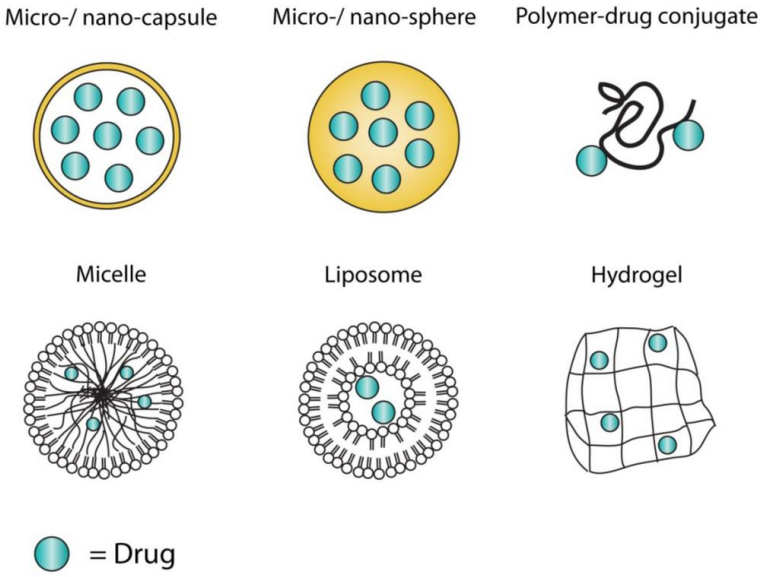

Figure 19. *Organic nanoparticle-based drug formulations.*[275]

Among the vast range of ONPs, biodegradable polymeric NPs have due to their flexible manufacturing and modification regimes and their potential to entrap a wide range of therapeutic agents shown great promise in the treatment of a wide range of diseases, including various cancers and central nervous system disorders,[269] cardiovascular diseases, viral infections and pulmonary and urinary tract infections. Their composition and structures, in terms of size, shape, internal morphology and surface properties, can readily be tuned to fit different purposes (see *Figure 20*). Particularly the hydrophilic polymer PEG is

often covalently conjugated to the surface of polymeric NPs in order to reduce immunogenicity and clearance by the cells of the reticuloendothelial system (RES), thus, prolonging blood circulation times, leading to improved therapeutic efficiency.[276] Polymeric particles can be either nanocapsules, i.e. (drug) reservoirs with a polymeric shell, or nanospheres, i.e. homogeneous polymeric matrices with encapsulated drug, made up of natural or synthetic polymers, or combinations of these.[275] Especially nanospheres exhibit excellent sustained release characteristics.[277] Through effective surface-functionalization, these NPs can furthermore be modified for targeted delivery, stimuli-responsive activation and efficient permeation over biological barriers,[82] making them especially useful for treatment of various cancers. Most polymeric NPs are biodegradable and biocompatible, which naturally is a prerequisite for any material intended for biomedical applications.[269] Existing drug delivery formulations employing biodegradable polymers include, among others, PLA,[78] PLGA,[79,278] PACA,[271,279,280] gelatin[281,282] and chitosan[283–286] NPs. In fact, PLA and PLGA NPs formulated to carry various low molecular weight compounds have also, by the FDA, been approved for clinical use.[287]

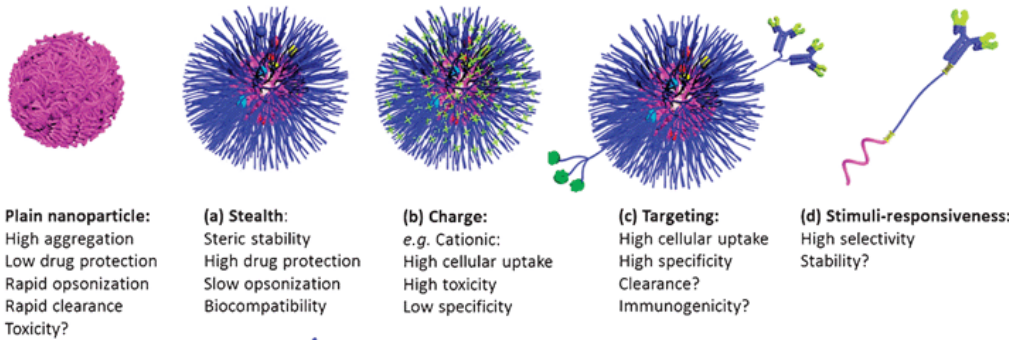

Figure 20. *Surface properties of polymeric NPs: (a) stealth: imparts biocompatibility, steric stability and drug protection, reduces opsonization and clearance by cells of the RES, may also reduce cellular uptake and endosomal escape, (b) charge: cationic charge enhances cellular uptake and endosomal escape, but is associated with uncontrolled tissue distribution and toxicity, (c) targeting: enhances specific cellular uptake, but may also accelerate clearance and/or immunogenicity, (d) stimuli-responsiveness: controls cargo release dynamics of NPs at specific sites. Modified from Elsabahy and Wooley (2012).*[82]

4.1 Poly(alkylcyanoacrylate) nanoparticles

Alkylcyanoacrylate polymers are well known for their excellent adhesive properties, which have been exploited in both the commercially available Superglue for the repair of everyday items, and surgical glues for repair and closure of skin and surgical wounds.[288–291] During the past three decades, alkylcyanoacrylates have also broken ground in the field of nanomedicine as PACA-based biocompatible and biodegradable NPs, first introduced in 1979 by Couvreur *et al.*,[292] have been developed as colloidal drug carriers for the treatment of various cancers and viral, bacteriologic and parasite infections as well as for metabolic an autoimmune diseases.[293–297] The easy and convenient *in situ* polymerization of PACA NPs by various emulsification techniques,[298] allows for simultaneous incorporation of a wide range of drugs, fluorescent dyes and contrast agents for magnetic resonance imaging (MRI) or positron emission tomography (PET).[299,300] The NP surface is often PEGylated in order to impart stealth properties to the nanocarrier, thus, achieving better dispersion stability and longer blood circulation times for passive targeting to tumors by the enhanced permeability and retention (EPR) effect,[301] although various ligands can furthermore be conjugated to the NP surface in order to achieve selective, targeted delivery.[82] PACA NPs have more recently also gained increasing attention as potential drug carriers over the BBB, which sets perhaps the biggest challenge in drug delivery by effectively limiting drug penetration into the brain.[295,302,22] For instance, ultrasound treatment in combination with microbubbles (MBs) has been explored as a means of improving PACA NP-mediated drug delivery, both to different tumors and over the BBB.[303,304]

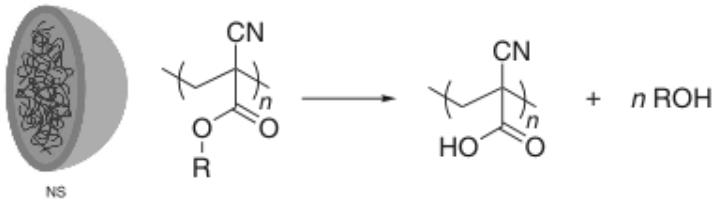

Figure 21. *Schematic representation of a polymeric nanosphere and the primary degradation mechanism of PACA by hydrolysis of alkyl side chain ester functions. Modified from Nicolas and Couvreur (2009).*[305]

As for all drug carriers the degradation, excretion and toxicity of PACA NPs and their degradation by-products are crucial aspects for their applicability in biomedicine. The main degradation mechanism of PACA NPs involves hydrolysis of their side chain ester,[297] into the corresponding alkyl alcohol and poly(cyanoacrylic acid) (*Figure 21*), both of which can potentially be harmful to cells.[306] The latter is, however, completely water-soluble and can be excreted by renal filtration.[305] The biodegradation process can in biological fluids be catalyzed by esterases from serum, lysosomes, or pancreatic fluid.[307,308] Other mechanisms have also been proposed, but are thought to be less significant in biological conditions. The typically very fast degradation of PACA NPs is strongly dependent on the alkyl side chain length of the monomer (**Publication II**). Shorter alkyl chains are associated with faster hydrolysis, but also higher toxicity due to resulting high concentrations of degradation by-products.[309,310] Since drug release from polymeric NPs occurs mainly in connection to the biodegradation of the carrier (**Publication II**) or by diffusion out of the carrier,[311] careful tuning of the NP monomer composition could both potentially minimize toxic responses, and offer control over drug release kinetics, through manipulation of the biodegradation rate. Although showing great promise as nanomedicines for cancer therapy, PACA NPs have, due to remaining concerns regarding their safety and efficiency, not yet been authorized for clinical use. Some PACA-based drug formulations have, however, reached Phase II and III clinical trials.[282,312]

5 Nanoparticles in pharmaceutical technology

One of the fundamental aspects of pharmaceutical technology and drug development is proper drug delivery and distribution within the patient's body.[313] This poses a challenge, especially for the effective and safe administration of highly toxic and poorly water-soluble compounds, such as many cytostatic drugs intended for cancer treatment, using conventional drug formulations. Pharmaceutical technology has hence, during the past three decades, experienced an upsurge, as a wide range of new NP-based DDSs with controllable properties have been designed with the intent of overcoming this obstacle by entrapping various drugs within the matrix of the nanocarrier. An ideal DDS, which should also be stable under various physiological conditions, would thereby increase the bioavailability and safety of the drug by providing control over the rate, time and place of drug release, in a reproducible manner.[314,315] In practice, this requires proper administration and transport across biological membranes to the desired site of action, while avoiding premature release or interaction with non-diseased tissue, which could lead to harmful side effects.

Among the countless varieties of NPs designed for pharmaceutical use, amorphous mesoporous silica-based NPs have emerged as especially promising candidates for the use as multifunctional DDSs. Their unique properties, such as large surface area and pore volume and flexible functional regimes allowing control over size, morphology and surface functionality, along with biocompatibility and biodegradability make them highly suitable for combined diagnostic and therapeutic approaches, as so called theranostic agents.[316] MSNs with fluorescent molecules and nanosized particles for optical imaging,[70,317–319] radionuclides for PET,[320,321] and various contrast agents, such as metal oxide NPs and quantum dots, for MRI[49,59,322,323] have been synthesized for diagnostic actions. Furthermore, silica NPs have successfully been loaded and conjugated with various drugs, proteins, peptides, vaccines and antigens, and their outer surface has been decorated with various ligands to achieve targeted therapies[19,324–327] Some recent efforts to create MSN-based theranostics include MSNs conjugated with lanthanide ions, such as europium or gadolinium that have recently been explored for *in* vitro and *in vivo* targeted delivery of the anti-cancer drug camptothecin (CPT) to cancer cells, during simultaneous monitoring of the course of events by MRI and fluorescence imaging.[328] MSN-encapsulated carbon and silicon nanocrystals, conjugated with hyaluronic acid and PEGylated phospoholipids have also been studied *in vitro* in combination with luminescence imaging for combined imaging and targeting of breast cancer.[90] Furthermore, Chen *et al.* presented a hollow MSN-based theranostic DDS that showed promising results both *in vitro* in human umbilical vein

endothelial cells (HUVEC) and human breast cancer cells as well as *in vivo* in the treatment of breast cancer upon IV injection.[329]

Also polymeric NPs have due to their biocompatibility and flexibility in terms of surface functionalization for targeted actions and high loading capacity for various diagnostic and therapeutic molecules shown great promise for theranostic applications.[330] PACA nanocarriers that have previously demonstrated successful drug delivery both to solid tumors and over the BBB,[22] have more recently also emerged as potential theranostic agents when used in conjunction with hard-shell MBs, MRI and molecular ultrasound (US) imaging.[299,300] For example, Fokong *et al.* recently demonstrated successful combined targeting and US imaging of PBCA MBs *in vitro* on HUVEC and *in vivo* in human ovarian carcinoma bearing mice.[331] Similarly, Fokong *et al.* also demonstrated the efficient US-mediated delivery of both hydrophilic and hydrophobic model drugs *in vitro*, and *in vivo* in tumor-bearing mice with the help of PBCA MBs.[332] The future of both MSN- and PACA-based cancer theranostics most certainly looks bright, both in the light of already achieved results and due to the multitude of diagnostic molecules and techniques, therapeutic compounds, targeting strategies and administration routes available that offer endless new possibilities for multimodal and personalized medical treatment. However, additional *in vivo* investigation to ensure the safety and efficacy of these DDSs will be required in order for them to achieve real clinical applicability.

5.1 Incorporation of hydrophobic drug

Due to their high surface area and pore volume, MSNs are capable of carrying large payloads of therapeutic molecules, mainly inside the pore structure, but also conjugated to the outer surface of the particle.[333] Some therapeutic molecules, such as e.g. antibodies that are conjugated to the outer surface of the particle may serve dual purposes, also acting as targeting ligands. The incorporation of drug to MSNs typically occurs as a post-synthetic procedure, either by adsorption or through covalent conjugation.[334–336] These procedures differ significantly from the drug incorporation into e.g. polymeric (PACA) NPs, in which the drug is generally incorporated during the emulsification synthesis of the NPs.[303] Though this approach is generally very successful for a variety of drugs and results in homogeneous drug dispersion within the polymeric structure, it should be kept in mind that alkylcyanoacrylates are highly reactive compounds and may react with any substances containing nucleophilic groups. On one hand, this can be exploited to promote association between the drug molecules and the NPs by covalent binding. On the other, it may also compromise drug activity or NP formation.[337] The method

furthermore offers poor control over the amount of drug being incorporated and typically allows incorporation of much smaller drug amounts than those, which can be incorporated by adsorption to mesoporous silica.[102,338–341] Incorporation of therapeutic molecules into nanocarriers allow for drugs with poor hydrolytic stability and low aqueous solubility to be efficiently delivered to their target organs. Furthermore, the matrix of the NP may protect various drugs or biomolecules from enzymatic degradation.

The extent of drug adsorption to any NP is dependent on interactions between the adsorbent (carrier) and adsorbate (drug) as well as their interactions with the solvent. Hence the solvent can be chosen based on the chemical properties of the drug as to promote drug-adsorbent over drug-solvent interactions.[337] Since the silica matrix is unaffected in organic solvents, adsorption of hydrophobic drugs from various organic solvents is very convenient. Adsorption from organic solvents mainly relies on hydrogen bonding and interactions between polar groups on the drug molecule and the carrier. For silica NPs, the surface silanol groups typically serve as anchoring points for the drug. Functionalization of the silica surface can further be performed to enhance the affinity between drug and carrier. One such example is the functionalization of silica with amino groups in order to promote adsorption of carboxylic acids.[342–344] By performing the drug loading in organic media, repulsive forces between drug and nanocarrier that might occur in aqueous media due to electrostatic interactions, pH-dependencies and hydrophobicity of the drug, can be avoided. Conversely, in the case of hydrophilic drugs, the exact same interactions can be used for fine-tuning the drug adsorption extent in hydrophilic media.[344,345]

5.2 Drug release

The release of drug from silica NPs is dependent on both carrier and drug characteristics. The degradation behavior of the nanocarrier is linked to its pore size, morphology and surface chemistry. These factors, along with the drug loading degree, affect the surface wettability of the nanocarrier, i.e. the ability of the solvent to wet the surface of the carrier.[346] Dissolution and subsequent diffusion of the drug from the carrier or erosion of the carrier matrix due to wetting of inner and outer surfaces may thereby cause drug release.[208,347] Naturally, solvent properties such as pH, temperature, polarity, electrolyte concentration, enzyme or protein content may also affect the carrier degradation and drug release behavior (**Publication I**). For polymeric NPs, such as PACA, the release of hydrophobic cargo (dye/drug) is in addition to hydrophobic and electrostatic interactions between the cargo molecules and NPs (**Supporting Publication II)**, strongly connected to the degradation of the

polymer matrix,[348,349] which causes liberation of the encapsulated drug molecules, as furthermore investigated in **Publication II**. There are also cases, in which direct contact between the PACA nanocarrier and biological membranes has been shown to cause release of the hydrophobic content into the cells by diffusion through the plasma membrane.[311] The physical state (crystalline or amorphous) of the drug also affects its solubility and, hence, its release, amorphous drug forms having higher solubility than crystalline ones. It has been shown that several drugs can be maintained in their amorphous form when confined within the mesopores of NPs, thus, improving the solubility and release of an otherwise poorly soluble crystalline drug form.[350–352] To avoid premature release, the drug can be covalently attached to functional groups on the inner pore walls.[229,353,354] Depending on the physicochemical properties of the drug as well as the carrier, confining the drug molecules inside the porous matrix of the nanocarrier may allow delayed or sustained release of the drug.[355] A delayed release profile can be of crucial importance in providing a substantial amount of circulation time for the carrier to reach the target organ. Controlled or sustained release, on the other hand, can provide a slow, continuous release profile in order to maintain the plasma drug concentration within a certain therapeutic window (see *Figure 22*). The release profile can furthermore be adjusted by employing various capping molecules and release-on-demand systems to the NP that rely on external stimuli to trigger the release of drug.[356–358]

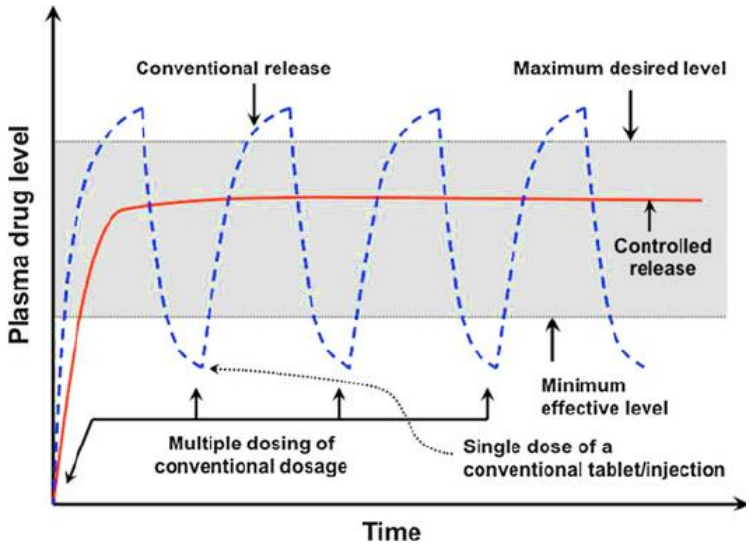

Figure 22. *Drug levels in the plasma released from a traditional release system, i.e. multiple oral capsules or injections (blue dashed curve), and a controlled release system (red continuous curve).*[359]

5.3 Targeted drug delivery

Drug targeting can be achieved by either passive or active actions (*Figure 23*). Passive targeting takes advantage of physicochemical factors, mainly size and surface charge, of particulate carrier systems in order to promote uptake by cells of the RES, also called the mononuclear phagocyte system (MPS).[266] Another targeting strategy involves exploiting the EPR effect for the uptake of materials within a certain size range. By contrast, active targeting requires establishment of a specific connection between targeting molecules on the surface of the NP and receptors or ligands on the cell membrane to induce cellular uptake. Such targeting strategies include conjugation of the particle surface with e.g. antibodies,[19] also presented in **Supporting Publication IV**, peptides,[360] sugars[361] or folate[325] (**Supporting Publication VII**). Passive and active drug targeting of nanocarriers to tumors may reduce toxic side effects, increase therapeutic efficacy and improve the bioavailability of poorly soluble or stable drugs. In this thesis, we have not aimed at active targeting, but instead investigated various passive targeting strategies to achieve efficient intracellular NP uptake.

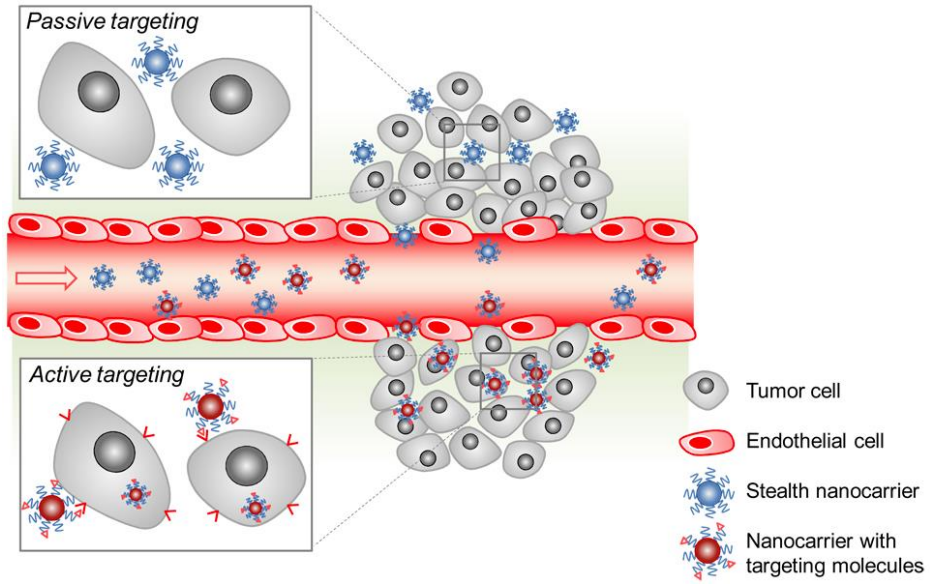

Figure 23. *Schematic representation of passive and active tumor targeting with nanocarriers. Both types of nanocarriers reach tumors selectively through the leaky vasculature surrounding the tumors. Stealth nanocarriers can be taken up unspecifically by the cells, whereas the nanocarriers with targeting molecules can bind to the target cells and enter them via specific receptor–mediated interactions.*[362]

5.3.1 Passive targeting

Passive targeting occurs when the physicochemical characteristics of a NP induce cellular uptake or accumulation in cells and tissue (e.g. tumors). The two main parameters that determine the pharmacokinetics and biodistribution of NPs are size and surface charge, which are, thus, the main characteristics responsible for passive targeting and intracellular uptake of NPs.[363,364] Foreign materials, such as various NPs that are introduced intravenously to the body are typically rapidly recognized and cleared by the body's own immune system, the RES. The RES is the body's first line of defense against pathogens and consists of different phagocytic cells.[365] The efficient uptake of material by phagocytic cells, mainly macrophages and neutrophils, abundantly present in the spleen, liver, lungs and bone marrow can also be exploited to achieve passive targeting of drugs to treat cancer localized in these organs.[366] Non-phagocytic cells do typically not efficiently internalize particles larger than 500 nm.[367,368] Thus, NPs can be designed for uptake by phagocytic cells by tuning the particle size.

The uptake and fast clearance of NPs by the RES from the blood circulation is, however, not desirable when aiming for treatment of other organs or tissues. Recognition of foreign materials by the RES is typically preceded by a process called opsonization, which involves binding of plasma proteins and glycoproteins to the surface of the material in order to facilitate recognition by the phagocytic cells. For instance, hydrophobic particles have been found to efficiently bind plasma proteins and as a result be rapidly cleared from the circulation.[365,369] With the help of surface engineering, NPs can be made unrecognizable to the cells of the immune system, leading to longer blood circulation times and consequently better ability to reach the target site.[363] The ability to avoid opsonization and clearance by the RES is commonly referred to as 'stealth' effect, and is in general achieved by coating the surface of the NPs with a hydrophilic polymer, such as the nonionic polymer PEG,[370–372] either by electrostatic adsorption or covalent conjugation to the NP surface or by incorporation of PEG into the polymeric backbone of the NP.[256,373] Passive targeting for cancer treatment can be achieved with long-circulating PEGylated NPs that accumulate in some tumors as a result of fenestrations in the tumor capillaries and lack of functional lymphatics, which causes retention of the NPs in the tumor tissue.[374] This so called EPR effect serves as a possibility for particles or molecules of a certain size to enter into the cancerous tissue due to the leaky and defective tumor vasculature that develop as a result of rapid vascularization in fast-growing tumors.[375,376] Since smaller particles permeate more easily over biological barriers, drug-containing NPs tuned to the right size can be used for passive targeting of cancerous tissue.

Although charged NPs typically have short circulation times due to adsorption of plasma proteins, which leads to fast recognition and removal by the RES,[377] passive targeting with NPs carrying a high positive charge, such as PEI-grafted NPs, may also be an efficient way of inducing intracellular uptake by promoting non-specific binding with the typically negatively charged cell membrane.[378] Furthermore the high positive charge of PEI helps maintain good dispersion stability also at physiological conditions by electrostatic stabilization of the particles. PEI has furthermore been proposed to exhibit a unique proton-sponge or endosomal buffering effect, arising from protonation of the tertiary amines in the interior of PEI at acidic endosomal pH, causing destabilization of the endosomal membrane, and subsequent endosomal escape.[244,379] The basis of this hypothesis has been more thoroughly discussed in chapter 3.4.3.

5.4 Intracellular uptake of nanoparticles

Cells possess a variety of mechanisms for transferring materia across the plasma membrane. Ions and small molecules use both passive and active transport routes, while larger macromolecules and particulate systems rely on endocytosis and exocytosis to traverse the cell membrane (see *Figure 24*).[380–382] The most well-described routes of endocytosis are the clathrin-mediated route, which typically requires recognition of some ligand by a specific receptor,[59] and the non-specific caveolin-mediated route.[383] The clathrin-mediated route has, however, also been suggested to take part in endocytosis through unspecific binding.[384,385] The rate and pathway of NP uptake depends strongly on cell type and on the size, shape, charge and surface chemistry of the NP that can naturally be manipulated in order to promote receptor-specific intracellular uptake.[386,387] Particles ≤200 nm in diameter, are typically more efficiently taken up through the clathrin- and caveolin-mediated routes.[252] Caveolin-mediated uptake has, however, also been reported for NPs as large as 500 nm.[367] Larger particles and complexes (>500 nm) are taken up by phagocytosis performed by macrophages and neutrophils.[59] The endocytic process is moreover affected by the temperature, pH and energy of the system as well as the time of exposure to the external stimulus.[388]

Receptor-mediated endocytosis is initiated by ligand-receptor binding on the extracellular side of the cell membrane. The binding gives off a chemical signal to the cellular machinery, which causes invagination of the particle and receptor-ligand complex inside clathrin-coated vesicles that are internalized by the cell by budding off from the plasma membrane.[389,390] Caveolin-coated vehicles form in a similar fashion as a result of unspecific binding of ligands or other constituents to the plasma membrane. Inside the cell the clathrin- or caveolin-coated vesicle is fused with the endosome, which functions as a

sorting compartment and can either recycle the material back to the cell membrane or transfer it to the lysosomes, where material is broken down by different hydrolytic enzymes.[59,391,392] Caveolin-coated vehicles may also be delivered directly to the endoplasmic reticulum or Golgi apparatus, thus, escaping degradation by lysosomes.[393] Achieving endosomal escape is of crucial importance for many NPs intended for drug delivery, as a large number of drug targets are located within the cytoplasm. The ability of drug carriers to release their cargo into the cytoplasm, either by transfer of the active substance over the endosomal membrane or by escaping the endosome and subsequently releasing their cargo into the cytosol, is hence a decisive parameter in achieving efficient intracellular drug delivery.[394] NPs that absorb protons in the acidic endosomal environment have been found to disrupt the endosomal membrane by causing swelling and an increase in osmotic pressure, thus, enabling endosomal escape.[395]

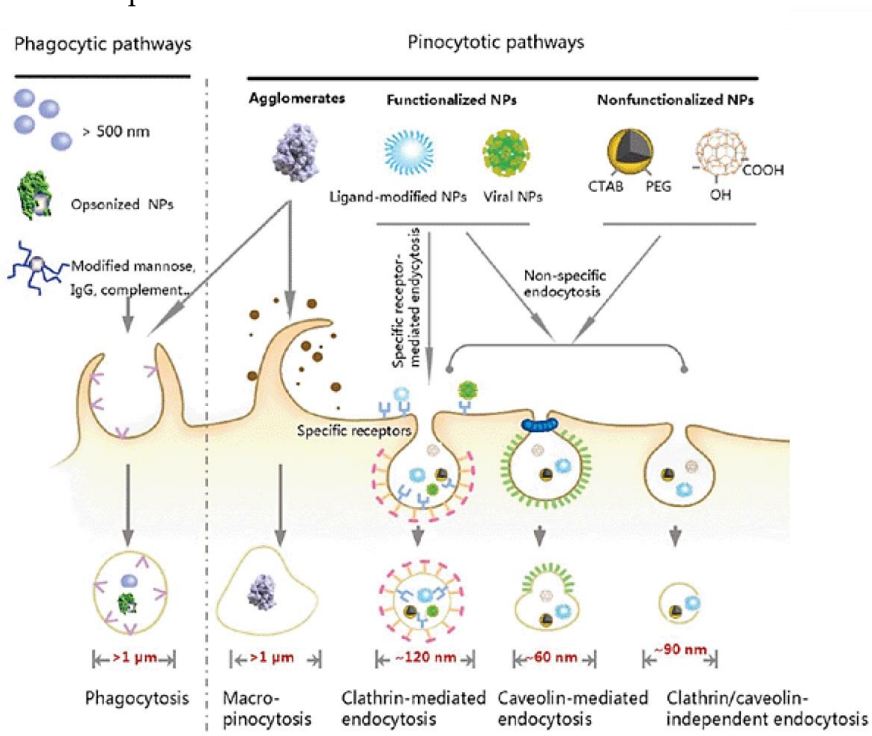

Figure 24. *The cellular uptake of particles is determined by the natural size rules and gatekeepers within the cell. Phagocytes can take up large particles or NP aggregates, opsonized NPs, or particles with certain ligand modification. Active particle uptake by a non-phagocytic cell occurs mainly through pinocytosis. Particles with different surface modifications, may be taken up either by specific (receptor-mediated) or nonspecific routes. The heterogeneity of particle dispersions and surfaces always cause uptake through multiple pathways. Modified from Zhu et al. 2013.*[252]

AIMS OF THE STUDY

The aim of the present study is the rational and stepwise design and development of multifunctional NP-based delivery systems for cancer theranostics. The degradation and hydrophobic cargo release behavior of inorganic MSNs will be studied *in vitro*, in order to enable future control and prediction over these parameters, to understand their interdependency and pinpoint the mechanism of intracellular drug release. The same parameters will also be studied for an organic delivery system, based on biodegradable PACA NPs, in order to elucidate the relationship between NP monomer composition and biodegradation rate as well as intracellular biodegradation behavior and cargo release. Finally, a core-shell composite NP, comprising a photoluminescent ND core coated with mesoporous silica, will be developed to achieve combined long-term biomedical imaging and tracking, as well as therapeutic actions. By employing a ND core, we aim for superior diagnostic properties over conventional fluorescently labeled NPs, in terms of fluorescence intensity and stability. Efficient cargo delivery and release is aimed for by taking advantage of the flexible functionalization regimes of MSNs in terms of cargo loading and surface modification.

The specific aims of this thesis are to:

- pinpoint the interdependency of the degradation and cargo release behavior for both an inorganic and organic NP-based delivery system
- develop a novel core-shell composite NP comprising diagnostic and therapeutic functions
- verify the applicability of the delivery systems in terms of intracellular delivery and cargo release, imaging and tracking

CHARACTERIZATION METHODS

A wide set of characterization techniques is typically needed in order to define the properties and phenomena exhibited by NPs intended for biomedical applications. *Table 1* presents a summary of the techniques used in this thesis and the properties or phenomena they have been used for elucidating. In the following section, these techniques will be discussed to the extent required for understanding the results that will be presented.

Table 1. *Summary of characterization techniques used for studying different properties and phenomena in the presented publications.*

Characterization method	Studied properties/events	Publication No
Dynamic light scattering	Particle size	I-IV
Electrokinetic measurement	Net surface charge (zeta potential)	I-IV
Small-angle x-ray scattering	Pore structure	I, III-IV
Nitrogen physisorption	Surface area, pore size and pore volume	I
UV-vis spectrophotometry	Silica dissolution	I, III
	Cargo loading/release	I, III-IV
Thermogravimetric analysis	ND/silica mass ratio	III
	Cargo loading, surface functionalization	I
Scanning electron microscopy	Particle morphology	I, III
Transmission electron microscopy	Particle and pore morphology	I, III-IV
	Intracellular NP uptake and trafficking	IV
Flow cytometry	Intracellular uptake	II, IV
Confocal laser scanning microscopy	Intracellular uptake and localization	I-II, IV
	Internalization pathways	II
Fluorescence recovery after photobleaching	Intracellular cargo release	I
Fluorescence lifetime imaging microscopy	Intracellular localization and NP degradation	II
Förster resonance energy transfer	Intracellular NP degradation	II
Stimulated emission depletion	ND imaging and intracellular tracking	IV

1 Dynamic light scattering[396–398]

Dynamic Light Scattering (DLS) is commonly used to measure the hydrodynamic size of particles in a suspension. The technique is based on measuring the spontaneous random diffusion of particles within a liquid, i.e. the Brownian motion that arises due to bombardment of particles by the surrounding solvent molecules. By using the patented technique called Non-Invasive Back-Scatter (NIBS), where the scattered light is collected at a 173° angle relative to the light source, typically a laser beam, better sensitivity can be achieved and samples containing large particles and higher concentrations of particles can be measured.[396]

When hit by a light source, particles scatter light in all directions. The constant random movement of the particles, which is dependent on their size, causes intensity fluctuations in the scattered light. Smaller particles move faster than larger ones, thus also resulting in larger intensity fluctuations. As the intensity fluctuates randomly with time, the scattered light causes either constructive or destructive interference, which is detected and registered as a continuously changing interference pattern. A number of different algorithms are then used for translating the pattern into a correlation function, based on which both the size and size distribution of the particles can be determined. As the size of the spherical colloidal particles is related to their translational diffusion coefficient, D, their hydrodynamic radius, r, may be calculated using the Stokes-Einstein relationship,

$$D = \frac{k_B T}{3\pi\eta r} \qquad \textbf{(Eq. 1)}$$

where k_B is the Boltzmann's constant, T the absolute temperature, and η the viscosity of the solvent.[399]

The resulting particle size is typically displayed as the *Z* or *Z-average*, also called *Intensity PSD* (Particle Size Distribution), because it is the mean particle size calculated based on the intensity of the sample. For the *Z-average* a polydispersity index (PdI) is given, which describes the width of the size distribution. The *Z-average* value is best used if the particles are spherical and the sample monomodal and monodisperse. A sample with a PdI below 0.5 can be considered suitable for comparative analysis. A PdI over 0.5 indicates a fairly polydisperse sample, in which case a distribution analysis is preferred. In the case of polymodal samples, the size distribution can also be displayed as either *Volume PSD* or *Number PSD*, which are calculated based on the mean particle volume or number, respectively (*Figure 25*).

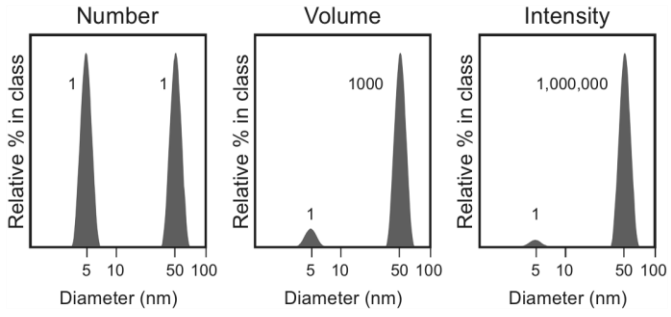

Figure 25. *The size distribution of a sample, containing only two sizes of particles in equal numbers, shown as number, volume and intensity distributions.*[396]

2 Electrokinetic measurement of zeta potential[400,401]

When particles are dispersed in a liquid, they obtain an electrical charge as a result of ionization of surface functional groups or adsorption of ions onto the particle surface. This gives rise to electrostatic forces that are either attractive or repulsive and that affect the electrophoretic mobility of the particles in a medium. The charged particles attract counterions, i.e. ions of opposite charge, in such a way that an inner layer with a higher concentration and more strongly bound counterions is formed close to the particle, while an outer layer of more loosely associated ions is formed further away from the particle surface (*Figure 26*).[402] The inner Stern layer and the outer diffuse layer together form the electrical double layer. When the particle moves within a liquid due to gravity or an applied voltage, counterions up until a certain distance from the particle move along with the particle. Ions at a farther distance do not move with the particle. This theoretical boundary, beyond which the ions do not follow the movements of the particle, exists within the diffuse layer and is called the surface of hydrodynamic shear or the slipping plane. The electric potential that exists at the slipping plane is called the zeta (ζ) potential. The zeta potential can thus be defined as the double layer potential close to the slipping plane, at the interface between the surrounding medium that is attached to the particle and the dispersion medium. It is, however, noteworthy that the exact location of the zeta potential cannot be specified.[398]

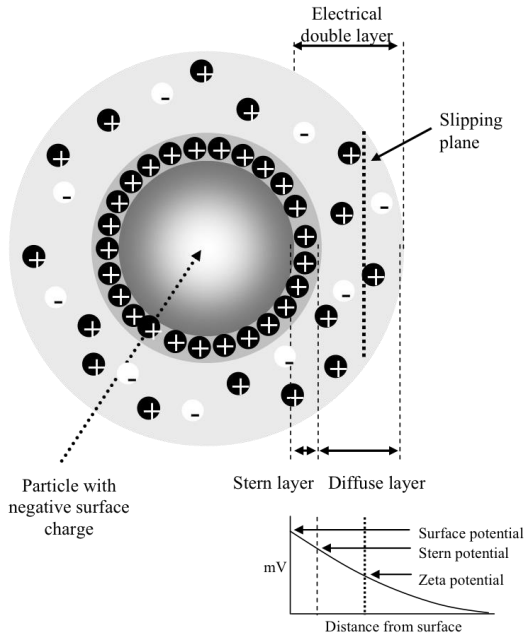

Figure 26. *Schematic representation of the electrical double layer and zeta potential.*[402]

The electrophoretic mobility of the particles can be obtained by performing an electrophoresis measurement using laser Doppler velocimetry (LDV). When an electric field is applied across a sample in dispersion, placed in a sampling cell equipped with electrodes, it induces the charged particles to move towards the oppositely charged electrode. The velocity of the particles depends on the strength and direction of the electric field, the dielectric constant and viscosity of the medium and on the zeta potential. By measuring the electrophoretic mobility, the zeta potential can be determined using the Henry equation:

$$U_E = \frac{2\varepsilon f(\kappa a)\zeta}{3\eta} \qquad \textbf{(Eq. 2)}$$

where U_E is the electrophoretic mobility, ε the dielectric constant of the medium, $f(\kappa a)$ Henry's function, ζ the zeta potential and η the viscosity of the medium. Two values are generally used for Henry's function. For aqueous solutions, the value 1.5, referred to as the Smoluchowski approximation, is used and for non-polar solvents, the value 1.0, also known as the Hückel approximation, is used.

The zeta potential value is of crucial importance considering the dispersion stability. A colloidal dispersion is considered electrostatically stable if it has a large negative or positive zeta potential value, $\zeta \leq$ -30 mV or $\zeta \geq$ 30 mV, which creates sufficient repulsion between the particles to keep them from flocculating. Since pH greatly affects the surface charge and thereby also the stability of the dispersion, a zeta potential value without the accompanying pH is virtually meaningless. The pH of the medium should therefore always be noted. The pH-dependence can also be exploited for determination of the IEP of the dispersion through electrokinetic titration. The IEP is the pH value at which the net effective charge (ζ) of the particle is zero and, thus, where the colloidal dispersion is least stable. In addition to the pH value, the electrolyte concentration should furthermore be stated, since added electrolytes screen the surface charges and thus distort the absolute zeta potential value.

3 Small-angle X-ray scattering

X-ray diffraction (XRD) is a powerful nondestructive and widely used technique for studying the porosity and periodic atomic arrangement of materials. With Small-angle X-ray Scattering (SAXS) it is possible to determine both microscale or nanoscale structural characteristics, such as the atomic position, bond lengths and bond angles of molecules in a lattice, of various well-ordered particulate systems. Hence, SAXS can serve as a useful tool for

studying the structural characteristics of inorganic mesoporous materials, such as silica NPs.

The technique involves bombarding a sample with a monochromatic X-ray beam and then recording the elastic scattering of electrons at very low angles, between 0.1° and 10°. The measurement is performed in vacuum to minimize interference effects caused by air. The scattering, which is caused by the electron clouds of the atoms in the irradiated sample, creates a scattering pattern, which describes the intensity of the scattered x-rays measured as a function of scattering angle, and is dependent on the electron density in the sample. This means that in the absence of adsorption effects the intensity of the scattered electrons is directly proportional to the electron density differences in the system. The scattering pattern provides information about the size and shape, size distribution and surface-to-volume ratio of the studied material.

The position of diffraction peaks in a pattern is determined by the unit cell of the crystal, whereas the peak intensity is a function of the positions of the atoms in the crystal. Depending on the structure of the sample the scattered waves can thus give rise to either constructive or destructive interference.[403] Heterogeneities in the material's structure causes the scattered waves to interfere destructively, canceling each other out. Contradictory, well-ordered materials, where the atoms are periodically arranged in lattices, cause constructive interference, which gives rise to a diffraction pattern. Diffraction thus occurs when the wavelength of the constructively interfering waves is of the same order of magnitude as the repeat distance, i.e. the phase shift 2θ, between the scattering centers within a crystal. The diffraction then follows Bragg's law,[404]

$$n\lambda = 2d_{hkl}\sin\theta \qquad \textbf{(Eq. 3)}$$

where n describes the integer number of wavelengths, i.e. the order of diffraction, λ is the wavelength of the x-ray beam, d_{hkl} the repeating distance between the lattice planes and θ the scattering angle. Bragg's law hereby relates the distance (d_{hkl}) between the periodically repeated crystal lattices to the angle (θ) of diffraction.

The lattice spacings and scattering intensities of materials with different unit cells vary greatly. The materials therefore display very different diffraction patterns that are specific for the atomic composition of the material. Because the diffraction arises from scattering by a periodically ordered material, not only crystalline, but also amorphous materials, with an ordered molecular structure, can be characterized. *Figure 27* shows the diffraction pattern for three

mesoporous materials with different unit cell structures, where also the Bragg diffraction peaks are displayed.[405]

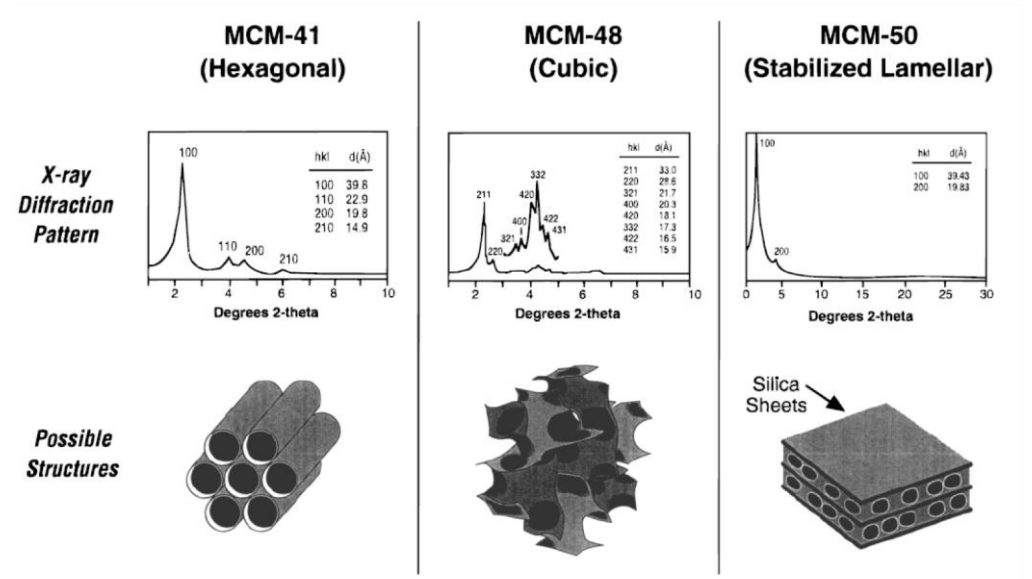

Figure 27. *X-ray diffraction patterns for some mesoporous materials.*[405]

The Bragg diffraction peaks refer to the d-spacing between the lattice planes and are indexed accordingly. For a hexagonal unit cell the lattice planes are indexed (100), (110), (200), (210), and (300). The Bragg spacing ratio is specific for the composition of matter. For materials with a two-dimensional hexagonal structure, the Bragg spacing ratio is 1: 1√3: 1√4: 1√7: 1√12. The repeating distance d_{100} can directly be used to calculate the lattice parameter, a, of the hexagonal structure, through application of the Bragg spacing ratio in the following expression:

$$a = \frac{2d_{hkl}}{\sqrt{3}} \qquad \textbf{(Eq. 4)}$$

where a is the lattice parameter, the distance between the centers of two cylinders in the hexagonal structure, and d_{hkl} equals d_{100} and is the spacing of the hexagonal structure. The d_{100}-spacings of a hexagonal and lamellar structure are illustrated in *Figure 28.*

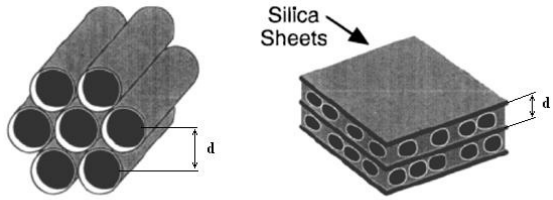

Figure 28. *Illustration of a hexagonal and lamellar structure and their d_{100}-spacing. Modified from Barton et al.*[405]

The d_{100}-spacing provides direct information about the lattice spacing if the mesoscopic order of the material is known. Additional information about the pore width and pore wall thickness can be obtained by using SAXS results in conjunction with physisorption data.

4 Nitrogen physisorption[108,406]

Gas physisorption is of major importance for the characterization of a large variety of porous materials, such as industrial adsorbents, ceramics, pigments and building materials, since it can be used for determining both the pore size and shape, pore volume, pore size distribution and specific surface area of the studied material. Determination of the physisorption isotherm is typically performed either by the conventional technique, by which the adsorption isotherm is constructed point-by-point by admission of successive amounts of nitrogen to the adsorbent, allowing the system to attain equilibrium between each gas admission. The more recent continuous technique, is used to determine the adsorption under quasi-equilibrium conditions; gas is then continuously admitted by a slow and constant flow. Volumetric or gravimetric means can be used to determine the adsorption at the gas-solid interface. Before determination of the adsorption isotherm, the sample must always be degassed at vacuum and typically at an elevated temperature in order to remove all psysisorbed molecules from the surface of the adsorbent that might otherwise distort the result.

4.1 Porosity and classification of pores[108]

According to the IUPAC classification of pores, porous materials can be divided into three classes based on pore width. Microporous materials have pores with a diameter less than 2 nm, mesoporous materials have pores with a diameter between 2 nm and 50 nm and finally macroporous materials have pores of a diameter more than 50 nm. These values are, however, to some extent indiscriminate as the process of pore filling depends largely also on pore

shape and adsorbent-adsorbate interactions. The complete volume of a microporous material can be considered as adsorption space, where micropore filling occurs, in contrast to surface coverage, which occurs on the walls of macro- and mesopores. While micropore filling can be regarded as a primary physisorption process, mesopore filling involves a two-step process consisting of monolayer-to-multilayer formation and capillary condensation.

5.5 Physisorption isotherms

The properties of the material, the adsorbent and adsorbent-adsorbate interactions all influence the physisorption process, while the equilibrium pressure and temperature of the system furthermore influence the adsorption efficiency. Based on the material characteristics and interactions of the gas-solid system, the adsorption follows a certain type of pattern, called isotherm. Although a wide range of physisorption isotherms have been experimentally recorded, the majority of the isotherms can be divided into six main classes (*Figure 29*) according to the IUPAC classification.[108]

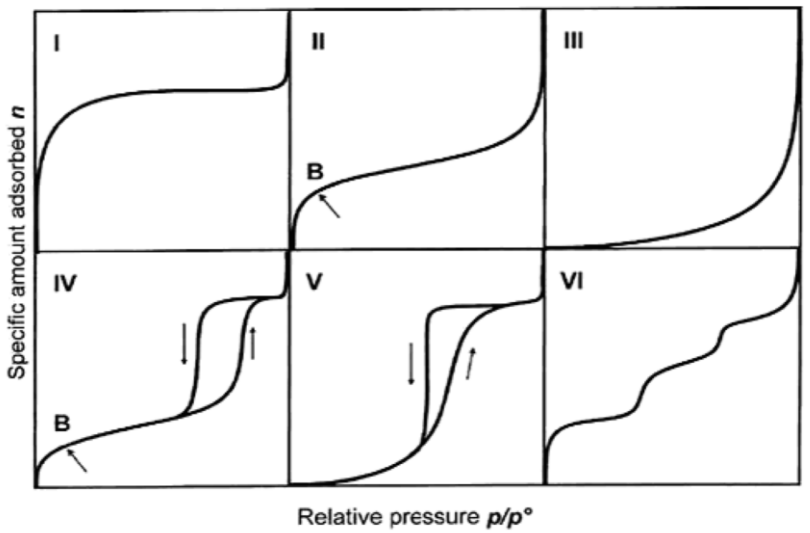

Figure 29. *The six main types of adsorption isotherms according to the IUPAC classification.*[108]

The type I isotherm is typical of materials with micropores (0.7-2 nm) of molecular dimension with strong adsorbent-adsorbate interactions. The steep slope of the adsorption curve is an indication of a relatively small pore size distribution and the wide plateau signifies a very small surface area. Type II isotherms are usually displayed by non-porous and macroporous solids, which allow unrestricted monolayer to multilayer adsorption on an open surface. The isotherm then describes the formation of an adsorbed layer, whose thickness

increases progressively as the relative pressure increases. Point B typically represents the completion of the monolayer and the start of multilayer formation. The type III isotherm is convex to the relative pressure over the whole range, which means that the monolayer coverage increases as the relative pressure is increased, but instead of reaching a point of completion of the monolayer, multilayer adsorption starts as gas molecules clusters at the most favorable sites. Therefore, no point B exists. The isotherm is indicative of very weak adsorbent-adsorbate interactions. Type IV isotherms resemble type II isotherms with the difference that they most often exhibit a second plateau at higher relative pressures. The characteristic hysteresis loop describes the progressive filling (lower branch) and emptying (upper branch) of the pores by capillary condensation. The type V isotherm resembles the type III isotherm, but levels off at high relative pressures. The isotherm is displayed by a number of inorganic oxides, such as e.g. amorphous silica gels, and indicative of weak adsorbent-adsorbate interactions. The type VI isotherm is quite rare and typically seen in materials where a layer-by-layer adsorption occurs on a highly uniform surface.

5.6 Surface area determination by the BET method

The most commonly used method for determining the surface area of porous materials is the Brunauer-Emmett-Teller (BET) gas adsorption method.[407] The BET theory is an extension of the Langmuir theory of monolayer adsorption, and also describes multilayer adsorption. The theory relies on two assumptions: a homogeneously adsorbed layer of molecules on the surface of the material and the absence of interaction between the adsorbed molecules, whereby it can be expressed in its linear form by the following equation:[108]

$$\frac{p}{n^a(p^\circ - p)} = \frac{1}{n_m^a C} + \frac{(C-1)}{n_m^a C}\frac{p}{p^\circ} \qquad \textbf{(Eq. 5)}$$

where n^a is the amount adsorbed at the relative pressure p/p° and n_m^a is the monolayer capacity. C is a constant, which is exponentially related to the adsorption enthalpy in the first adsorbed layer and provides an indication of the magnitude of the adsorbent-adsorbate interactions. The constant C typically has a value between 80 and 150 for many non-porous and mesoporous materials in nitrogen at 77 K. The specific surface area, also known as the BET area, can subsequently be calculated from the monolayer capacity, n_m^a:[108]

$$A_s(BET) = n_m^a L a_m \quad \textbf{(Eq. 6)}$$

$$a_s(BET) = A_s(BET)/m \quad \textbf{(Eq. 7)}$$

where $A_s(BET)$ is the total and $a_s(BET)$ the specific surface areas of the adsorbent mass (m), L is Avogadro's constant and a_m the average area occupied by each gas molecule in the complete monolayer (a_m for N_2 at 77K = 0.162 nm^2).

5.7 Pore size and shape determination

The most useful method for determination of mesopore size is the Barrett-Joyner-Halenda (BJH) method.[408] By using the corrected form of the Kelvin equation,[108,409] which accounts for multilayer thickness in the pore walls, the pore width can be determined. The Kelvin equation assumes a hemispherical liquid/vapor meniscus and a well-defined surface tension and can be expressed:

$$\ln \frac{p}{p^\circ} = \frac{2\gamma V_L}{RT}\left(\frac{1}{r_m}\right) \quad \textbf{(Eq. 8)}$$

where p/p° is the relative pressure, γ and V_L the surface tension and molar volume of liquid nitrogen at 77 K, r_m the mean radius of curvature of a liquid in a pore, R the universal gas constant and T the absolute temperature. For cylindrical pores, the BJH method makes the correction $r_p = r_m + t$, where r_p is the pore radius and t is the thickness of the multilayer. However useful for comparison of pores sizes, the BJH model is unable to accurately determine the absolute pore size, as it underestimates the pore size by approximately 1 nm within the size range 2–4 nm.[410]. A more accurate method for determination of pore size distribution is the non-local density functional theory (NLDFT),[408,410] which is based on statistical mechanics and calculates the adsorption and desorption isotherms based on intermolecular potentials of fluid-fluid and fluid-solid interactions, simultaneously taking into consideration the adsorption forces close to the pore walls. Hence, the NLDFT allows for calculation of pore sizes over the whole micro- and mesopore range. By combining nitrogen physisorption and SAXS analysis data the pore wall thickness can furthermore be calculated.[409]

5 UV-Vis spectrophotometry[411]

Spectroscopy studies the interaction between electromagnetic radiation and matter. When a molecule is illuminated by a light source with a specific wavelength or wavelength range, part of the light can be absorbed as it passes through the sample. As a molecule absorbs energy from the radiation, it is excited to a higher energy level. Ultraviolet and visible (UV-Vis) absorption spectrophotometry measures and calculates the amount of energy absorbed by comparing the transmitted (I_t) and incident (I_0) light intensities. The Beer-Lambert law expresses the linear relationship between absorbance and concentration (or path length) through the equation:[411,412]

$$A_\lambda = \log \frac{I_0}{I_t} = \varepsilon_\lambda c l \qquad \textbf{(Eq. 9)}$$

where A is the absorbance at the specific wavelength λ, ε_λ is the molar absorptivity (molar extinction coefficient) at that specific wavelength, c is the molar concentration of the sample and l is the path length. Typically, the experimental procedure involves measuring the transmittance through, rather than absorbance of, the sample. Since transmittance is defined as $T = I_t / I_0$, the following relationship between the absorbance and transmittance applies:

$$A = -\log T \qquad \textbf{(Eq. 10)}$$

When performing measurements with a sample cuvette a small amount of light is lost due to reflection at the cuvette walls. Corrections for the reflection and the absorption by the pure solvent, thus, need to be made. A reference sample containing only the pure solvent should therefore be measured and used as I_0 in the Beer-Lambert expression. Deviations from the Beer-Lambert law may arise for a number of reasons: sample inhomogeneity, scattering by particulates in the sample, a concentration-dependent equilibrium between chemical species within the sample, concentration-dependent changes in the refractive index of the solution or occurrence of aggregation due to high sample concentrations.[413] The predominate consequence of such effects, is the loss of linear relationship between increase in absorbance and concentration or path length.

6 Thermogravimetric analysis[414,415]

Thermogravimetric analysis (TGA) provides a means of analyzing the composition of a material by examining its mass change as a function of temperature when the material is subjected to a controlled temperature program. The sample is placed on a sensitive scale, the so-called thermobalance, which, during the program, measures the weight loss of the sample that occurs due to oxidation or decomposition of volatile substances in the studied material. The temperature program may involve heating, cooling, keeping the temperature constant, or any combination of these. Measurements can be performed from room temperature up 1500°C under controlled gas atmospheres. The result is typically displayed as the weight percent loss curve, or its first derivative, of the sample as a function of temperature or time. The first derivative, which describes the rate of mass loss against time plotted as a function of temperature or time, can be helpful when wanting to distinguish two overlapping reactions, as double peaks or gradient changes will occur in the first derivative curve. During heating also other reactions, such as different state transitions, that do not include mass loss, may take place in the sample. These can be detected by differential scanning calorimetry (DSC), which measures the change in heat flow in a sample as a function of temperature or time. A combined, simultaneous TGA and DSC analysis is therefore a convenient way of gaining additionally detailed information about the studied material. It is important to remember that the sample-heating rate distinctively affects the appearance of the resulting weight loss curve, wherefore the same setting for the heating program should always be used for samples that are to be compared to each other.

7 Electron microscopy[398,411]

To be able to directly observe particles of colloidal dimensions, the resolution of a microscope needs to be far beyond that of an optical microscope, meaning that the wavelength of the radiation must be far shorter than that of visible light. An electron microscope is able to produce electron beams with a very short wavelength, in the magnitude of 0.01 nm, which can be focused using electrostatic or magnetic lenses. As a consequence, it is possible to acquire images of several hundredfold better resolution by electron microscopy than by light microscopy. Electron microscopy techniques have therefore become increasingly important in the characterization and study of different nano- and microparticles, macromolecules and cellular components.

7.1 Scanning electron microscopy[416,417]

Scanning Electron Microscopy (SEM) is a useful technique for acquiring images of the outside morphology of different materials by scanning a small area of the sample with a focused, high-energy (0.1-50 keV) electron beam. The SEM can also obtain information about the chemical composition of the studied material. For a sample to be suitable for SEM analysis it must be electrically conductive, at least on the surface, and be electrically grounded in order to avoid accumulation of an electric charge on the sample surface. In order to analyze samples, such as silica, which are not naturally conductive, the sample first needs to be coated (sputtered) with an ultrathin layer of a conductive material, typically carbon, gold or platinum, prior to analysis.[418,419] The system must always be kept at vacuum during scanning to eliminate interference effects arising from interactions between the electrons and molecules in the air.

As the electron beam is scanned across the sample, the electrons interact with the sample and give rise to various signals, including secondary electrons, reflected or back-scattered electrons, x-rays, light (cathodoluminescence), absorbed current and transmitted electrons, which all can be detected by specific detectors. The different signals originate from interactions between the incident electron beam with atoms at varying depths within the sample and, thus, provide both quantitative and qualitative information about the structure and elemental composition of the studied sample. The two main signals used for generating images of the sample are the secondary electrons and the backscattered electrons. The inelastic scattering of electrons from the sample surface produces secondary electrons that are emitted from the k-orbitals of the sample atoms. The intensity of the recorded signal depends on the number of electrons arriving at the detector. A topographical image is therefore obtained as a result of electron emissivity variations on the sample surface, where the intensity fluctuations result in variations in brightness on the detected image. Elastic scattering occurs due to interactions between the primary electrons and the sample atoms, and produces backscattered electrons. Since a greater number of electrons backscatter from heavier elements than from lighter ones, backscattered electrons provide important information about the elemental composition of the sample.[418]

The resolution of the resulting image from the different intensity signals is primarily dependent on the focusing capacity of the electron beam, but the sputter coating on the sample surface further enhances the signal and surface resolution, hence improving the obtained image. Although the resolution of a SEM is typically not as good as that of a transmission electron microscope (TEM), its major advantage is its ability to acquire images with a great depth of focus. This property, which is a consequence of the low numerical aperture of

the SEM, offers the possibility of obtaining sample images with three-dimensional characteristics, providing highly useful information about both bulk and surface characteristics of the sample.

7.2 Transmission electron microscopy[417,420,421]

TEM is a highly useful technique for studying particles and structures of nanoscopic dimensions as it examines their internal structure and provides detailed microstructural information of the material. By switching between different imaging modes[422] TEM can study e.g. the chemical composition, crystal orientation or electronic structure of a sample, in addition to the conventional absorption-based imaging. TEM can distinguish and image objects in the approximate size range 1 nm-5 μm. Using high resolution transmission electron microscopy (HRTEM), also called phase-contrast, images with even greater resolution have been achieved, enabling study of the periodic structure of solids, complex structures and crystal defects down to the atomic level. For a sample to be suitable for TEM analysis it needs to be extremely thin, typically <100 nm, and in extreme cases such as HRTEM even <50 nm or <10 nm. Since high-vacuum conditions are required for the electrons to travel unhindered the sample should furthermore be stable in vacuum and able to withstand radiation damage by the electron beam.

The components of a TEM are assembled into a vertical microscope column with an electron gun positioned at the top of the instrument.[421] Condenser lenses situated below the electron gun demagnify the electron beam, limiting its diameter, hence, controlling the intensity of the illumination and the size of the illuminated sample area. The sample, usually mounted on a thin electron-transparent plastic or carbon film supported by a copper mesh grid, is illuminated by accelerating an electron beam at a potential difference range 40-400 kV onto the sample. The applied voltage depends on the nature of the specimen and the desired information. The electrons interact with the specimen as they pass through it and form an image on the underlying fluorescent screen or photographic plate. One of the main requirements of the sample is that it needs to be ultra-thin in order for the transmitted electrons to have sufficient intensity for creating an interpretable image within a certain time limit, which generally is a function of the electron energy and the average atomic number of the sample.

Contrast formation in TEM is largely dependent on which imaging technique is used. The most common operation mode is bright-field imaging, in which only the transmitted electrons contribute to image-formation.[423] The result is a two-dimensional image where thicker specimen regions or regions with atoms of higher atomic number appear darker and thinner specimen

regions or regions with a lower atomic number appear brighter on the screen. Dark-field imaging exploits the scattering of electrons from the sample into locations in the back focal plane and can be useful e.g. in identifying lattice defects in crystals. By selecting certain reflections and excluding the unscattered beam and by projecting the back focal plane instead of the imaging plane onto the image device, a diffraction pattern, which appears dark at the locations lacking sample scattering can be created. For thin single-crystal samples, diffraction produces an image dotted pattern, which provides information about crystal orientation and space group symmetries in the crystal. In polycrystalline or amorphous materials diffraction causes a ring-pattern.[143]

8 Flow cytometry[424–426]

Fluorescence-based flow cytometry (FCM) is an effective technique for analyzing the physical and chemical characteristics of biological material, such as cells or other biological components in the same size range, based on their fluorescent characteristics. Thousands of cells can be quantitatively analyzed, counted and sorted each second,[427] as the cells are illuminated by a laser beam and pass through an electronic detection device in a fluid stream, called the sheath fluid. The liquid flow is regulated so that the cells are well separated and only one cell at a time passes the fluorescence measuring station, making it possible to record the fluorescent signal of each individual cell.[426] When the stream flows through the laser beam fluorescent molecules in or on the surface of the cell can be exited and emit light. The emitted light is detected by the forward scattering (FSC) and sideway scattering (SSC) detectors as well as by one or several fluorescence detectors. While FSC provides information about cell size or volume, SSC describes the granularity or inner structure of the cell. Each cell produces a separate signal that is converted by an analog-to-digital conversion detector system to electrical signals that can be processed and analyzed by a computer. The acquired data can then be viewed on a linear or logarithmic scale as a two-dimensional dot plot or as a single-dimension histogram. Based on fluorescence intensity one or several regions of interest, i.e. cell populations with similar properties, can be chosen or "gated" for analysis.[424] When using fluorescence as the means to obtain information about a sample it is always important taking into consideration factors such as fluorochrome quenching, bleaching and photon saturation that might potentially interfere with the measurement.[428]

9 Confocal laser scanning microscopy[429,430]

Confocal laser scanning microscopy (CLSM) is a valuable instrument for non-destructive examination of thin (0.5-1.5 μm) optical sections within or on the surface of a wide range of both living and fixed biological specimens. By scanning multiple layers, so-called stacks of the sample, also 3D-images of the object can be produced. Modern confocal fluorescence microscopes have 3-5 lasers with adjustable excitation intensity and several detectors, each able to collect emission in a certain wavelength range. One or several of the lasers and detectors may be operated simultaneously and the microscopes are able to detect fluorescence emission in the wavelength range 400-750 nm.[431] Due to the wide array of existing fluorochromes suitable for labeling of biological specimens, a variety of molecules as well as cellular and sub-cellular components, can be fluorescently labeled and simultaneously identified and imaged with high precision using CLSM.

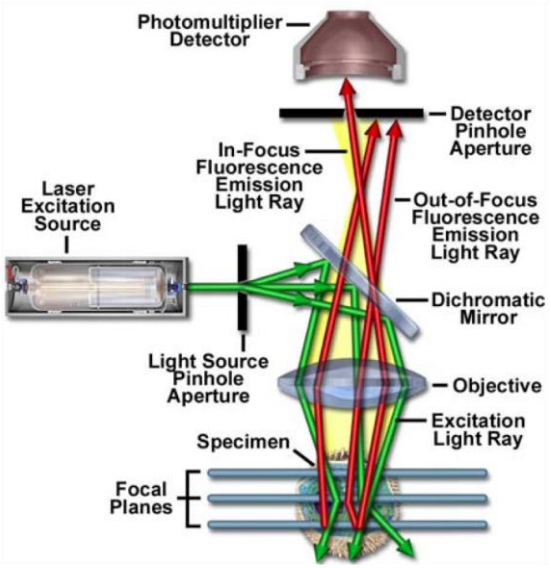

Figure 30. *Schematic diagram of the optical pathway and main components in a CLSM.*[431]

Within the instrument both the fluorescence and scattered light from the examined specimen is collected by the objective lens and passed forward to a beam splitter, which separates the light and carries only a part of it into the detector. The detector filtrates the light, letting through only the selected fluorescent wavelengths, while blocking the primary excitation wavelength. The signal then passes through a pinhole in the conjugate plane, allowing only

light from the focal plane to enter the detector, thus, contributing to creating a sharper image. The final signal passes through a photodetection device, which converts the light into an electric signal that can be registered by a computer.[430,431] The beam path and principal component of a CLSM is illustrated in *Figure 30*.

CLSM can additionally be used for studying varying cellular structures and dynamics by techniques, such as Stimulated emission depletion (STED) microscopy, Fluorescence-lifetime imaging microscopy (FLIM), Förster resonance energy transfer (FRET) and Fluorescence recovery after photobleaching (FRAP). STED microscopy enables enhancement of the image resolution by minimizing the area of illumination at the focal point by selectively deactivating the peripheral fluorescence.[432] This allows for highly detailed analysis of various structures in biological systems. In FLIM, the exponential decay, i.e. the lifetime of the fluorescent signal, instead of its intensity, is recorded and used for producing an image.[433] The technique is useful e.g. when investigating the intracellular degradation of fluorescently labeled samples and has the advantage of reducing the effects of photon scattering in thicker samples. FRET describes a mechanism, where energy is transferred from a donor chromophore to an acceptor chromophore through radiationless dipole-dipole coupling.[434] Since the distance required for interaction is extremely short (≤10 nm), FRET is highly useful for studying the colocalization of different structures. FRAP is performed by selectively illuminating a small area of a specimen at a low light intensity, while the emitted fluorescence is measured. [435] The illumination is then briefly increased to a very high level to rapidly bleach the fluorescent molecules in that region. The recovery of fluorescence intensity, by diffusion of new unbleached fluorescent molecules into the bleached region, is then monitored to obtain information about the molecular transfer dynamics into the specified region.[436]

SUMMARY OF RESULTS

1 Design of MSNs for drug delivery

1.1 Synthesis and functionalization of MSNs

MCM-41 type amino-functionalized MSNs of approximately ~200-300 nm in diameter were synthesized for investigating their degradation behavior and drug release mechanism *in vitro*, as well as the interdependency of the two above-mentioned parameters. The materials were synthesized and surface-functionalized using already thoroughly documented protocols and the obtained characterization data from SAXS and N_2-sorption measurements corresponded well with literature data.[111,437,438] Moreover, additional characterization methods (DLS, SEM and TEM) confirmed that the obtained materials were of the desired size and shape, had a narrow size distribution, good dispersion stability at physiological pH and maintained their porous structure throughout all functionalization steps. Successful surface grafting with PEI was confirmed by electrokinetic measurements and the grafted amount (22 wt%) was quantitatively determined by TGA.

1.2 Drug loading

The fluorescent lipophilic cationic indocarbocyanine dye 1,1'-dioctadecyl-3,3,3,3'-tetra-methylindocarbocyanineperchlorate (DiI or $DiIC_{18}$) is widely used as a membrane stain, as it diffuses laterally to stain the entire cell membrane and has a bright fluorescence with good photostability in physiological environment. It is well suited for use as a model drug, for labeling purposes and as a long-term tracer in various cells.[439] DiI was thereby, in the drug release experiments, used as a model drug for the gamma(γ)-secretase inhibitor (GSI) drug N-[(3,5-difluorophenyl)acetyl]- L-alanyl-2-phenyl]glycine- 1,1-dimethyl-ethylester (DAPT) and, moreover, since we have previously verified DiI to be a suitable model drug for DAPT when studying cancer targeting in vivo (**Supporting Publication VII**). DAPT was also used as a control substance for confirming that the release behavior of DiI resembled that of a real hydrophobic drug. DAPT is a highly hydrophobic drug that has been studied as an inhibitor of e.g. autoimmune and lymphoproliferative diseases, cancer cell growth and angiogenesis. Both DiI and DAPT are insoluble in water and aqueous buffers, but soluble in some organic solvents, such as dimethylformamide (DMF) and dimethylsulfoxide (DMSO), which is why they are typically adsorbed to the substrate from organic media. The adsorption of DiI and DAPT was, hence, performed from cyclohexane to avoid competition

between adsorbent-adsorbate and solvent-adsorbate interactions.[440] The adsorption efficiency of both adsorbates was through dye/drug elution from the loaded NPs in methanol and characterization with UV-vis spectrophotometry (DiI) and high-performance liquid chromatography (HPLC) (DAPT) found to equal 100% when a 5 wt% (with regard to particle mass) dye/drug amount was applied. An impregnation time of one day was found sufficient for reaching complete adsorption.

1.3 Degradation of MSNs *in vitro*

The degradation of MSNs with varying surface-functionalization and dye/drug-loading was investigated using a dialysis setup in the aqueous buffer 4-(2-hydroxyethyl)-1-piperazineethanesulfonic acid (HEPES) at pH 7.2 and 37°C, in order to mimic intracellular cytosolic conditions. The dissolution of silica was determined spectrophotometrically using the molybdenum blue method.[14] The results of the degradation experiments, which were carried out over one week, are displayed in *Figure 31*. The surface chemistry (PEI-functionalization) as well as cargo (DiI/DAPT)-loading were found to clearly influence the degradation behavior of the investigated materials. All PEI-functionalized samples, regardless of dye/drug-loading, were found to initially degrade faster than the amino-functionalized particles (MSN). This phenomenon was thought to relate to the abundance of amino groups grafted onto the silica surface, which is known to boost silica degradation in neutral and alkaline conditions in the presence of water.[212,213] The degradation profiles of the dye/drug-loaded samples (MSN-PEI/DiI and MSN-PEI/DAPT) and the amino-functionalized sample (MSN) were fairly similar. As the pore filling with hydrophobic molecules would be expected to retard the material degradation through delayed wetting by the solvent, these results pointed to a possible difference in degradation mechanism between the cargo-containing and amino-functionalized MSNs. As further investigation of the

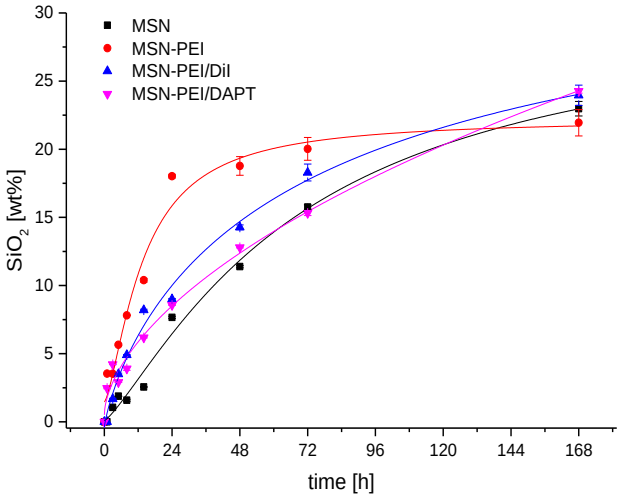

Figure 31. *Dissolution of MSNs with different functionalization as wt% dissolved SiO_2 over time. Error bars are SD; n=3.*

degradation samples with TEM (*Figure 32*) displayed a very intact outer spherical shape of the amino-functionalized MSNs while the pore structure had clearly been deformed, we proposed that these particles had primarily degraded from the inside by bulk erosion, which agrees with previously published data.[441,442] The PEI-grafted unloaded sample (MSN-PEI), which displayed a more intact pore structure, was suggested to degrade by a combined bulk and surface erosion, since the absence of cargo would allow pore wetting and the surface amino groups would promote hydrolysis of Si-O-Si bonds, leading to surface erosion. Based on the same statements, the cargo-containing samples were suggested to degrade in a similar fashion as MSN-PEI with the addition of an initial retardation in dissolution rate due to the presence of hydrophobic cargo. The low asymptote value of 20-25 wt% silica dissolution for all investigated samples that was reached after one week of testing was thought to be related to limitations set by the experimental setup, including potential dissolution-reprecipitation behavior and the absence of solvent-exchange in the system. Naturally, at physiological conditions, the exchange of fluids would ultimately result in complete dissolution of the NPs.

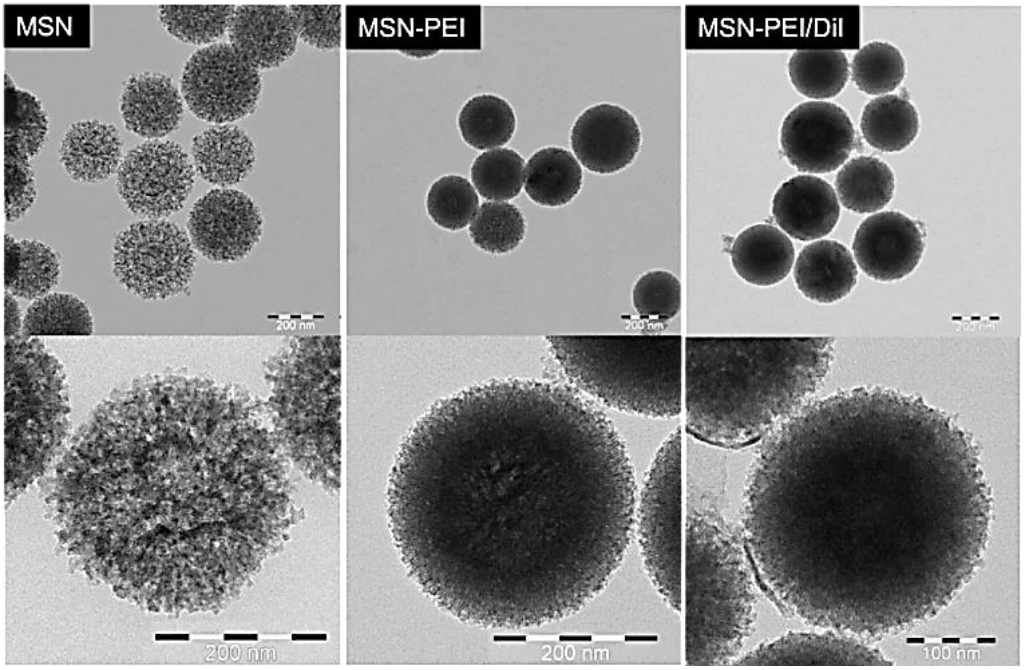

Figure 32. *TEM overview and single-particle images of MSN, MSN-PEI and MSN-PEI/DiI after dissolution and drug release testing for one week.*

1.4 Drug release

The release of hydrophobic cargo (DiI/DAPT) from PEI-functionalized NPs was investigated in HEPES buffer at various solvents over one week, mimicking intracellular conditions in terms of temperature, pH, polarity, protein, enzyme or lipid content, presence of hydrophobic structures and finally also in live cancer cells. As can be seen in *Figure 33*, the release of cargo in pure aqueous buffer (HEPES) at pH 7.2 was very low both due to the limited water-solubility of the hydrophobic active agents and the presence of cargo that counteracted degradation-related release by preventing penetration of water molecules into the pore structure. A strong positive correlation between the release profiles and their corresponding carrier degradation profiles suggested that the release of poorly water-soluble cargo in a simple aqueous environment is strongly connected to the degradation of the carrier.

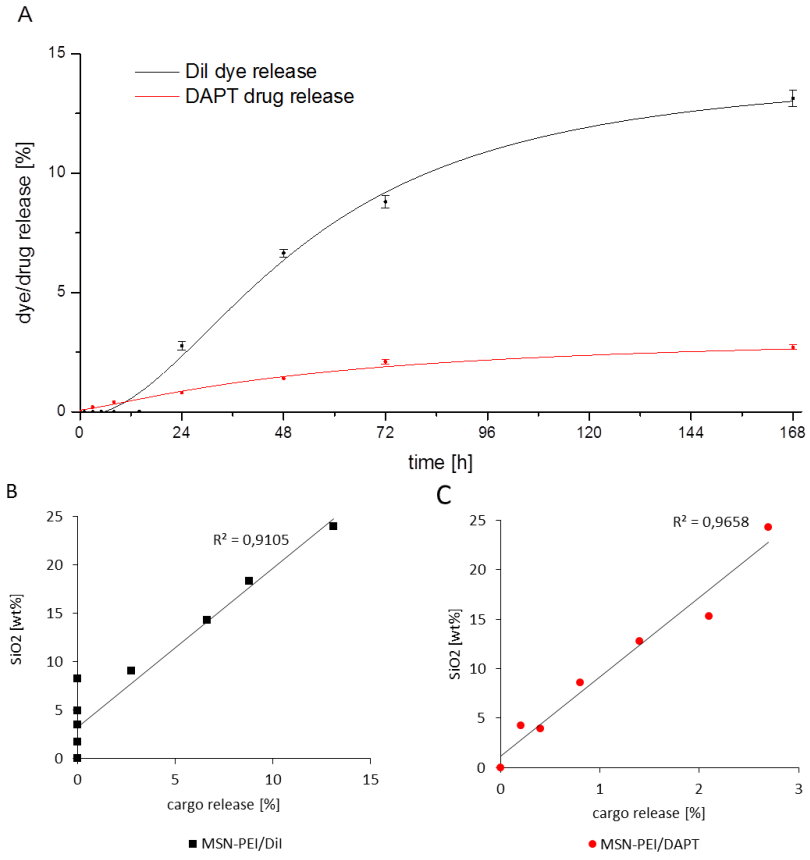

Figure 33. *A) Dye and drug release profiles from MSN-PEI/DiI and MSN-PEI/DAPT particles in HEPES buffer (pH 7.2) at 37°C. Error bars are SD; n=3. The correlation between carrier degradation and cargo release is shown for B) DiI-loaded and C) DAPT-loaded particles.*

Since only a small fraction of the total cargo amount was released at the employed conditions, further investigations of model drug (DiI) release in more complex media were performed (*Figure 34*). A decrease in pH to 4.8 of the release medium, which corresponds to the acidic environment found in late endosomes and lysosomes, where NPs typically end up after intracellular uptake, showed no signs of increasing the release rate. The dye release rather decreased, which reinforces the earlier statement that the release of hydrophobic agents in aqueous buffer is primarily dependent on carrier degradation, and agrees with knowledge of the pH-dependent solubility of silica.[14,106] The presence of surfactants (concentration below CMC), enzymes or proteins in the release medium was also excluded as release-triggering factors. Upon the addition of an organic apolar solvent to the release medium, an almost immediate release of adsorbed model drug was observed. Further investigations revealed that only the hydrophobic dye moved into the apolar phase, while the NPs resided in the aqueous phase. The desorption of model drug moreover reached a higher completion following an increased concentration (>CMC) of amphiphilic molecules or other hydrophobic components, such as cellular membranes and organelles, in the release medium. The drug-solubilizing capacity of the micellar and hydrophobic structures was clearly displayed and is possible to predict based on the high log P value (12.0) of DiI,[443,444] which signals that DiI preferentially partitions into a more apolar substance.[445] The strong mechanical agitation applied during experimental conditions should be taken into consideration when comparing the drug release profile to the drug release in actual intracellular conditions in live cancer cells. The lack of such a mechanical agitation at intracellular conditions is expected to result in a less pronounced contact between cargo molecules confined to the pores of the nanocarrier and surrounding hydrophobic structures, consequently resulting in a delayed release of cargo.

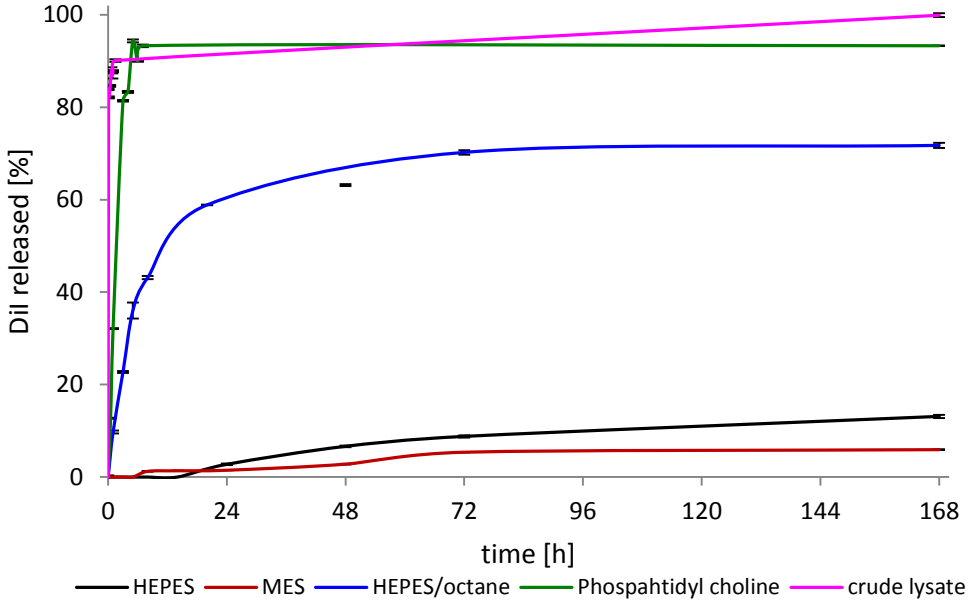

Figure 34. *DiI release in different media plotted as % of dye released over time. Error bars are SD; n=3.*

1.5 Intracellular drug delivery and release

The presented nanocarrier system has previously been extensively studied and established as non-cytotoxic, biocompatible and biodegradable.[19,224,361] The cancer-specific uptake of nanocarriers, along with the delivery of hydrophobic cargo *in vitro* and *in vivo* has furthermore been demonstrated in a number of publications,[19,224,286,325,361,446] including **Supporting Publication VII**. The nanocarriers have been efficiently taken up into intracellular compartments and the release of drug has been restricted to the intracellular environment without any premature leakage.[224,325] Investigation of the intracellular uptake of MSN-PEI/DiI particles and their subsequent intracellular release of hydrophobic cargo (DiI) in HeLa cervical cancer and MDA-MB-231 breast cancer cells was hereby performed as a verification of the proposed drug release mechanism, ascribed to interaction between apolar substances.[447] The nanocarriers were efficiently taken up into intracellular compartments, from which a sudden release of cargo into the cytosol was observed after approximately 48 h (*Figure 35*). The active intracellular release was verified by bleaching a cytosolic area containing previously released dye and subsequently recording the continuous dye-release from cytoplasmic vesicles into the pre-bleached spot, using FRAP.

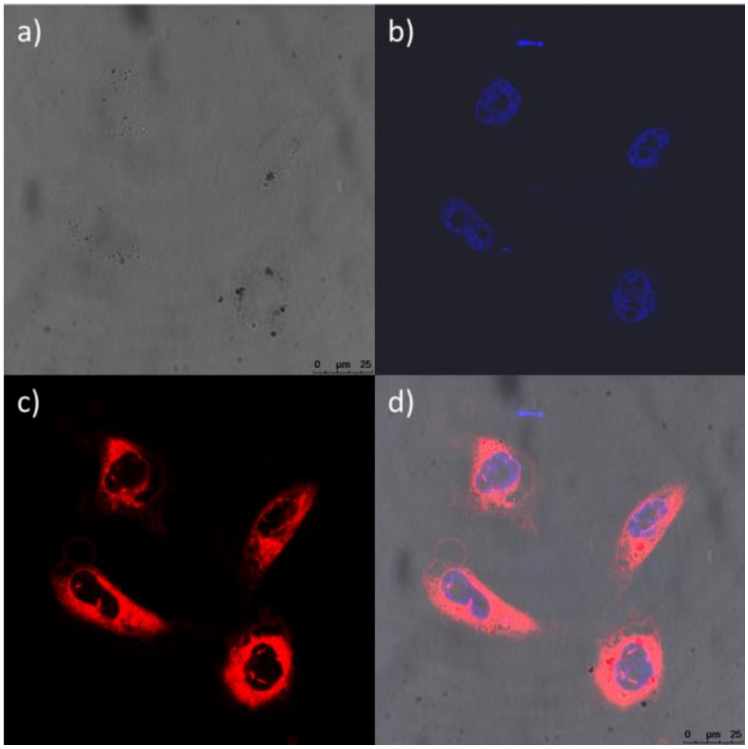

Figure 35. *Confocal microscopy images of MDA-MB-231 breast cancer cells after 48 h incubation with MSN-PEI/DiI NPs. a) Bright-field image of cells, b) 4',6-diamidino-2-phenylindole (DAPI)-stained cell nuclei, c) intracellularly delivered and released DiI, and d) overlay image.*

1.6 Summary of results

The intracellular release of hydrophobic cargo from an MSN-based DDS was evaluated in various mimicked intracellular conditions as well as in live cancer cells. The release of cargo in purely aqueous solvents was found to correlate strongly with the degradation of the nanocarrier. The release was not affected by changes in pH or by the presence of enzymes or protein in the release medium. We found that the release from MSNs was triggered as a result of close association with high concentrations (>CMC) of amphiphilic molecules or hydrophobic structures, such as cellular membranes and organelles. At these conditions the physicochemical characteristics of the cargo molecules, thereby, became the release-governing factors. The release of cargo was observed as a sudden burst from the nanocarrier; very similar to the intracellular release observed from cytoplasmic vesicles in live cancer cells 24-48 h after NP uptake.

2 Intracellular uptake and degradation of PACA NPs

2.1 The nanocarrier system

PEG-functionalized PACA NPs with different monomer compositions (PBCA, POCA and P(BCA/OCA)), containing the fluorescent hydrophobic dye NR668 (model drug), were synthesized at SINTEF Materials and Chemistry (Trondheim, Norway) by an oil-in-water miniemulsion polymerization process.[303] The produced NPs had the approximately same size (d~150-175 nm) and surface charge (ζ~-10 mV). Due to their easy fabrication and functionalization, biocompatibility and controllable degradation rate[21] PACA NPs can potentially serve as drug carriers both to solid tumors and across the blood-brain barrier.[22] PACA degradation in aqueous environment occurs predominantly by surface-erosion through the hydrolysis of esters,[448] which produces the corresponding alkyl alcohol and water-soluble poly(cyanoacrylic acid).[348,349] This process can potentially also be catalyzed by esterases.[308] The degradation rate is furthermore strongly dependent on the alkyl chain-length of the monomer.[349] As the release of hydrophobic drugs from PACA NPs occurs primarily as a result of carrier degradation the intracellular uptake and degradation of the NPs are the two main factors that determine the bioavailability of the drug. Since the knowledge of these processes are still fairly limited, they were evaluated as a function of NP monomer composition in two different cells lines.

2.2 Intracellular uptake of PACA nanoparticles

The intracellular uptake of PBCA and POCA NPs in the PC3 human prostate cancer and RBE4 rat brain endothelial cell lines was quantified by FCM. The results are presented in *Figure 36* as fluorescence intensity and percentage positive (fluorescent) cells. RBE4 cells displayed a significantly faster and overall higher uptake of both particle samples than the PC3 cells. Roughly, 90% of the RBE4 cells were fluorescence positive after only 1 h of incubation, whereas the same level was reached in PC3 cells after 24 h. The RBE4 cells furthermore showed higher uptake of PBCA NPs, while POCA NPs were more efficiently taken up in PC3 cells, suggesting that intracellular uptake is dependent both on cells line as well as on the alkyl chain-length of the monomer. NP size and surface charge are furthermore known to affect intracellular uptake.[51] NP enlargement due to swelling or protein corona formation, or changes in net surface charge (ζ) as a result of protein adsorption or NP degradation were therefore also thought to influence the uptake.

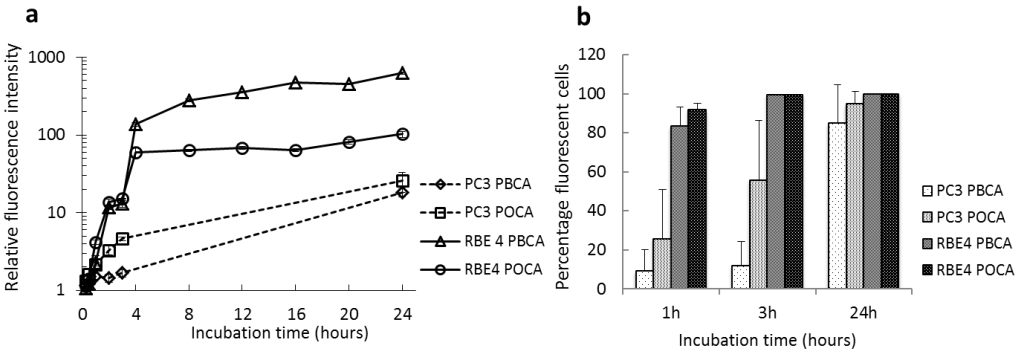

Figure 36. *a) PBCA and POCA NP uptake kinetics in PC3 and RBE4 cells expressed as fluorescence intensity relative to untreated cells. b) Percentage positive cells. Error bars are SD; n=2.*

The uptake of NPs was analyzed by CLSM after 3 h, displaying some colocalization of PBCA NPs with early endosomes, late endosomes and lysosomes in RBE4 cells and of POCA NPs with lysosomes in PC3 cells. The level of colocalization was, however, low and the vast majority of endocytic compartments did not contain any NPs. This corroborates findings by other research groups,[449,450] possibly indicating that PACA NPs are capable of early endosomal escape, the mechanism of escape, however, remaining unclear. The lack of cellular fluorescence upon incubation at 4°C also confirmed the uptake of NPs to be an energy-requiring process, which proceeds through active endocytosis. These results agree with previous studies[279,451] and furthermore demonstrated that no fluorophore-leaking occurred prior to cellular uptake as a result of NP-cell contact that has previously been observed for nile red from PACA NPs.[311] Both clathrin-mediated (CME) and caveolin-mediated endocytosis (CavME), which were inhibited using chlorpromazine and genistein, respectively, were found to participate actively in particle uptake in both cell lines (*Figure 37*). Active endocytosis by CavME was found to be less prominent for PBCA than POCA NPs in PC3 cells, while inhibition of CME reduced the uptake of both particle samples by approximately 40%. Inhibition of CME and CavME in RBE4 cells both resulted in significant reduction of cellular uptake of both particles. PBCA uptake was reduced by 83% (CME) and 56% (CavME), while POCA uptake was reduced by 73% and 43%, respectively, indicating that these endocytic routes played a greater role for NP uptake in the RBE4 than the PC3 cell line. Previously published results,[51,380,452] have shown similar high NP uptake efficiency by RBE4 cells compared to other cell types, suggesting that the high uptake efficiency might be a cell type-specific characteristic of brain endothelial cells, something that may potentially be exploited for delivering NPs over the blood-brain barrier.[22,302] CME and CavME

inhibition showed that both pathways were active, CME being particularly dominant in RBE4 cells. The combined reduction in uptake efficiency by RBE4 cells through inhibition of the CME and CavME pathways exceeded 100% inhibitors, which suggested poor inhibitor-selectivity for the respective internalization pathways, as has also been stated by others.[453] The overall low inhibition effect in PC3 cells may also indicate that other endocytic pathways were active.

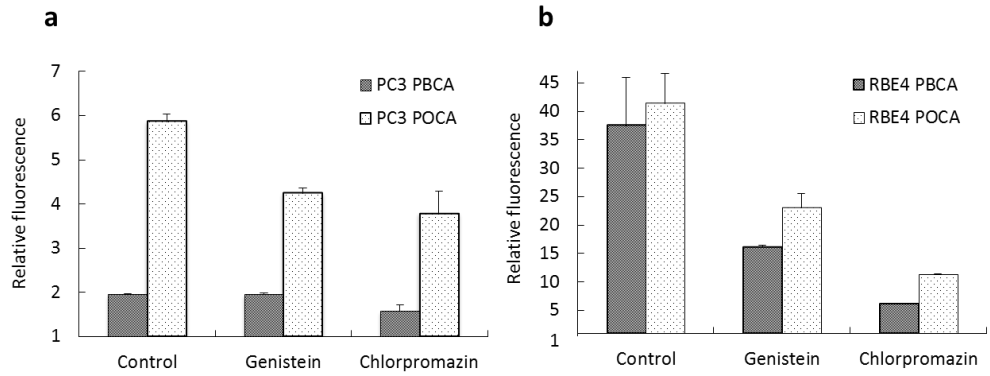

Figure 37. *The inhibition effect of genistein and chlorpromazine on endocytosis of PBCA and POCA NPs in a) PC3 cells and b) RBE4 cells. Control is untreated cells. The median fluorescence intensity is expressed relative to autofluorescence. Error bars are SD; n = 2.*

2.3 Intracellular degradation and drug release

The degradation rate of PACA NPs was studied by monitoring the change in particle size and concentration as a function of time in physiologically relevant buffers of different pH, in cell medium and human blood serum. PBCA NPs were found to degrade in all media, increasingly fast upon increase in pH of the medium, whereas POCA NPs displayed little sensitivity to pH. For both particles an initial increase in size was observed at physiological pH 7.4, as well as in cell medium and serum, the former most likely relating to polymer swelling[454] and the latter to adsorption of proteins[455]m onto the particle surface. Quantitative determination of the degradation products butyl and octyl alcohol by gas chromatography (GC) revealed 88% degradation of PBCA, 45% of the hybrid polymer NP P(BCA/OCA) and only 3% of POCA, after 48 h (*Figure 38*). Assuming linear degradation rates for all samples, half-lives of 25 h for PBCA, 48 h for P(BCA/OCA), and ~500 h for POCA were obtained. The above-presented values indicate that the degradation rate of the NPs can be manipulated by mixing two monomers with different alkyl chain-lengths.

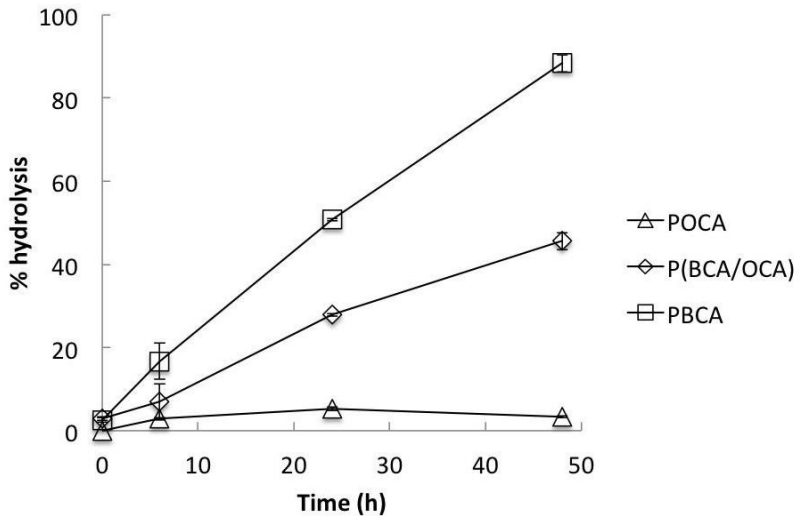

Figure 38. *Degradation of PACA NPs as % hydrolysis of the NPs as a function of time at pH 7.4. 100 % hydrolysis was obtained in glycine buffer at pH 9. Error bars are SD; n = 3.*

Intracellular degradation of NPs and drug release was studied in PC3 cells by exploiting the spectral properties of the incorporated hydrophobic fluorescent dye (model drug) NR668. The dye was strongly associated with the polymeric matrix since no diffuse cytoplasmic staining, resulting from dye leaking, could be observed at 4°C. Dye-labeling of cytoplasmic lipid droplets and hydrophobic molecules should, hence, be a result of degradation-associated release of NR668. FLIM and spectral analysis of free dye NR668, PBCA and POCA NPs was used to investigate NP degradation (*Figure 39*). The significant shift in fluorescence lifetime distribution of the PBCA NPs indicated that the NPs were constantly degrading. The POCA NPs underwent virtually no shift, but the change in distribution profile and large standard deviation at 6-7 days suggests that the particle underwent some physical or chemical changes. Fluorescence emission spectra of PC3 cells incubated with PBCA and POCA NPs for 24 h were compared to that of NPs prior to incubation and PC3 cells incubated with free NR668 dye for 24 h. The PBCA NPs displayed clear spectral differences at 0 and 24 h, while at 24 h the emission spectra shifted towards that of PC3 cells incubated with free NR668. The emission spectrum of POCA NPs did, however, not shift after 24 h and were more similar to that of the corresponding free NPs. To confirm that the observed changes in fluorescence lifetime and spectral emission originated from the release of dye of NPs, the hydrophobic dye pentamer hydrogen thiophene acetic acid methyl ester (p-HTAM) was used to create a FRET pair with NR668. PC3 cells were stained with p-HTAM following 24 h of NP incubation, whereupon a FRET signal was detected in

cells incubated with PBCA NPs, while no signal was detected in cells incubated with POCA (*Figure 40*). Formation of a FRET pair requires the immediate proximity (10 nm) of the fluorescent molecules to each other, wherefore FRET could not occur unless the dye had been released from the NPs.[434] The presence of a FRET signal, thus indicates dye release as a consequence of particle degradation in PBCA.

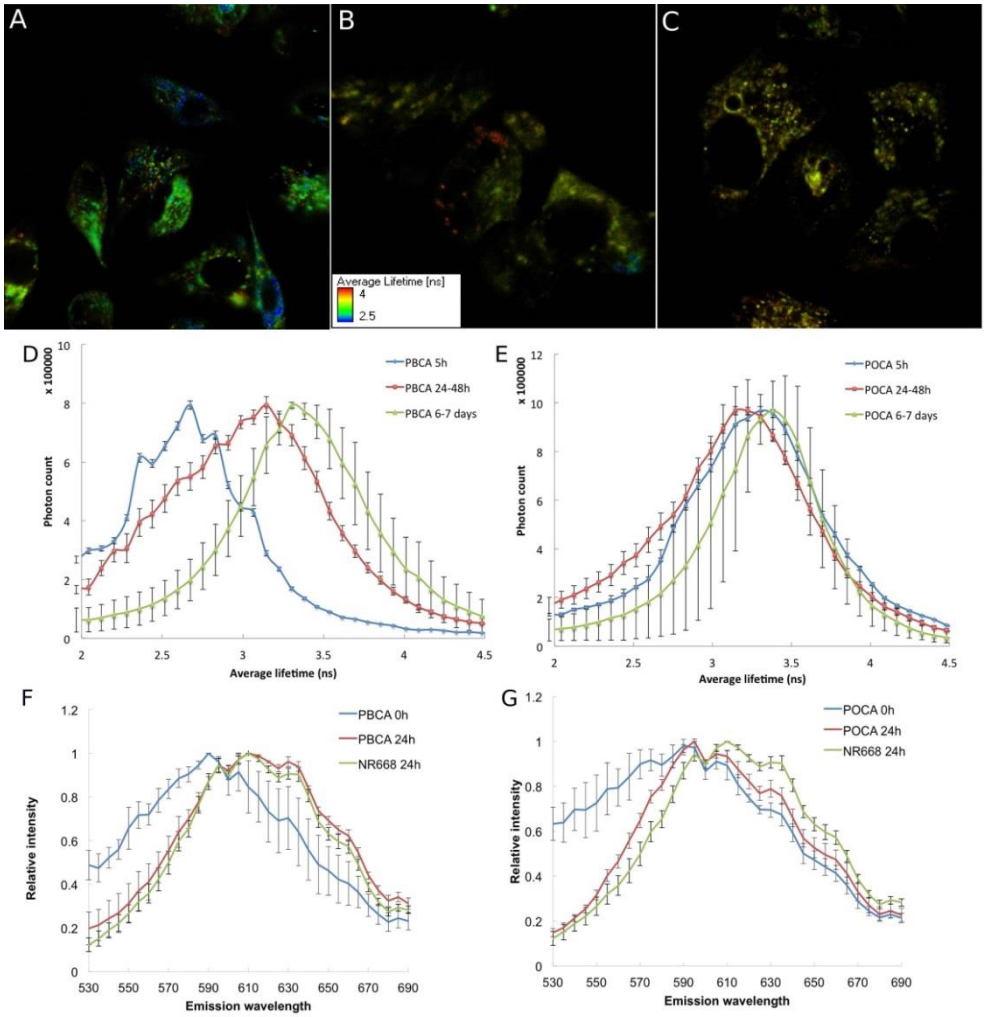

Figure 39. *A-C) FLIM images of PC3 cells incubated for 24 h with A) free NR668, B) PBCA and C) POCA NPs and grown for an additional 5 days. Each pixel is colored based on the average lifetime. Fluorescence lifetime distribution for D) PBCA, and E) POCA NPs inside cells at 5 h, 24–48 h and 6-7 days. Emission spectra from NPs prior to incubation (blue) and PC3 cells incubated with free NR688 (green), F) PBCA or G) POCA NPs after 24 h (red). Error bars are SD; n=5.*

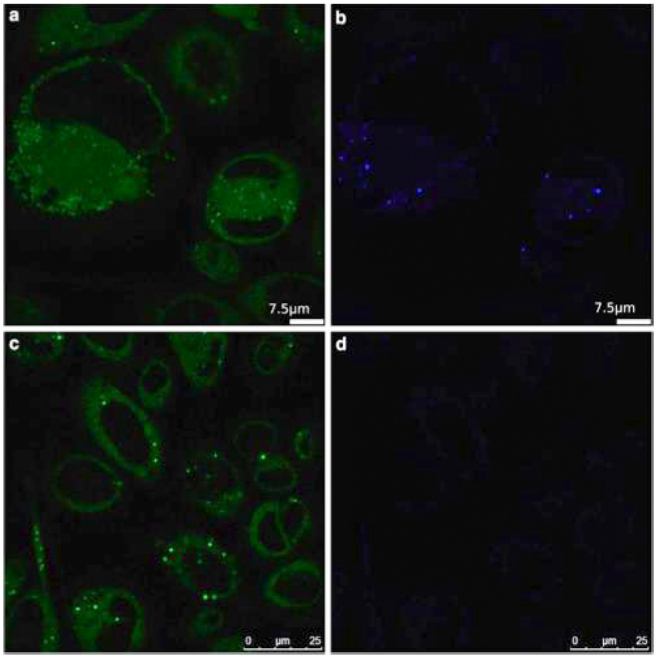

Figure 40. *PC3 cells incubated with a-b) PBCA and c-d) POCA NPs for 24 h and grown for an additional 72 h before p-HTAM staining. Excitation at 405 nm, a) & c) emission signal from p-HTAM at 500–540, and b & d) FRET signal at 650–710 nm.*

2.4 Summary of results

NPs with different polymeric compositions (PBCA, POCA, PBCA/POCA) containing the fluorescent hydrophobic dye NR668 as a model drug were assessed for intracellular degradation and uptake in the RBE4 and PC3 cell lines. Analysis by various optical imaging techniques showed that the PBCA NPs were intracellularly degraded within 24 h of administration and consequently released their payload into the cytosol, whereas the POCA NPs remained intact and displayed no release of model drug after the same incubation time. An intermediate degradation and drug release rate was observed for the PBCA/POCA hybrid NPs, which indicates that the drug release profile could be fine-tuned by choosing the appropriate PACA monomers. The intracellular uptake of PACA NPs was furthermore shown to depend both on the chain length of the monomer as well as on the choice of cell line. The overall NP uptake was considerably higher in RBE4 than in PC3 cells. CME and CavME were actively involved in PACA NP uptake, the former being particularly dominant in RBE4 cells.

3 Design of core-shell nanoparticles for theranostics

3.1 The core-shell nanocarrier system

A multifunctional core-shell composite NP comprising a photoluminescent ND core and a mesoporous silica shell was designed for combined diagnostic and therapeutic – theranostic – actions. The nanocarrier was functionalized with a hydrophilic copolymer for efficient permeation over the cell plasma membrane in order to enable delivery of hydrophobic cargo into cancer cells with subsequent cargo release into the cytosol. NDs containing luminescent NV color centers present bright and stable fluorescence and do not suffer from photobleaching or toxicity.[151] The structural defects on the surface of NDs also contribute to the luminescent signal but is, contrary to the NV-center luminescence, dependent on particle size and may be affected by interaction with the surrounding medium or additional surface functions attached to the particle.[456] Thus, the applied silica coating could potentially protect the ND surface fluorescence and serve as a protective coating against a degradative environment. In addition to its apparent function as a drug-carrying matrix, the mesoporous silica shell furthermore provides the otherwise rough ND surface with a smoother, physicochemically more homogeneous, and subsequently easily functionalizable surface. Based on the many advantageous properties and excellent compatibility of these two materials we set out to create a new core-shell ND@MSN nanocomposite for combined imaging and drug delivery.

3.2 Formation of porous silica shells

Silica-coating of hydrophilic, net negatively charged DNDs (*Table 2*) was performed using the same chemical components (water, CTAB, ammonia and TEOS) as used in the synthesis of conventional base-catalyzed MCM-41 MSNs, with the crucial addition of ethanol when aiming for a core-shell structure, similar to conditions employed when coating non-porous Stöber silica NPs with porous shells.[457] DLS analysis of the materials prior to and following coating with silica displayed an increase in particle size along with an apparent decrease in PdI, suggesting that the ND cores had been successfully coated. Morphological and structural analysis of the composite NPs by TEM (*Figure 41*) confirmed that spherical porous nanocomposites containing a single ND had been formed. Elemental analysis by X-ray energy dispersive spectroscopy (EDS) (*Figure 41d & e*) at spot 1 and 2, respectively, in *Figure 41b* furthermore confirmed the presence of a diamond core surrounded by a silica shell. The silica shell presented radially aligned pores with a size of 3-4 nm in diameter, but was structurally less well-ordered than bulk MCM-41 materials.[92]

Table 2. *Characteristics of the used DND core materials.*

Sample	Methods of synthesis and treatment of samples	Crystallite size[a]	ζ[b]	Particle size of ND dispersion[b]
ND-1	Detonation of a mixture of graphite and hexogen, singlet oxygen and acid purification	34 nm	23 mV	200 nm
ND-2	Detonation of a mixture of trinitrotoluene and hexogen, acid purification	6 nm	36 mV	120 nm

[a] Size was determined by SAXS.

[b]Zeta potential and size (DLS) measurements were performed in HEPES buffer (25 mM; pH 7.2).

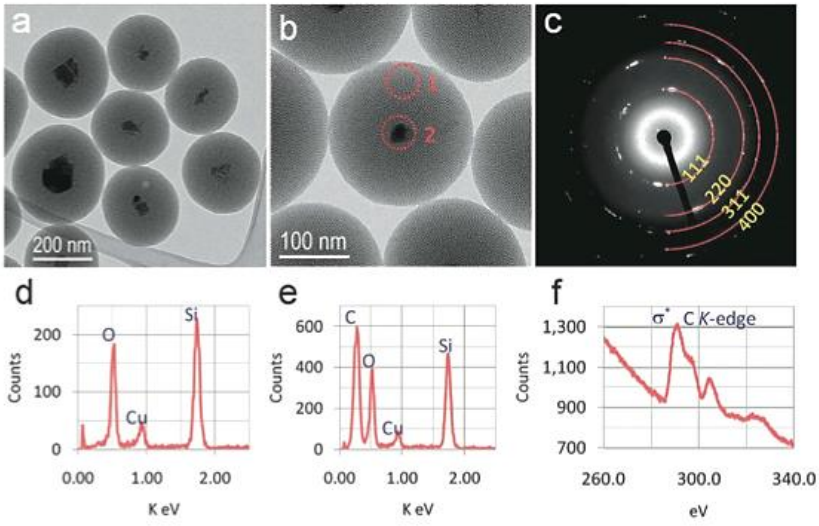

Figure 41. *TEM studies of sample ND-1. a) bright-field image; b) single-particle bright-field image; c) electron diffraction pattern of a selected area, indexed for diamond structure; d) & e) EDS spectra collected at spot 1 and spot 2 in b), respectively; and f) C K-edge energy electron energy-loss spectrum (EELS) at spot 2 in b).*

3.3 Optimization of coating parameters

Having established a working coating protocol, we attempted to control the silica coating thickness. As the approximate reaction yield of the silica precursor was determined to be ~ 60%, we hypothesized that the coating thickness could be reduced as the yield fell below 100%. Thus, by reducing the silica precursor (TEOS) volume in respect to ND amount and synthesis volume, still keeping the CTAB/TEOS ratio of the reaction constant, the effect on coating thickness was investigated. Results presented in *Figure 42* show that no reduction of hydrodynamic particle size was achieved, until a sudden decrease of DLS size (*z-average*) to the size of the ND core. Elemental analysis confirmed that no silica was present in these samples that were clearly also structurally different from the silica-coated samples. The silica precursor amount was, thus,

not the decisive parameter for tuning the coating thickness, as was expected based on knowledge of coating of non-porous silica.[458,459] Instead any amount exceeding the critical CTAB/TEOS value 30 mg/60 µL resulted in formation of equally sized particles.

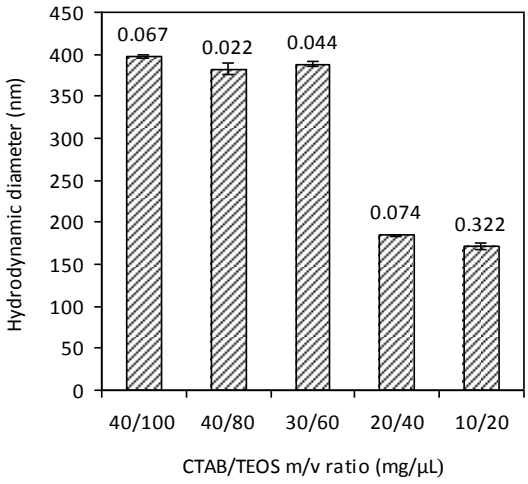

Figure 42. *DLS size of ND-1@MSN, synthesized with varying CTAB/ TEOS amounts. Error bars are SD; n=3. PdI values are given above the columns.*

Given the fact that co-solvents affect the formation of pristine MSN synthesized by the Stöber method,[86] the water-to-ethanol ratio of the reaction solution was expected to influence particle size and morphology. Since ethanol is also produced as a result of alcohol condensation during silica polymerization, the addition of ethanol causes the chemical equilibrium of the reaction to shift, consequently reducing the reaction rate. This in turn reduces the high surface curvature energy at the nanosized core particle, thus facilitating formation of curved morphologies.[184] A range of samples displayed in *Figure 43* were synthesized using different H_2O/EtOH ratios in order to investigate its influence on the silica coating thickness. The particle size was analyzed by DLS, and furthermore investigated by SEM and TEM, the two latter also for the purpose of studying the morphology and pore structure of the samples. The particles show a decreasing size trend upon increased H_2O/EtOH ratio. The SEM images also revealed a systematic size decrease of the spherical particles (*Figure 43*a & c) until a point where larger irregular particles start to form (*Figure 43*e & g). The corresponding HRTEM images indicated that thinning of the silica layer resulted in formation of separate silica spheres due to self-nucleation of excess precursor molecules. The irregularity of the larger composite NPs with thin silica layers (*Figure 43f & h*) also seemed a result of the irregular shape of the core. The applicable coating thickness range (within the limits of the study) reached from ~90 nm for the lowest H_2O/EtOH ratio value to a coating thickness of ~45 nm of the core structures with an average size of 80 nm. The coating thickness was, thus, limited to approximately the size of the core radius.

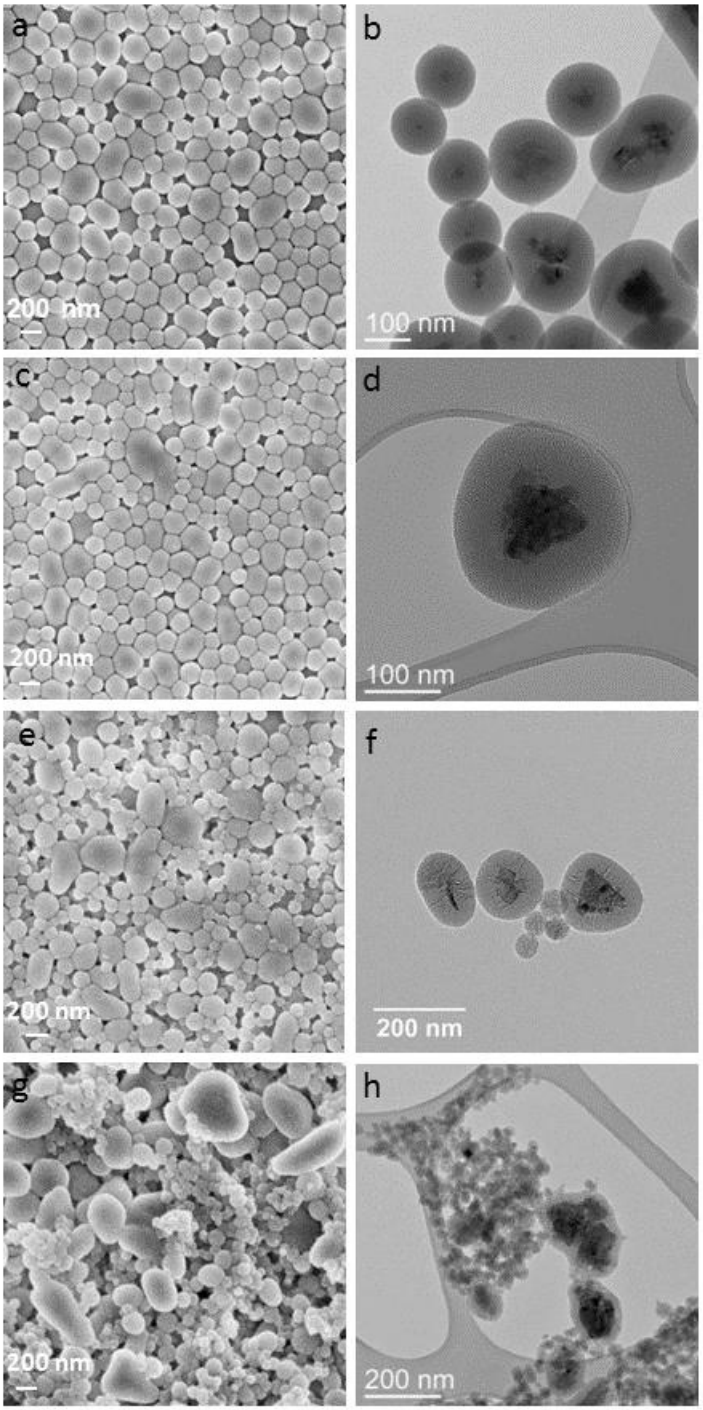

Figure 43. *SEM and corresponding TEM images of selected ND-1@MSN samples, with increasing H_2O/EtOH ratio starting from the lowest at a) & b).*

3.4 Hosting of hydrophobic molecules

The fluorescent hydrophobic dye DiI that had previously be established as a well-suited model substance for highly water-insoluble drugs **(Publication I)** was adsorbed to the particle in order to investigate the cargo-carrying capacity of our composite NP (ND@MSN). An ND@MSN sample with the average particle size 200 nm was loaded with DiI, successively adding dye until complete adsorption was no longer observed. Spectrophotometric quantification of adsorbed dye revealed a loading degree of 110 wt% in respect to total particle mass (DiI/ND@MSN). In contrast, direct adsorption of dye to ND cores resulted in a loading degree of 1 wt%, clearly displaying the huge advantage of mesoporous silica as a drug-carrying matrix over conventional direct adsorption to NDs. Naturally the adsorptive properties of silica will vary depending on the physicochemical characteristics of the loaded compound. For confirmation, a range of hydrophobic drugs was adsorbed under the same loading conditions. The obtained results showed similar loading degrees (>100 wt%) as for the model drug. Drug loading by direct adsorption to ND cores has commonly been used as the loading strategy of NDs intended for drug delivery.[460,461] Based on the above-presented results our ND@MSN composite NP can be considered a significant improvement in ND-based drug delivery, both in terms of drug-carrying capacity and carrier uniformity.

3.5 Photoluminescence of nanodiamonds

In order to confirm the functionality of the ND core and our core-shell design PL measurements of two ND samples of different origin, ND-1 and ND-2, were performed. *Figure 44* shows the PL spectra for both samples and their corresponding composite ND@MSN excited at 488 nm. High bulk PL from active neutral (NV^0) and negatively charged (NV^-) vacancy color centers in *Figure 44a* of ND-1, typical of such NDs, produced from a mixture of graphite and hexogen,[146] display ZPLs at 576 nm and 639 nm, respectively. The PL spectrum of ND-2 (produced from a mixture of trinitrotoluene and hexogen) (*Figure 44b*) consisted of a broad featureless band with a maximum PL around 600 nm, which is typical of detonation ND and can be assigned to surface defects.[166,171] The bulk PL of ND-1 was not affected by silica coating, while the surface PL was in fact enhanced by 30% as a result of silica coating. This confirms that coating NDs with silica does not impair the luminescent properties of the core, but can instead enhance them, in addition to acting as a protective shield in potentially damaging environments. PL stability measurements moreover confirmed excellent stability of the ND probes, showing no deterioration following silica coating.

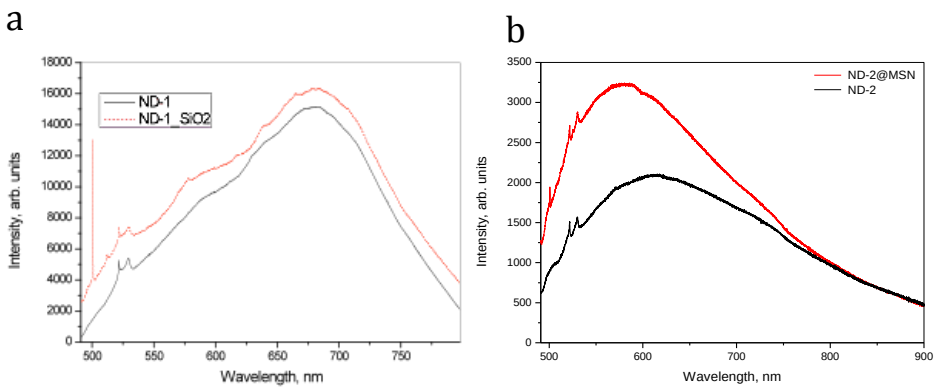

Figure 44. *PL spectra of ND-1 and ND-2 recorded at 488 nm laser excitation at RT. a) PL spectra of ND-1 and ND-1@MSN. The Raman diamond line, and ZPL of NV^0 and NV^- are indicated by arrows at 522 nm, 576 nm, and 639 nm, respectively. b) PL spectra of ND-2 and ND-2@MSN.*

3.6 Intracellular uptake and localization

Electron-irradiated HPHT-synthesized ND cores exhibiting bright PL were used for studying the intracellular uptake and localization of NDs and its composites in HeLa cells. The optical detectability of composite ND@MSN was studied using standard confocal microscopy. In addition to the composite's fluorescent signal, which was detected over a range of 650-730 nm a fairly strong reflection signal at 500-550 nm could also be recorded (*Figure 45*), thus, providing an alternative option for localization of the fluorescent probe. In accordance with previously published data,[168] NDs were found to be suitable labels for super-resolution STED imaging, the technique demonstrating superior resolution of individual NV centers as compared to conventional confocal microscopy. STED microscopy could thereby be a valuable method for intracellular tracking and investigation of cell fate of ND-based NPs. Since biocompatibility is the basis for any NP system intended for biomedical use, it should be evaluated after each separate system modification. Toxicity evaluation of ND and its composites showed low toxicity to cells at a concentration of 10 mg/mL, which was the concentration used in all cell-based experiments. These results affirm previously published statements of NDs being biocompatible in terms of cell viability and cytotoxicity *in vitro*[152,462–465] and *in vivo*.[151] Furthermore silica is regarded as safe in biological context[16] and capable even of enhancing the biocompatibility of other materials.[28]

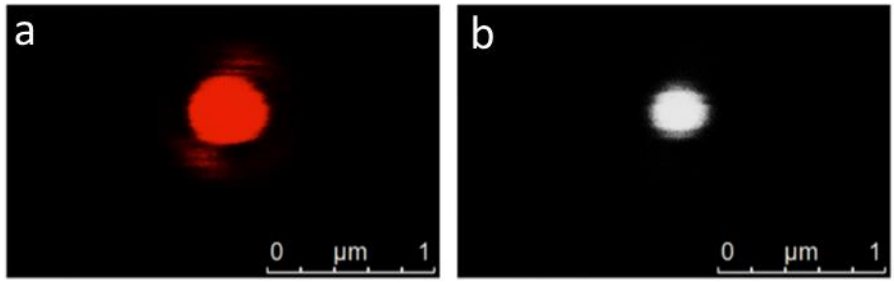

Figure 45. *Confocal microscopy images of ND@MSN. a) Reflection signal in red (500-550 nm) and b) PL signal in grayscale (650-730 nm).*

The intracellular uptake of ND and its composites ND@MSN and copolymer-coated ND@MSN@cop in HeLa cancer cells was investigated by confocal microscopy. An emission signal at 650-730 nm was clearly distinguishable from all samples, indicating efficient particle uptake after 6h (*Figure 46*). Stronger emission intensity/cell was recorded for the composite NPs, than for pure ND, clearly demonstrating the potential of these composite NPs as labeling probes for bioimaging and intracellular tracking purposes. Larger aggregates of ND@MSN were seen probably as a result of compartmentalization inside endosomal vesicles. A strong, and more evenly distributed emission signal was seen especially for ND@MSN@cop that seemed to be localized throughout the cytoplasm. This may be owing to the PEG-PEI copolymer coating, which enhances cellular uptake and promotes endosomal escape by the endosomal membrane-destabilizing capacity of PEI at acidic pH (4-6).[248] As most drugs require delivery into the cell cytoplasm, such a composite NP can, thus, by promoting endosomal escape or at least preventing particle aggregation, potentially serve as an efficient probe for combined intracellular tracking and drug delivery.

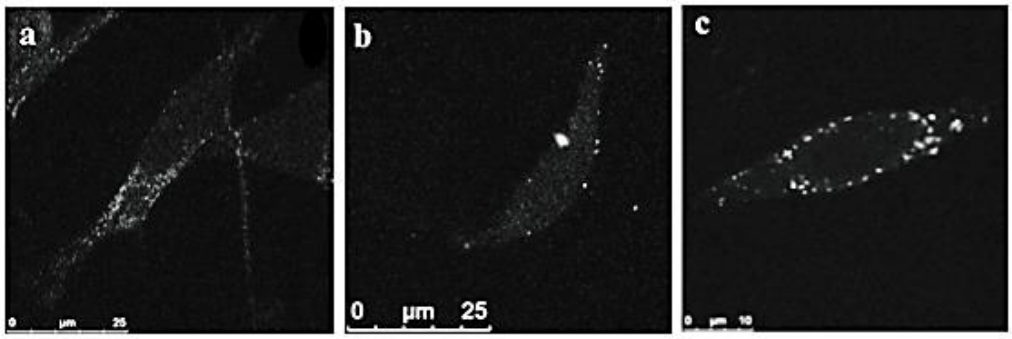

Figure 46. *PL from fixed HeLa cells incubated with a) ND, b) ND@MSN and c) ND@MSN@cop. (Ex. 488 nm; Em. 650– 730 nm).*

Subcellular localization by TEM found composite NPs to be localized inside endosomal vesicles throughout the cell 48 h following incubation. Opening of the cell membrane upon particle uptake in vesicular bodies, followed by movement across the cytoplasm and aggregation into multivesicular bodies can be seen in *Figure 47*. The resemblance of these structures to internalized ND cores was very high, suggesting that the ND cores were collected in the multivesicular bodies, from which they were unable to escape, whereas the coating had degraded, whereupon potential cargo molecules would have been released.

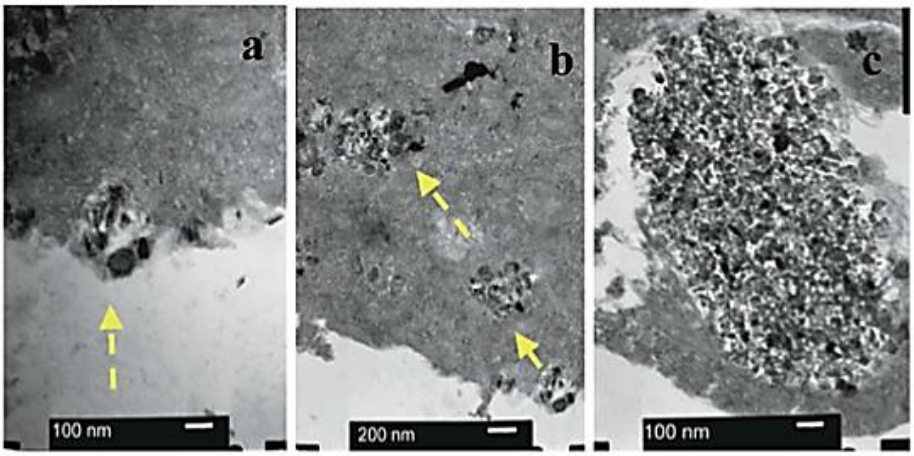

Figure 47. *Intracellular uptake and trafficking of ND@MSN@cop in thin sections of HeLa cells imaged by TEM. a) Opening of the plasma membrane to internalize the composite NP (indicated by arrow) present in the extracellular space. b) Illustration of the movement (indicated by arrows) of internalized ND@MSN@cop across the cytoplasm. c) Large multivesicular body of aggregated particles at 48 h.*

3.7 Intracellular delivery and release of hydrophobic cargo

Live cell imaging of dye-loaded (2.5 wt% DiI) composite NPs ND@MSN/DiI and ND@MSN@cop/DiI was performed over a period of 72 h in order to investigate the intracellular uptake efficiency and cargo-release from the nanocomposites. *Figure 48* demonstrates efficient uptake of the ND@MSN@cop/DiI sample (*Figure 48b*), seen as green ND cores and intracellular release of red DiI dye. Whereas the ND signal was localized to intracellular compartments (dotted pattern), the DiI dye was disseminated throughout the cells. Cells incubated with the ND@MSN/DiI particle, lacking copolymer coating and corresponding amounts of free dye show slight uptake (*Figure 48c & d*). The polymer coating prevents aggregation, enhances intracellular uptake and promotes intracellular release of cargo into the cytoplasm through endosomal escape. In sharp contrast, ND@MSN/DiI tended

to form aggregates in the cell medium, leading to decreased uptake efficiency. Regardless of the hydrophilicity of the silica coating, the adsorbed hydrophobic payload renders the particle hydrophobic, thus, impairing its ability to permeate over the cell membrane. Quantitative determination of uptake with confocal microscopy and flow cytometry corroborated the above-mentioned results, highlighting the superior uptake efficiency of composite NPs as compared to free dye. However, since lipophilic carbocyanine dyes such as DiI are commonly used as membrane stains, some degree of uptake of free dye, mainly in the plasma membrane, can be expected.

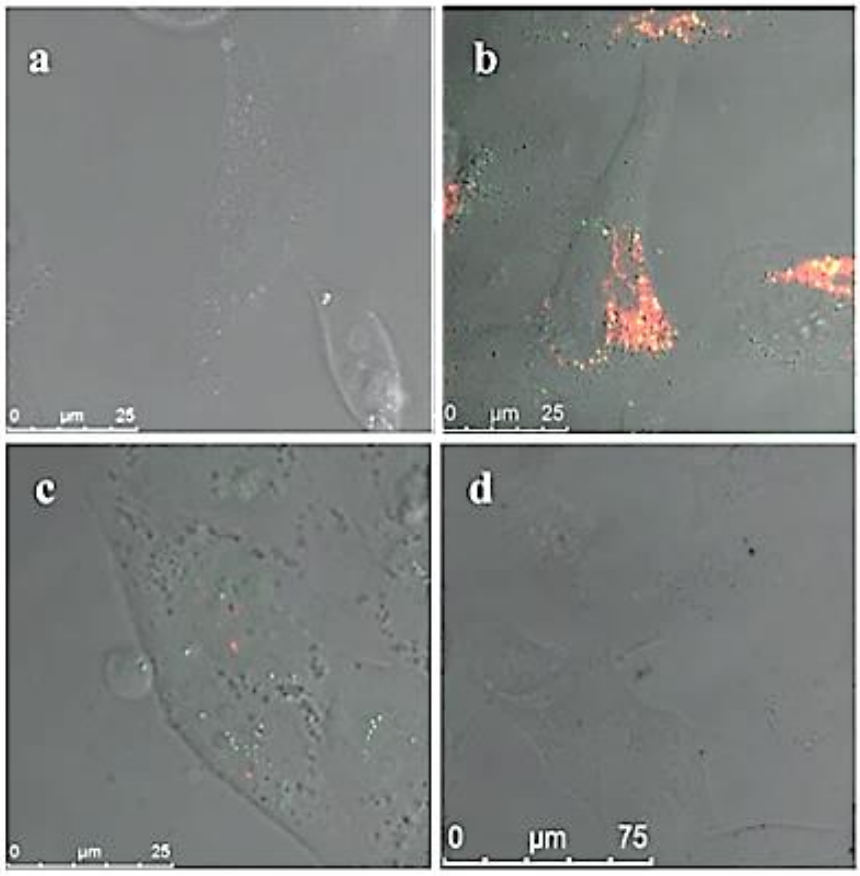

Figure 48. *Microscopic evaluation of intracellular delivery efficacy by measuring DiI fluorescence after particle (loaded with 2.5 wt% DiI) incubation in HeLa cells for 72 h. a) Control cell, b) ND@MSN@cop/DiI, c) ND@MSN/DiI, and d) DiI. Red channel shows DiI emission, green/yellow a reflection from ND cores and grey- scale was set to show transmission signal.*

3.8 Summary of results

Successful coating of PL NDs with uniform layers of mesoporous silica through a one-step coating procedure was demonstrated. The thickness of the silica layer could be varied, allowing tuning of the composite particle size over a broad range. PL from NV-color centers was detectable by spectrophotometric measures also after silica coating. The silica coating did thus not impair the PL properties of the ND core, but could instead serve as a protective layer. The composite NPs were capable of carrying their own weight of hydrophobic cargo (100 wt%), in apparent contrast to ND cores, which had a loading-capacity of 1 wt%. Surface-modification with a PEG-PEI copolymer enabled intracellular uptake of the cargo-containing composite NPs and subsequent release of cargo into the cytosol. The ND cores, however, remained inside intracellular vesicles and were aggregated into multivesicular bodies. Both NDs and cargo molecules were detectable by optical imaging techniques and readily distinguishable in the intracellular environment. The final fate of the NDs was not investigated in the presented study. We, however, note that ND exocytosis and subsequent excretion from the body following intracellular drug release would naturally be necessary for the applicability of such a drug delivery system. A few publications report very limited exocytosis and excretion of NDs,[466,467] while others have found them to distribute in lung, spleen and liver, with subsequent excretion into the urinary tract after intravenous administration[468]. Several publications also report low ND toxicity, both *in vitro* and *in vivo* regardless of cell or organ accumulation.[469] Although these results seem promising, it is important to keep in mind that the biobehavior of NDs may vary greatly depending on physicochemical characteristics and administration route. As the data on this subject is still quite scarce, and the result somewhat inconsistent, it is without doubt an area of research that needs to be further investigated.

CONCLUSIONS AND OUTLOOK

The rational design and characterization of multifunctional mesoporous silica-based NPs have been presented with focus on developing a biodegradable and efficient DDS with bright and stable fluorescence, tunable properties and predictable biobehavior for theranostic applications. For future control and prediction of the biobehavior of our DDS, the release mechanism of poorly water-soluble drugs and its relation to the degradation of the nanocarrier was established. The release of cargo was found to be dependent on both carrier degradation and the physicochemical properties of the cargo molecule in a given environment. For purely hydrophilic environments, the release of cargo was connected to the degradation of the nanocarrier, while in an intracellular setting, release occurred due to interactions between the cargo molecules and hydrophobic structures in the surrounding environment. For comparison, the intracellular uptake and release of hydrophobic cargo in relation to the biodegradation of PEGylated PACA NPs was studied. For these particles, the cargo release was strongly associated with the degradation of the nanocarrier, the behavior of which was closely related to its monomer composition. The obtained results elucidate the relationship between degradation and drug release behavior in the studied systems and highlight the importance of its understanding in order to enable better prediction and manipulation of the pharmacokinetics of DDSs.

To improve the applicability of our MSN-based DDS, core-shell structures of optically detectable and stable, PL ND cores coated with mesoporous silica (ND@MSN) were developed. Fluorescence from both NDs and their composites was optically detectable in live cancer cells. The surface composition of functional groups was found to crucially influence the dispersion stability and, consequently, also the intracellular uptake of the composite NPs. The efficient intracellular uptake and movement of these surface-functionalized composite NPs with subsequent release of cargo into the cytosol of cancer cells was readily detectable by optical microscopy. These results confirmed the feasibility of this novel core-shell composite as a probe for simultaneous intracellular imaging, tracing and drug delivery. Core-shell ND@MSNs with combined imaging and drug delivery functions, show great promise for theranostics. Moreover, additional surface-functionalization of such NPs to develop so called stimuli-responsive DDSs that react on an external stimulus to release the active compound, and modification with active targeting molecules, could naturally further enhance their efficacy and applicability. As for any DDS, the complete degradation and excretion of all degradation products, without cytotoxic effects or organ accumulation would

naturally be the ultimate aim. The knowledge of these processes concerning diamond nanostructures is, however, still scarce and would therefore certainly be an interesting aspect of future studies. Hence, further *in vitro* and *in vivo* research regarding the biocompatibility of NDs is still required before their full biomedical potential can be realized.

Although significant progress within the field of nanomedicine has been made during the last three decades, only a few cancer-targeted DDSs have to date been approved for clinical use. Moreover, a recent literature survey published by Wilhelm *at al.* showed that, on average, only 0.7% of the injected dose of IV administered NPs accumulated in tumor tissue.[470] Is this low number reason for concern, and what is the reason for the poor translation of nanomedicines? From a clinical perspective, the accumulated percent of the injected dose is not necessarily the most important aspect for patient benefit. Rather, improving the balance between on- and off-target accumulation plays a greater role, as it ultimately improves quality of life of the patient. Thus, instead of focusing on targeting as such, more attention should be payed to developing and improving nanocarrier-based drug formulations, combination therapies and patient selection protocols, in order to improve clinical translation. The main reason for the poor translation of nanomedicines may be the lack of "true" interdisciplinarity within the field, to drive the collective progress. Multifunctional theranostic nanocarriers can perhaps promise improved chemotherapies by enabling better patient selection through diagnostic screening and by offering improved therapeutic efficiency-to-toxicity ratios. However, for the overall goal to be realized, and in order for materials chemistry, colloid science and nanotechnology to continue contributing to the development of nanomedicine, better integration with biology, pharmacology, immunology and clinical needs is required. A joined technological push and clinical pull, strengthened by proof of efficacy and safety in biological systems are thus needed for achieving efficient clinical translation of new nanomedicines.

ACKNOWLEDGEMENTS

Completing a PhD thesis and achieving good results demand hard work, persistence and patience, good teamwork and communication, and every now and then a kind helping hand from a random someone. There are numerous people, to whom I am grateful for supporting me along my PhD journey. First of all, I would like to express my gratitude towards Adjunct Prof. Hélder A. Santos and Prof. Dr. Dr. Twan Lammers for the time and effort put in, reviewing my thesis and, in particular, Prof. Lennart Bergström for agreeing to act as my opponent.

During my PhD studies, I have had the good fortune of working under the watching eyes of Prof. Jessica Rosenholm. Thank you for taking me along for the ride from FyKe to Biocity and for allowing me to complete my PhD thesis at the Pharmaceutical Sciences Laboratory under your supervision. I'm very grateful for the freedom you have given me to shape my own research, to develop into a confident and independent researcher, yet always staying close by, ready to help in case of emergency. Thank you for always keeping your office door open, for eagerly sharing your knowledge and for having such good patience and of course, for laughing a lot and for being also a friend. I want to thank the entire Bionanomaterials group, especially Tina, Didem, Neeraj, and Diti for creating a positive and prosperous work environment.

Of course, I also want to thank Prof. Jouko Peltonen and the whole Laboratory of Physical Chemistry for the years on Gado's 3rd floor and for being the FyKe family you are. A special thanks goes out to our lab engineer Kenneth "Kena" Stenlund for always trying to make our lives a little bit easier and safer, for all the technical help and support you've given me, no matter the issue or time of day, and for always greeting me with a smile.

For an incredibly inspiring, enlightening and memorable research period at the Biophysics Department at NTNU in Trondheim, I sincerely thank Prof. Catharina de Lange Davies and her team. I am immensely grateful for getting to be part of your team and for learning so many new and exciting things over a relatively short time. I also especially want to thank Andreas Åslund for being a huge inspiration, research mastermind, scientific partner in crime, big brother and friend to me.

Furthermore, I'd like to collectively thank all of my co-authors for your collaboration and contribution to our joint work and publications.

Naturally, there are also several organizations and societies, whose economic support has made it possible for me to proceed with and complete my doctoral degree. For this, I want to thank the Academy of Finland, Alfred Kordelinin Säätiö (Suomalaisten Kemistien Seura), Waldemar von Frenkells

Stiftelse, Magnus Ehrnrooths Stiftelse, the Rector of Åbo Akademi University, Tekniikan Edistämissäätiö and the Finnish Pharmaceutical Society.

As if a PhD in itself isn't hard enough, I in parallel played American football (far beyond hobby level) for the whole duration of my PhD studies. It sure felt like an almost impossible equation at times, but in retrospect I'm sure I would never have succeeded in one without the other. It has brought me more value, both as a person and as a researcher, than it ever claimed in time or energy. I owe a huge thanks to all my teammates, coaches, organizations; everyone I've met involved in American football. You have taught me selfless team work, given me the mental strength and courage to test and exceed my limits, taught me that bruises are inevitable if you want to succeed and that only the restrictions I put on myself are the ones that hold me back.

I also want to thank my amazing friends for your encouragement and for all the non-scientific discussions, laughs, trips, dinners and wine bottles we've shared over the years. What would I do without you? And Eetu: Thank you for being not only the best, but the only *pludi* a girl can have!

Finally, I want to thank my family. Mom and Dad, even if you probably have very little idea of what I'm *actually* doing, and may still think I'm studying organic chemistry ;), and though you are my worst critics, you also are, and always have been, my best supporters. Thank you for putting up with my excessive babble about everything and nothing, my stubbornness and "sometimes" bad temper, for believing in my potential, for cheering with me when I succeed and for kicking my butt to push me further when I don't and for never letting me walk on there where the fence is lowest. I'm truly grateful for all the support and the toolbox of life skills you've given me. Anna and Soffi! No words could ever express my love, gratitude, and admiration for you. You are everything sisters should be: the craziest, most awesome, and most annoying people that make everything in life just **THAT** much better!

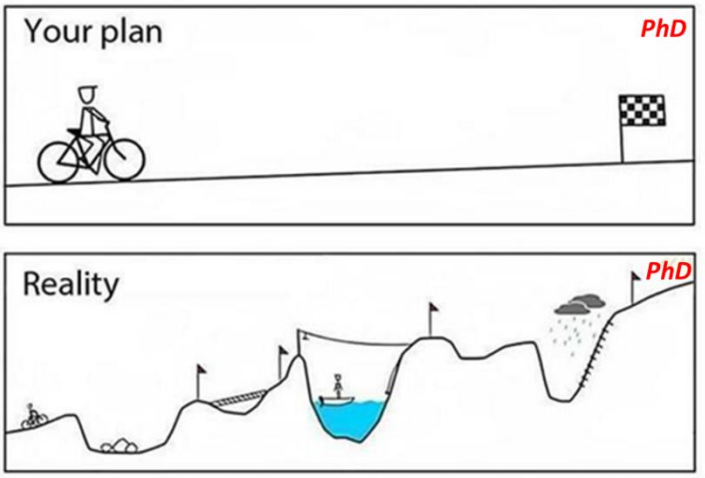

REFERENCES

(1) Emerich, D. F. Nanomedicine – Prospective Therapeutic and Diagnostic Applications. *Expert Opin. Biol. Ther.* **2005**, *5* (1), 1–5.

(2) Moghimi, S. M. Nanomedicine: Current Status and Future Prospects. *FASEB J.* **2005**, *19* (3), 311–330.

(3) Riehemann, K.; Schneider, S. W.; Luger, T. A.; Godin, B.; Ferrari, M.; Fuchs, H. Nanomedicine-Challenge and Perspectives. *Angew. Chem. Int. Ed.* **2009**, *48* (5), 872–897.

(4) Chow, E. K.-H.; Ho, D. Cancer Nanomedicine: From Drug Delivery to Imaging. *Sci. Transl. Med.* **2013**, *5* (216), 216rv4-216rv4.

(5) Niemeyer, C. M. Nanoparticles, Proteins, and Nucleic Acids: Biotechnology Meets Materials Science. *Angew Chem Int Ed* **2001**, *40*, 4128–4158.

(6) Chan, W. C. W. Bionanotechnology Progress and Advances. *Biol. Blood Marrow Transplant.* **2006**, *12* (1), 87–91.

(7) Nanotechnology 101 - What It Is and How It Works www.nano.gov (accessed Oct 31, 2016).

(8) Weissig, V.; Pettinger, T.; Murdock, N. Nanopharmaceuticals (Part 1): Products on the Market. *Int. J. Nanomedicine* **2014**, 4357.

(9) Goesmann, H.; Feldmann, C. Nanoparticulate Functional Materials. *Angew. Chem. Int. Ed.* **2010**, *49* (8), 1362–1395.

(10) Mirza, A. Z.; Siddiqui, F. A. Nanomedicine and Drug Delivery: A Mini Review. *Int. Nano Lett.* **2014**, *4* (1).

(11) Owen, A.; Rannard, S.; Bawa, R.; Feng, S.-S. Interdisciplinary Nanomedicine Publications through Interdisciplinary Peer-Review. *J. Interdiscip. Nanomedicine* **2016**, *1* (1), 4–8.

(12) *Handbook of Clinical Nanomedicine: Nanoparticles, Imaging, Therapy, and Clinical Applications*; Bawa, R., Audette, G. F., Rubinstein, I., Eds.; CRC, Taylor & Francis: Boca Raton, FL, USA, 2015; Vol. Pan Stanford Series on Nanomedicine Vol. 1.

(13) Saad, M. Receptor-Targeted Nanocarriers for Tumor Specifictreatment and Imaging. **2008**.

(14) Iler, R. K. *The Chemistry of Silica: Solubility, Polymerization, Colloid and Surface Properties, and Biochemistry*; Wiley: New York, 1979.

(15) Lee, J. E.; Lee, N.; Kim, T.; Kim, J.; Hyeon, T. Multifunctional Mesoporous Silica Nanocomposite Nanoparticles for Theranostic Applications. *Acc. Chem. Res.* **2011**, *44* (10), 893–902.

(16) Barbé, C.; Bartlett, J.; Kong, L.; Finnie, K.; Lin, H. Q.; Larkin, M.; Calleja, S.; Bush, A.; Calleja, G. Silica Particles: A Novel Drug-Delivery System. *Adv. Mater.* **2004**, *16* (21), 1959–1966.

(17) Desai, D.; Karaman, D. S.; Prabhakar, N.; Tadayon, S.; Duchanoy, A.; Toivola, D. M.; Rajput, S.; Näreoja, T.; Rosenholm, J. M. Design Considerations for Mesoporous Silica Nanoparticulate Systems in Facilitating Biomedical Applications. *Mesoporous Biomater.* **2014**, *1* (1), 16–43.

(18) Zhang, J.; Rosenholm, J. M. The Viability of Mesoporous Silica Nanoparticles for Drug Delivery. *Ther. Deliv.* **2015**, *6* (8), 891–893.

(19) Mamaeva, V.; Rosenholm, J. M.; Bate-Eya, L. T.; Bergman, L.; Peuhu, E.; Duchanoy, A.; Fortelius, L. E.; Landor, S.; Toivola, D. M.; Lindén, M.; Sahlgren, C. Mesoporous Silica Nanoparticles as Drug Delivery Systems for Targeted Inhibition of Notch Signaling in Cancer. *Mol. Ther. J. Am. Soc. Gene Ther.* **2011**, *19* (8), 1538–1546.

(20) Crespy, D.; Landfester, K. Miniemulsion Polymerization as a Versatile Tool for the Synthesis of Functionalized Polymers. *Beilstein J. Org. Chem.* **2010**, *6*, 1132–1148.

(21) Kumari, A.; Yadav, S. K.; Yadav, S. C. Biodegradable Polymeric Nanoparticles Based Drug Delivery Systems. *Colloids Surf. B Biointerfaces* **2010**, *75* (1), 1–18.

(22) Andrieux, K.; Couvreur, P. Polyalkylcyanoacrylate Nanoparticles for Delivery of Drugs across the Blood-Brain Barrier. *Wiley Interdiscip. Rev. Nanomed. Nanobiotechnol.* **2009**, *1* (5), 463–474.

(23) M. Rosenholm, J.; Sahlgren, C.; Linden, M. Multifunctional Mesoporous Silica Nanoparticles for Combined Therapeutic, Diagnostic and Targeted Action in Cancer Treatment. *Curr. Drug Targets* **2011**, *12* (8), 1166–1186.

(24) Chang, Y.-R.; Lee, H.-Y.; Chen, K.; Chang, C.-C.; Tsai, D.-S.; Fu, C.-C.; Lim, T.-S.; Tzeng, Y.-K.; Fang, C.-Y.; Han, C.-C.; Chang, H.-C.; Fann, W. Mass Production and Dynamic Imaging of Fluorescent Nanodiamonds. *Nat. Nanotechnol.* **2008**, *3* (5), 284–288.

(25) Boudou, J.-P.; Curmi, P. A.; Jelezko, F.; Wrachtrup, J.; Aubert, P.; Sennour, M.; Balasubramanian, G.; Reuter, R.; Thorel, A.; Gaffet, E. High Yield Fabrication of Fluorescent Nanodiamonds. *Nanotechnology* **2009**, *20* (23), 235602.

(26) Baker, M. Nanotechnology Imaging Probes: Smaller and More Stable. *Nat. Methods* **2010**, *7* (12), 957–962.

(27) Guerrero-Martínez, A.; Pérez-Juste, J.; Liz-Marzán, L. M. Recent Progress on Silica Coating of Nanoparticles and Related Nanomaterials. *Adv. Mater.* **2010**, *22* (11), 1182–1195.

(28) Ghosh Chaudhuri, R.; Paria, S. Core/Shell Nanoparticles: Classes, Properties, Synthesis Mechanisms, Characterization, and Applications. *Chem. Rev.* **2012**, *112* (4), 2373–2433.

(29) Sahoo, S. K.; Parveen, S.; Panda, J. J. The Present and Future of Nanotechnology in Human Health Care. *Nanomedicine Nanotechnol. Biol. Med.* **2007**, *3* (1), 20–31.

(30) *Nanomaterials Handbook*; Gogotsi, Y., Ed.; CRC/Taylor & Francis: Boca Raton, 2006.

(31) Cao, G.; Wang, Y. *Nanostructures & Nanomaterials: Synthesis, Properties, and Applications*, 2nd ed.; World scientific series in nanoscience and nanotechnology; World Scientific: New Jersey, 2011.

(32) Guo, Z.; Tan, L. *Fundamentals and Applications of Nanomaterials*; Artech House nanoscale science and engineering; Artech House: Boston, 2009.

(33) Ageitos, J. M.; Chuah, J.-A.; Numata, K. Chapter 1. Design Considerations for Properties of Nanocarriers on Disposition and Efficiency of Drug and Gene Delivery. In *RSC Drug Discovery*; Braddock, M., Ed.; Royal Society of Chemistry: Cambridge, 2016; pp 1–22.

(34) *Understanding Nanotechnology: From the Editors of Scientific American*; Fritz, S., Scientific American, inc, Eds.; Science made accessible; Warner Books: New York, 2002.

(35) Shaffer, C. Nanomedicine Transforms Drug Delivery. *Drug Discov. Today* **2005**, *10* (23–24), 1581–1582.

(36) Emerich, D. F.; Thanos, C. G. Nanotechnology and Medicine. *Expert Opin. Biol. Ther.* **2003**, *3* (4), 655–663.

(37) Klabunde, K. J. *Nanoscale Materials in Chemistry*; Wiley-Interscience: New York, 2001.

(38) Zhang, J. Z.; Noguez, C. Plasmonic Optical Properties and Applications of Metal Nanostructures. *Plasmonics* **2008**, *3* (4), 127–150.

(39) Liu, J.-H.; Yang, S.-T.; Chen, X.-X.; Wang, H. Fluorescent Carbon Dots and Nanodiamonds for Biological Imaging: Preparation, Application, Pharmacokinetics and Toxicity. *Curr. Drug Metab.* **2012**, *13* (8), 1046–1056.

(40) Gupta, A. K.; Gupta, M. Synthesis and Surface Engineering of Iron Oxide Nanoparticles for Biomedical Applications. *Biomaterials* **2005**, *26* (18), 3995–4021.

(41) Roduner, E. *Nanoscopic Materials: Size-Dependent Phenomena*; RSC nanoscience & nanotechnology; RSC Pub: Cambridge, 2006.

(42) Lin, C.-A. J.; Liedl, T.; Sperling, R. A.; Fernández-Argüelles, M. T.; Costa-Fernández, J. M.; Pereiro, R.; Sanz-Medel, A.; Chang, W. H.; Parak, W. J. Bioanalytics and Biolabeling with Semiconductor Nanoparticles (Quantum Dots). *J Mater Chem* **2007**, *17* (14), 1343–1346.

(43) de Farias, P. M. A.; Santos, B. S.; Menezes, F. D.; Brasil Jr., A. G.; Ferreira, R.; Motta, M. A.; Castro-Neto, A. G.; Vieira, A. A. S.; Silva, D. C. N.; Fontes, A.; Cesar, C. L. Highly Fluorescent Semiconductor Core–shell CdTe–CdS Nanocrystals for Monitoring Living Yeast Cells Activity. *Appl. Phys. A* **2007**, *89* (4), 957–961.

(44) Oberdörster, G.; Oberdörster, E.; Oberdörster, J. Nanotoxicology: An Emerging Discipline Evolving from Studies of Ultrafine Particles. *Environ. Health Perspect.* **2005**, *113* (7), 823–839.

(45) Vasir, J.; Reddy, M.; Labhasetwar, V. Nanosystems in Drug Targeting: Opportunities and Challenges. *Curr. Nanosci.* **2005**, *1* (1), 47–64.

(46) Kim, J.; Lee, J. E.; Lee, J.; Yu, J. H.; Kim, B. C.; An, K.; Hwang, Y.; Shin, C.-H.; Park, J.-G.; Kim, J.; Hyeon, T. Magnetic Fluorescent Delivery Vehicle Using Uniform Mesoporous Silica Spheres Embedded with Monodisperse Magnetic and Semiconductor Nanocrystals. *J. Am. Chem. Soc.* **2006**, *128* (3), 688–689.

(47) Kim, J.; Kim, H. S.; Lee, N.; Kim, T.; Kim, H.; Yu, T.; Song, I. C.; Moon, W. K.; Hyeon, T. Multifunctional Uniform Nanoparticles Composed of a Magnetite Nanocrystal Core and a Mesoporous Silica Shell for Magnetic Resonance and Fluorescence Imaging and for Drug Delivery. *Angew. Chem. Int. Ed.* **2008**, *47* (44), 8438–8441.

(48) Le Droumaguet, B.; Nicolas, J.; Brambilla, D.; Mura, S.; Maksimenko, A.; De Kimpe, L.; Salvati, E.; Zona, C.; Airoldi, C.; Canovi, M.; Gobbi, M.; Magali, N.; La Ferla, B.; Nicotra, F.; Scheper, W.; Flores, O.; Masserini, M.; Andrieux, K.; Couvreur, P. Versatile and Efficient Targeting Using a Single Nanoparticulate Platform: Application to Cancer and Alzheimer's Disease. *ACS Nano* **2012**, *6* (7), 5866–5879.

(49) Chen, Y.; Yin, Q.; Ji, X.; Zhang, S.; Chen, H.; Zheng, Y.; Sun, Y.; Qu, H.; Wang, Z.; Li, Y.; Wang, X.; Zhang, K.; Zhang, L.; Shi, J. Manganese Oxide-Based Multifunctionalized Mesoporous Silica Nanoparticles for pH-Responsive MRI, Ultrasonography and Circumvention of MDR in Cancer Cells. *Biomaterials* **2012**, *33* (29), 7126–7137.

(50) Zimmer, J. P.; Kim, S.-W.; Ohnishi, S.; Tanaka, E.; Frangioni, J. V.; Bawendi, M. G. Size Series of Small Indium Arsenide–Zinc Selenide Core–Shell Nanocrystals and Their Application to In Vivo Imaging. *J. Am. Chem. Soc.* **2006**, *128* (8), 2526–2527.

(51) He, C.; Hu, Y.; Yin, L.; Tang, C.; Yin, C. Effects of Particle Size and Surface Charge on Cellular Uptake and Biodistribution of Polymeric Nanoparticles. *Biomaterials* **2010**, *31* (13), 3657–3666.

(52) Chithrani, B. D.; Ghazani, A. A.; Chan, W. C. W. Determining the Size and Shape Dependence of Gold Nanoparticle Uptake into Mammalian Cells. *Nano Lett.* **2006**, *6* (4), 662–668.

(53) Lin, W.; Huang, Y.; Zhou, X.-D.; Ma, Y. In Vitro Toxicity of Silica Nanoparticles in Human Lung Cancer Cells. *Toxicol. Appl. Pharmacol.* **2006**, *217* (3), 252–259.

(54) Slowing, I. I.; Trewyn, B. G.; Giri, S.; Lin, V. S.-Y. Mesoporous Silica Nanoparticles for Drug Delivery and Biosensing Applications. *Adv. Funct. Mater.* **2007**, *17* (8), 1225–1236.

(55) Slowing, I.; Vivero-Escoto, J.; Wu, C.; Lin, V. Mesoporous Silica Nanoparticles as Controlled Release Drug Delivery and Gene Transfection Carriers. *Adv. Drug Deliv. Rev.* **2008**, *60* (11), 1278–1288.

(56) Rieter, W. J.; Kim, J. S.; Taylor, K. M. L.; An, H.; Lin, W.; Tarrant, T.; Lin, W. Hybrid Silica Nanoparticles for Multimodal Imaging. *Angew. Chem. Int. Ed.* **2007**, *46* (20), 3680–3682.

(57) Jaganathan, H.; Godin, B. Biocompatibility Assessment of Si-Based Nano- and Micro-Particles. *Adv. Drug Deliv. Rev.* **2012**, *64* (15), 1800–1819.

(58) Chen, M.; Vonmikecz, A. Formation of Nucleoplasmic Protein Aggregates Impairs Nuclear Function in Response to SiO Nanoparticles. *Exp. Cell Res.* **2005**, *305* (1), 51–62.

(59) Garnett, M. C. Nanomedicines and Nanotoxicology: Some Physiological Principles. *Occup. Med.* **2006**, *56* (5), 307–311.

(60) Kang, S. H.; Dickey, M. D. Patterning via Self-Organization and Self-Folding: Beyond Conventional Lithography. *MRS Bull.* **2016**, *41* (02), 93–96.

(61) Sotiropoulou, S.; Sierra-Sastre, Y.; Mark, S. S.; Batt, C. A. Biotemplated Nanostructured Materials †. *Chem. Mater.* **2008**, *20* (3), 821–834.

(62) Schmitz-Antoniak, C. X-Ray Absorption Spectroscopy on Magnetic Nanoscale Systems for Modern Applications. *Rep. Prog. Phys.* **2015**, *78* (6), 062501.

(63) Feynman, R. There's Plenty of Room at the Bottom. *Caltech Eng. Sci.* **1960**, *23* (5), 22–36.

(64) Biswas, A.; Bayer, I. S.; Biris, A. S.; Wang, T.; Dervishi, E.; Faupel, F. Advances in Top–down and Bottom–up Surface Nanofabrication: Techniques, Applications & Future Prospects. *Adv. Colloid Interface Sci.* **2012**, *170* (1–2), 2–27.

(65) Niederberger, M. Nonaqueous Sol–Gel Routes to Metal Oxide Nanoparticles. *Acc. Chem. Res.* **2007**, *40* (9), 793–800.

(66) Cui, H.; Liu, Y.; Ren, W. Structure Switch between α-Fe2O3, γ-Fe2O3 and Fe3O4 during the Large Scale and Low Temperature Sol–gel Synthesis of Nearly Monodispersed Iron Oxide Nanoparticles. *Adv. Powder Technol.* **2013**, *24* (1), 93–97.

(67) Sui, R.; Charpentier, P. Synthesis of Metal Oxide Nanostructures by Direct Sol–Gel Chemistry in Supercritical Fluids. *Chem. Rev.* **2012**, *112* (6), 3057–3082.

(68) Caruso, F.; Spasova, M.; Susha, A.; Giersig, M.; Caruso, R. A. Magnetic Nanocomposite Particles and Hollow Spheres Constructed by a Sequential Layering Approach. *Chem. Mater.* **2001**, *13* (1), 109–116.

(69) Caruso, F.; Spasova, M.; Salgueiriño-Maceira, V.; Liz-Marzán, L. M. Multilayer Assemblies of Silica-Encapsulated Gold Nanoparticles on Decomposable Colloid Templates. *Adv. Mater.* **2001**, *13* (14), 1090–1094.

(70) Aslan, K.; Wu, M.; Lakowicz, J. R.; Geddes, C. D. Fluorescent Core−Shell Ag@SiO $_2$ Nanocomposites for Metal-Enhanced Fluorescence and Single Nanoparticle Sensing Platforms. *J. Am. Chem. Soc.* **2007**, *129* (6), 1524–1525.

(71) Ganguli, A. K.; Ganguly, A.; Vaidya, S. Microemulsion-Based Synthesis of Nanocrystalline Materials. *Chem Soc Rev* **2010**, *39* (2), 474–485.

(72) Boutonnet, M.; Kizling, J.; Stenius, P.; Maire, G. The Preparation of Monodisperse Colloidal Metal Particles from Microemulsions. *Colloids Surf.* **1982**, *5* (3), 209–225.

(73) Naoe, K.; Petit, C.; Pileni, M. P. Use of Reverse Micelles to Make Either Spherical or Worm-like Palladium Nanocrystals: Influence of Stabilizing Agent on Nanocrystal Shape. *Langmuir* **2008**, *24* (6), 2792–2798.

(74) Petit, C.; Lixon, P.; Pileni, M. P. Synthesis of Cadmium Sulfide in Situ in Reverse Micelles. 2. Influence of the Interface on the Growth of the Particles. *J. Phys. Chem.* **1990**, *94* (4), 1598–1603.

(75) Eastoe, J.; Hollamby, M. J.; Hudson, L. Recent Advances in Nanoparticle Synthesis with Reversed Micelles. *Adv. Colloid Interface Sci.* **2006**, *128–130*, 5–15.

(76) Yu, Y.; Che, B.; Si, Z.; Li, L.; Chen, W.; Xue, G. Carbon Nanotube/Polyaniline Core-Shell Nanowires Prepared by in Situ Inverse Microemulsion. *Synth. Met.* **2005**, *150* (3), 271–277.

(77) Xing, S.; Chu, Y.; Sui, X.; Wu, Z. Synthesis and Characterization of Polyaniline in CTAB/Hexanol/Water Reversed Micelle. *J. Mater. Sci.* **2005**, *40* (1), 215–218.

(78) Musumeci, T.; Ventura, C. A.; Giannone, I.; Ruozi, B.; Montenegro, L.; Pignatello, R.; Puglisi, G. PLA/PLGA Nanoparticles for Sustained Release of Docetaxel. *Int. J. Pharm.* **2006**, *325* (1–2), 172–179.

(79) Acharya, S.; Sahoo, S. K. PLGA Nanoparticles Containing Various Anticancer Agents and Tumour Delivery by EPR Effect. *Adv. Drug Deliv. Rev.* **2011**, *63* (3), 170–183.

(80) Krauel, K.; Davies, N. M.; Hook, S.; Rades, T. Using Different Structure Types of Microemulsions for the Preparation of Poly(alkylcyanoacrylate) Nanoparticles by Interfacial Polymerization. *J. Controlled Release* **2005**, *106* (1–2), 76–87.

(81) Vauthier, C.; Labarre, D.; Ponchel, G. Design Aspects of Poly(alkylcyanoacrylate) Nanoparticles for Drug Delivery. *J. Drug Target.* **2007**, *15* (10), 641–663.

(82) Elsabahy, M.; Wooley, K. L. Design of Polymeric Nanoparticles for Biomedical Delivery Applications. *Chem. Soc. Rev.* **2012**, *41* (7), 2545.

(83) *Sol-Gel Processing*; Kozuka, H., Ed.; Sakka, S., Series Ed.; Handbook of sol-gel science and technology Processing, Characterization and Applications; Kluwer Academic Publishers: Boston, 2005; Vol. 1.

(84) Stöber, W.; Fink, A.; Bohn, E. Controlled Growth of Monodisperse Silica Spheres in the Micron Size Range. *J. Colloid Interface Sci.* **1968**, *26* (1), 62–69.

(85) Liu, S.; Lu, L.; Yang, Z.; Cool, P.; Vansant, E. F. Further Investigations on the Modified Stöber Method for Spherical MCM-41. *Mater. Chem. Phys.* **2006**, *97* (2–3), 203–206.

(86) Yamada, Y.; Yano, K. Synthesis of Monodispersed Super-Microporous/Mesoporous Silica Spheres with Diameters in the Low Submicron Range. *Microporous Mesoporous Mater.* **2006**, *93* (1–3), 190–198.

(87) Kambara, K.; Shimura, N.; Ogawa, M. Larger Scale Syntheses of Surfactant-Templated Nanoporous Silica Spherical Particles by the Stöber Method. *J. Ceram. Soc. Jpn.* **2007**, *115* (1341), 315–318.

(88) Kobayashi, Y.; Katakami, H.; Mine, E.; Nagao, D.; Konno, M.; Liz-Marzán, L. M. Silica Coating of Silver Nanoparticles Using a Modified Stöber Method. *J. Colloid Interface Sci.* **2005**, *283* (2), 392–396.

(89) Gorelikov, I.; Matsuura, N. Single-Step Coating of Mesoporous Silica on Cetyltrimethyl Ammonium Bromide-Capped Nanoparticles. *Nano Lett.* **2008**, *8* (1), 369–373.

(90) He, Q.; Ma, M.; Wei, C.; Shi, J. Mesoporous Carbon@silicon-Silica Nanotheranostics for Synchronous Delivery of Insoluble Drugs and Luminescence Imaging. *Biomaterials* **2012**, *33* (17), 4392–4402.

(91) Xu, Z.; Gao, Y.; Huang, S.; Ma, P. an; Lin, J.; Fang, J. A Luminescent and Mesoporous Core-Shell Structured Gd2O3 : Eu3+@nSiO2@mSiO2 Nanocomposite as a Drug Carrier. *Dalton Trans.* **2011**, *40* (18), 4846.

(92) Kresge, C. T.; Leonowicz, M. E.; Roth, W. J.; Vartuli, J. C.; Beck, J. S. Ordered Mesoporous Molecular Sieves Synthesized by a Liquid-Crystal Template Mechanism. *Nature* **1992**, *359* (6397), 710–712.

(93) Beck, J. S.; Vartuli, J. C.; Roth, W. J.; Leonowicz, M. E.; Kresge, C. T.; Schmitt, K. D.; Chu, C. T. W.; Olson, D. H.; Sheppard, E. W.; McCullen, S. B.; Higgins, J. B.; Schlenker, J. L. A New Family of Mesoporous Molecular Sieves Prepared with Liquid Crystal Templates. *J. Am. Chem. Soc.* **1992**, *114* (27), 10834–10843.

(94) Hoffmann, F.; Cornelius, M.; Morell, J.; Fröba, M. Silica-Based Mesoporous Organic-Inorganic Hybrid Materials. *Angew. Chem. Int. Ed Engl.* **2006**, *45* (20), 3216–3251.

(95) Moliner, M. Direct Synthesis of Functional Zeolitic Materials. *ISRN Mater. Sci.* **2012**, *2012*, 1–24.

(96) Cundy, C. S.; Cox, P. A. The Hydrothermal Synthesis of Zeolites: History and Development from the Earliest Days to the Present Time. *Chem. Rev.* **2003**, *103* (3), 663–702.

(97) Grün, M.; Lauer, I.; Unger, K. K. The Synthesis of Micrometer- and Submicrometer-Size Spheres of Ordered Mesoporous Oxide MCM-41. *Adv. Mater.* **1997**, *9* (3), 254–257.

(98) Nooney, R. I.; Thirunavukkarasu, D.; Chen, Y.; Josephs, R.; Ostafin, A. E. Synthesis of Nanoscale Mesoporous Silica Spheres with Controlled Particle Size. *Chem. Mater.* **2002**, *14* (11), 4721–4728.

(99) Cai, Q.; Luo, Z.-S.; Pang, W.-Q.; Fan, Y.-W.; Chen, X.-H.; Cui, F.-Z. Dilute Solution Routes to Various Controllable Morphologies of MCM-41 Silica with a Basic Medium †. *Chem. Mater.* **2001**, *13* (2), 258–263.

(100) Cai, Q.; Cui, F. Z.; Chen, X. H.; Zhang, Y.; Luo, Z. S. Nanosphere of Ordered Silica MCM-41 Hydrothermally Synthesized with Low Surfactant Concentration. *Chem. Lett.* **2000**, No. 9, 1044–1045.

(101) Gulin-Sarfraz, T.; Sarfraz, J.; Didem Şen Karaman; Zhang, J.; Oetken-Lindholm, C.; Duchanoy, A.; Rosenholm, J. M.; Abankwa, D. FRET-Reporter Nanoparticles to Monitor Redox-Induced Intracellular Delivery of Active Compounds. *RSC Adv.* **2014**, *4* (32), 16429.

(102) von Haartman, E.; Jiang, H.; Khomich, A. A.; Zhang, J.; Burikov, S. A.; Dolenko, T. A.; Ruokolainen, J.; Gu, H.; Shenderova, O. A.; Vlasov, I. I.; Rosenholm, J. M. Core–shell Designs of Photoluminescent Nanodiamonds with Porous Silica Coatings for Bioimaging and Drug Delivery I: Fabrication. *J. Mater. Chem. B* **2013**, *1* (18), 2358.

(103) Graf, C.; Vossen, D. L. J.; Imhof, A.; van Blaaderen, A. A General Method To Coat Colloidal Particles with Silica. *Langmuir* **2003**, *19* (17), 6693–6700.

(104) Teng, Z.; Su, X.; Zheng, Y.; Sun, J.; Chen, G.; Tian, C.; Wang, J.; Li, H.; Zhao, Y.; Lu, G. Mesoporous Silica Hollow Spheres with Ordered Radial Mesochannels by a Spontaneous Self-Transformation Approach. *Chem. Mater.* **2013**, *25* (1), 98–105.

(105) Şen Karaman, D.; Gulin-Sarfraz, T.; Zhang, J.; Rosenholm, J. M. One-Pot Synthesis of Pore-Expanded Hollow Mesoporous Silica Particles. *Mater. Lett.* **2015**, *143*, 140–143.

(106) Brinker, C. J.; Scherer, G. W. *Sol-Gel Science: The Physics and Chemistry of Sol-Gel Processing*; Academic Press: Boston, 1990.

(107) Ostwald, W. *Lehrbuch Der Allgemeinen Chemie*; Leipzig, Germany, 1896; Vol. 2.

(108) Sing, K. S. W. Reporting Physisorption Data for Gas/Solid Systems with Special Reference to the Determination of Surface Area and Porosity (Recommendations 1984). *Pure Appl. Chem.* **1985**, *57* (4).

(109) Meynen, V.; Cool, P.; Vansant, E. F. Verified Syntheses of Mesoporous Materials. *Microporous Mesoporous Mater.* **2009**, *125* (3), 170–223.

(110) Huo, Q.; Margolese, D. I.; Ciesla, U.; Feng, P.; Gier, T. E.; Sieger, P.; Leon, R.; Petroff, P. M.; Schüth, F.; Stucky, G. D. Generalized Synthesis of Periodic Surfactant/Inorganic Composite Materials. *Nature* **1994**, *368* (6469), 317–321.

(111) Huo, Q.; Margolese, D. I.; Ciesla, U.; Demuth, D. G.; Feng, P.; Gier, T. E.; Sieger, P.; Firouzi, A.; Chmelka, B. F. Organization of Organic Molecules with Inorganic Molecular Species into Nanocomposite Biphase Arrays. *Chem. Mater.* **1994**, *6* (8), 1176–1191.

(112) Lin, H.-P.; Mou, C.-Y. Structural and Morphological Control of Cationic Surfactant-Templated Mesoporous Silica. *Acc. Chem. Res.* **2002**, *35* (11), 927–935.

(113) Broekhoff, J. C. P. Mesopore Determination from Nitrogen Sorption Isotherms: Fundamentals, Scope, Limitations. In *Studies in Surface Science and Catalysis*; Elsevier, 1979; Vol. 3, pp 663–684.

(114) Nagarajan, R. Molecular Packing Parameter and Surfactant Self-Assembly: The Neglected Role of the Surfactant Tail †. *Langmuir* **2002**, *18* (1), 31–38.

(115) Rosen, M. J.; Kunjappu, J. T. *Surfactants and Interfacial Phenomena*, 4th ed.; Wiley: Hoboken, N.J, 2012.

(116) Singh, L. P.; Bhattacharyya, S. K.; Mishra, G.; Ahalawat, S. Functional Role of Cationic Surfactant to Control the Nano Size of Silica Powder. *Appl. Nanosci.* **2011**, *1* (3), 117–122.

(117) ALOthman, Z. A Review: Fundamental Aspects of Silicate Mesoporous Materials. *Materials* **2012**, *5* (12), 2874–2902.

(118) Liu, C.; Wang, X.; Lee, S.; Pfefferle, L. D.; Haller, G. L. Surfactant Chain Length Effect on the Hexagonal-to-Cubic Phase Transition in Mesoporous Silica Synthesis. *Microporous Mesoporous Mater.* **2012**, *147* (1), 242–251.

(119) Zhang, J.; Li, X.; Rosenholm, J. M.; Gu, H. Synthesis and Characterization of Pore Size-Tunable Magnetic Mesoporous Silica Nanoparticles. *J. Colloid Interface Sci.* **2011**, *361* (1), 16–24.

(120) Kruk, M.; Cao, L. Pore Size Tailoring in Large-Pore SBA-15 Silica Synthesized in the Presence of Hexane. *Langmuir* **2007**, *23* (13), 7247–7254.

(121) Song, K.; Guan, J.; Wang, Z.; Xu, C.; Kan, Q. Post-Treatment of Mesoporous Material with High Temperature for Synthesis Super-Microporous Materials with Enhanced Hydrothermal Stability. *Appl. Surf. Sci.* **2009**, *255* (11), 5843–5846.

(122) Kruk, M.; Jaroniec, M.; Sayari, A. A Unified Interpretation of High-Temperature Pore Size Expansion Processes in MCM-41 Mesoporous Silicas. *J. Phys. Chem. B* **1999**, *103* (22), 4590–4598.

(123) Singh, L. P.; Bhattacharyya, S. K.; Kumar, R.; Mishra, G.; Sharma, U.; Singh, G.; Ahalawat, S. Sol-Gel Processing of Silica Nanoparticles and Their Applications. *Adv. Colloid Interface Sci.* **2014**, *214*, 17–37.

(124) Coll, C.; Bernardos, A.; Martínez-Máñez, R.; Sancenón, F. Gated Silica Mesoporous Supports for Controlled Release and Signaling Applications. *Acc. Chem. Res.* **2013**, *46* (2), 339–349.

(125) Yu, T.; Malugin, A.; Ghandehari, H. Impact of Silica Nanoparticle Design on Cellular Toxicity and Hemolytic Activity. *ACS Nano* **2011**, *5* (7), 5717–5728.

(126) Trewyn, B. G.; Slowing, I. I.; Giri, S.; Chen, H.-T.; Lin, V. S.-Y. Synthesis and Functionalization of a Mesoporous Silica Nanoparticle Based on the Sol–Gel Process and Applications in Controlled Release. *Acc. Chem. Res.* **2007**, *40* (9), 846–853.

(127) Yu, B.; Tai, H. C.; Xue, W.; Lee, L. J.; Lee, R. J. Receptor-Targeted Nanocarriers for Therapeutic Delivery to Cancer. *Mol. Membr. Biol.* **2010**, *27* (7), 286–298.

(128) Lee, Y.-G.; Park, J.-H.; Oh, C.; Oh, S.-G.; Kim, Y. C. Preparation of Highly Monodispersed Hybrid Silica Spheres Using a One-Step Sol−Gel Reaction in Aqueous Solution. *Langmuir* **2007**, *23* (22), 10875–10878.

(129) Rosenholm, J. M.; Sahlgren, C.; Lindén, M. Towards Multifunctional, Targeted Drug Delivery Systems Using Mesoporous Silica Nanoparticles – Opportunities & Challenges. *Nanoscale* **2010**, *2* (10), 1870.

(130) He, Q.; Ma, M.; Wei, C.; Shi, J. Mesoporous Carbon@silicon-Silica Nanotheranostics for Synchronous Delivery of Insoluble Drugs and Luminescence Imaging. *Biomaterials* **2012**, *33* (17), 4392–4402.

(131) Ma, G. H.; He, J.; Rajiv, K.; Tang, S. H.; Yang, Y.; Nogami, M. Observation of Resonant Energy Transfer in Au:CdS Nanocomposite. *Appl. Phys. Lett.* **2004**, *84* (23), 4684.

(132) Kamat, P. V.; Shanghavi, B. Interparticle Electron Transfer in Metal/Semiconductor Composites. Picosecond Dynamics of CdS-Capped Gold Nanoclusters. *J. Phys. Chem. B* **1997**, *101* (39), 7675–7679.

(133) Chomoucka, J.; Drbohlavova, J.; Huska, D.; Adam, V.; Kizek, R.; Hubalek, J. Magnetic Nanoparticles and Targeted Drug Delivering. *Pharmacol. Res.* **2010**, *62* (2), 144–149.

(134) Wang, Y.; Wang, K.; Zhang, R.; Liu, X.; Yan, X.; Wang, J.; Wagner, E.; Huang, R. Synthesis of Core–Shell Graphitic Carbon@Silica Nanospheres with Dual-Ordered Mesopores for Cancer-Targeted Photothermochemotherapy. *ACS Nano* **2014**, *8* (8), 7870–7879.

(135) Chen, S.; Li, Y.; Guo, C.; Wang, J.; Ma, J.; Liang, X.; Yang, L.-R.; Liu, H.-Z. Temperature-Responsive Magnetite/PEO–PPO–PEO Block Copolymer Nanoparticles for Controlled Drug Targeting Delivery. *Langmuir* **2007**, *23* (25), 12669–12676.

(136) Qin, S.; Wang, L.; Zhang, X.; Su, G. Grafting Poly(ethylene Glycol) Monomethacrylate onto Fe3O4 Nanoparticles to Resist Nonspecific Protein Adsorption. *Appl. Surf. Sci.* **2010**, *257* (3), 731–735.

(137) Mu, Q.; Yang, L.; Davis, J. C.; Vankayala, R.; Hwang, K. C.; Zhao, J.; Yan, B. Biocompatibility of Polymer Grafted Core/Shell Iron/Carbon Nanoparticles. *Biomaterials* **2010**, *31* (19), 5083–5090.

(138) *Carbon Nanomaterials*, 2. ed.; Gogocij, Y., Presser, V., Eds.; Advanced materials and technologies series; CRC, Taylor & Francis: Boca Raton, Fla., 2014.

(139) Dai, L.; Chang, D. W.; Baek, J.-B.; Lu, W. Carbon Nanomaterials for Advanced Energy Conversion and Storage. *Small* **2012**, *8* (8), 1130–1166.

(140) Jia, G.; Wang, H.; Yan, L.; Wang, X.; Pei, R.; Yan, T.; Zhao, Y.; Guo, X. Cytotoxicity of Carbon Nanomaterials: Single-Wall Nanotube, Multi-Wall Nanotube, and Fullerene. *Environ. Sci. Technol.* **2005**, *39* (5), 1378–1383.

(141) San-Miguel, A. Nanomaterials under High-Pressure. *Chem. Soc. Rev.* **2006**, *35* (10), 876.

(142) Dolmatov, V. Y. Detonation-Synthesis Nanodiamonds: Synthesis, Structure, Properties and Applications. *Russ. Chem. Rev.* **2007**, *76* (4), 339–360.

(143) Turner, S.; Lebedev, O. I.; Shenderova, O.; Vlasov, I. I.; Verbeeck, J.; Van Tendeloo, G. Determination of Size, Morphology, and Nitrogen Impurity Location in Treated Detonation Nanodiamond by Transmission Electron Microscopy. *Adv. Funct. Mater.* **2009**, *19* (13), 2116–2124.

(144) Neu, E.; Arend, C.; Gross, E.; Guldner, F.; Hepp, C.; Steinmetz, D.; Zscherpel, E.; Ghodbane, S.; Sternschulte, H.; Steinmüller-Nethl, D.; Liang, Y.; Krueger, A.; Becher, C. Narrowband Fluorescent Nanodiamonds Produced from Chemical Vapor Deposition Films. *Appl. Phys. Lett.* **2011**, *98* (24), 243107.

(145) Balmer, R. S.; Brandon, J. R.; Clewes, S. L.; Dhillon, H. K.; Dodson, J. M.; Friel, I.; Inglis, P. N.; Madgwick, T. D.; Markham, M. L.; Mollart, T. P.; Perkins, N.; Scarsbrook, G. A.; Twitchen, D. J.; Whitehead, A. J.; Wilman, J. J.; Woollard, S. M. Chemical Vapour Deposition Synthetic Diamond: Materials, Technology and Applications. *J. Phys. Condens. Matter* **2009**, *21* (36), 364221.

(146) Shenderova, O. A.; Vlasov, I. I.; Turner, S.; Van Tendeloo, G.; Orlinskii, S. B.; Shiryaev, A. A.; Khomich, A. A.; Sulyanov, S. N.; Jelezko, F.; Wrachtrup, J. Nitrogen Control in Nanodiamond Produced by Detonation Shock-Wave-Assisted Synthesis. *J. Phys. Chem. C* **2011**, *115* (29), 14014–14024.

(147) Faklaris, O.; Joshi, V.; Irinopoulou, T.; Tauc, P.; Sennour, M.; Girard, H.; Gesset, C.; Arnault, J.-C.; Thorel, A.; Boudou, J.-P.; Curmi, P. A.; Treussart, F. Photoluminescent Diamond Nanoparticles for Cell Labeling: Study of the Uptake Mechanism in Mammalian Cells. *ACS Nano* **2009**, *3* (12), 3955–3962.

(148) Tisler, J.; Balasubramanian, G.; Naydenov, B.; Kolesov, R.; Grotz, B.; Reuter, R.; Boudou, J.-P.; Curmi, P. A.; Sennour, M.; Thorel, A.; Börsch, M.; Aulenbacher, K.; Erdmann, R.; Hemmer, P. R.; Jelezko, F.; Wrachtrup, J. Fluorescence and Spin Properties of Defects in Single Digit Nanodiamonds. *ACS Nano* **2009**, *3* (7), 1959–1965.

(149) Sung, J. C.; Lin, J. *Diamond Nanotechnology: Syntheses and Applications*; Pan Stanford ; Distributed by World Scientific Pub: Singapore : Hackensack, NJ, 2009.

(150) *Ultrananocrystalline Diamond: Synthesis, Properties, and Applications*, Second edition.; Shenderova, O. A., Gruen, D. M., Eds.; Micro & nano technologies series; William Andrew, Elsevier: Amsterdam, 2012.

(151) Schrand, A.; Hens, S. A. C.; Shenderova, O. Nanodiamond Particles: Properties and Perspectives for Bioapplications. *Crit. Rev. Solid State Mater. Sci.* **2009**, *34* (1), 18–74.

(152) Yu, S.-J.; Kang, M.-W.; Chang, H.-C.; Chen, K.-M.; Yu, Y.-C. Bright Fluorescent Nanodiamonds: No Photobleaching and Low Cytotoxicity. *J. Am. Chem. Soc.* **2005**, *127* (50), 17604–17605.

(153) Fu, C.-C.; Lee, H.-Y.; Chen, K.; Lim, T.-S.; Wu, H.-Y.; Lin, P.-K.; Wei, P.-K.; Tsao, P.-H.; Chang, H.-C.; Fann, W. Characterization and Application of Single Fluorescent Nanodiamonds as Cellular Biomarkers. *Proc. Natl. Acad. Sci.* **2007**, *104* (3), 727–732.

(154) Huang, L.-C. L.; Chang, H.-C. Adsorption and Immobilization of Cytochrome *c* on Nanodiamonds. *Langmuir* **2004**, *20* (14), 5879–5884.

(155) Krüger, A.; Liang, Y.; Jarre, G.; Stegk, J. Surface Functionalisation of Detonation Diamond Suitable for Biological Applications. *J Mater Chem* **2006**, *16* (24), 2322–2328.

(156) Smith, B. R.; Inglis, D. W.; Sandnes, B.; Rabeau, J. R.; Zvyagin, A. V.; Gruber, D.; Noble, C. J.; Vogel, R.; Ōsawa, E.; Plakhotnik, T. Five-Nanometer Diamond with Luminescent Nitrogen-Vacancy Defect Centers. *Small* **2009**, *5* (14), 1649–1653.

(157) Liu, K.-K.; Cheng, C.-L.; Chang, C.-C.; Chao, J.-I. Biocompatible and Detectable Carboxylated Nanodiamond on Human Cell. *Nanotechnology* **2007**, *18* (32), 325102.

(158) Schrand, A. M.; Huang, H.; Carlson, C.; Schlager, J. J.; Ōsawa, E.; Hussain, S. M.; Dai, L. Are Diamond Nanoparticles Cytotoxic? *J. Phys. Chem. B* **2007**, *111* (1), 2–7.

(159) Schrand, A. M.; Dai, L.; Schlager, J. J.; Hussain, S. M.; Osawa, E. Differential Biocompatibility of Carbon Nanotubes and Nanodiamonds. *Diam. Relat. Mater.* **2007**, *16* (12), 2118–2123.

(160) Puzyr, A. P.; Baron, A. V.; Purtov, K. V.; Bortnikov, E. V.; Skobelev, N. N.; Mogilnaya, O. A.; Bondar, V. S. Nanodiamonds with Novel Properties: A Biological Study. *Diam. Relat. Mater.* **2007**, *16* (12), 2124–2128.

(161) Bakowicz, K.; Mitura, S. Biocompatibility of NCD. *J. Wide Bandgap Mater.* **2002**, *9* (4), 261–272.

(162) Yuan, Y.; Wang, X.; Jia, G.; Liu, J.-H.; Wang, T.; Gu, Y.; Yang, S.-T.; Zhen, S.; Wang, H.; Liu, Y. Pulmonary Toxicity and Translocation of Nanodiamonds in Mice. *Diam. Relat. Mater.* **2010**, *19* (4), 291–299.

(163) Gruber, A. Scanning Confocal Optical Microscopy and Magnetic Resonance on Single Defect Centers. *Science* **1997**, *276* (5321), 2012–2014.

(164) Wu, E.; Rabeau, J. R.; Treussart, F.; Zeng, H.; Grangier, P.; Prawer, S.; Roch, J.-F. Nonclassical Photon Statistics in a Single Nickel–nitrogen Diamond Color Center Photoluminescence at Room Temperature. *J. Mod. Opt.* **2008**, *55* (17), 2893–2901.

(165) Vlasov, I. I.; Barnard, A. S.; Ralchenko, V. G.; Lebedev, O. I.; Kanzyuba, M. V.; Saveliev, A. V.; Konov, V. I.; Goovaerts, E. Nanodiamond Photoemitters Based on Strong Narrow-Band Luminescence from Silicon-Vacancy Defects. *Adv. Mater.* **2009**, *21* (7), 808–812.

(166) Vlasov, I. I.; Shenderova, O.; Turner, S.; Lebedev, O. I.; Basov, A. A.; Sildos, I.; Rähn, M.; Shiryaev, A. A.; Van Tendeloo, G. Nitrogen and Luminescent Nitrogen-Vacancy Defects in Detonation Nanodiamond. *Small* **2010**, *6* (5), 687–694.

(167) Davies, G.; Hamer, M. F. Optical Studies of the 1.945 eV Vibronic Band in Diamond. *Proc. R. Soc. Math. Phys. Eng. Sci.* **1976**, *348* (1653), 285–298.

(168) Rittweger, E.; Han, K. Y.; Irvine, S. E.; Eggeling, C.; Hell, S. W. STED Microscopy Reveals Crystal Colour Centres with Nanometric Resolution. *Nat. Photonics* **2009**, *3* (3), 144–147.

(169) Han, K. Y.; Willig, K. I.; Rittweger, E.; Jelezko, F.; Eggeling, C.; Hell, S. W. Three-Dimensional Stimulated Emission Depletion Microscopy of Nitrogen-Vacancy Centers in Diamond Using Continuous-Wave Light. *Nano Lett.* **2009**, *9* (9), 3323–3329.

(170) Prabhakar, N.; Näreoja, T.; von Haartman, E.; Karaman, D. Ş.; Jiang, H.; Koho, S.; Dolenko, T. A.; Hänninen, P. E.; Vlasov, D. I.; Ralchenko, V. G.; Hosomi, S.; Vlasov, I. I.; Sahlgren, C.; Rosenholm, J. M. Core–shell Designs of Photoluminescent Nanodiamonds with Porous Silica Coatings for Bioimaging and Drug Delivery II: Application. *Nanoscale* **2013**, *5* (9), 3713–3722.

(171) Chung, P.-H.; Perevedentseva, E.; Cheng, C.-L. The Particle Size-Dependent Photoluminescence of Nanodiamonds. *Surf. Sci.* **2007**, *601* (18), 3866–3870.

(172) Bradac, C.; Gaebel, T.; Naidoo, N.; Rabeau, J. R.; Barnard, A. S. Prediction and Measurement of the Size-Dependent Stability of Fluorescence in Diamond over the Entire Nanoscale. *Nano Lett.* **2009**, *9* (10), 3555–3564.

(173) Turner, S.; Lebedev, O. I.; Shenderova, O.; Vlasov, I. I.; Verbeeck, J.; Van Tendeloo, G. Determination of Size, Morphology, and Nitrogen Impurity Location in Treated Detonation Nanodiamond by Transmission Electron Microscopy. *Adv. Funct. Mater.* **2009**, *19* (13), 2116–2124.

(174) Shenderova, O. Nanodiamonds Shine New Light on Bio Applications. *Biophotonics*. June 2015.

(175) Lu, J.; Liong, M.; Zink, J. I.; Tamanoi, F. Mesoporous Silica Nanoparticles as a Delivery System for Hydrophobic Anticancer Drugs. *Small* **2007**, *3* (8), 1341–1346.

(176) Kong, D.; Yang, P.; Wang, Z.; Chai, P.; Huang, S.; Lian, H.; Lin, J. Mesoporous Silica Coated CeF 3 : Tb 3+ Particles for Drug Release. *J. Nanomater.* **2008**, *2008*, 1–7.

(177) Liong, M.; France, B.; Bradley, K. A.; Zink, J. I. Antimicrobial Activity of Silver Nanocrystals Encapsulated in Mesoporous Silica Nanoparticles. *Adv. Mater.* **2009**, *21* (17), 1684–1689.

(178) Nooney, R. I.; Thirunavukkarasu, D.; Chen, Y.; Josephs, R.; Ostafin, A. E. Self-Assembly of Mesoporous Nanoscale Silica/Gold Composites. *Langmuir* **2003**, *19* (18), 7628–7637.

(179) Anderson, M. T.; Martin, J. E.; Odinek, J. G.; Newcomer, P. P. Surfactant-Templated Silica Mesophases Formed in Water:Cosolvent Mixtures. *Chem. Mater.* **1998**, *10* (1), 311–321.

(180) Pinho, S. L. C.; Pereira, G. A.; Voisin, P.; Kassem, J.; Bouchaud, V.; Etienne, L.; Peters, J. A.; Carlos, L.; Mornet, S.; Geraldes, C. F. G. C.; Rocha, J.; Delville, M.-H. Fine Tuning of the Relaxometry of γ-Fe_2O_3 @SiO_2 Nanoparticles by Tweaking the Silica Coating Thickness. *ACS Nano* **2010**, *4* (9), 5339–5349.

(181) Liz-Marzán, L. M.; Giersig, M.; Mulvaney, P. Synthesis of Nanosized Gold−Silica Core−Shell Particles. *Langmuir* **1996**, *12* (18), 4329–4335.

(182) Pastoriza-Santos, I.; Pérez-Juste, J.; Liz-Marzán, L. M. Silica-Coating and Hydrophobation of CTAB-Stabilized Gold Nanorods. *Chem. Mater.* **2006**, *18* (10), 2465–2467.

(183) Chou, K.-S.; Chen, C.-C. The Critical Conditions for Secondary Nucleation of Silica Colloids in a Batch Stöber Growth Process. *Ceram. Int.* **2008**, *34* (7), 1623–1627.

(184) Liu, S.; Cool, P.; Collart, O.; Van Der Voort, P.; Vansant, E. F.; Lebedev, O. I.; Van Tendeloo, G.; Jiang, M. The Influence of the Alcohol Concentration on the Structural Ordering of Mesoporous Silica: Cosurfactant versus Cosolvent. *J. Phys. Chem. B* **2003**, *107* (38), 10405–10411.

(185) Al Shamsi, M.; Al Samri, M. T.; Al-Salam, S.; Conca, W.; Shaban, S.; Benedict, S.; Tariq, S.; Biradar, A. V.; Penefsky, H. S.; Asefa, T.; Souid, A.-K. Biocompatibility of Calcined Mesoporous Silica Particles with Cellular Bioenergetics in Murine Tissues. *Chem. Res. Toxicol.* **2010**, *23* (11), 1796–1805.

(186) Kleitz, F.; Schmidt, W.; Schüth, F. Calcination Behavior of Different Surfactant-Templated Mesostructured Silica Materials. *Microporous Mesoporous Mater.* **2003**, *65* (1), 1–29.

(187) Kleitz, F. Ordered Mesoporous Materials: Template Removal, Frameworks and Morphology. PhD, Ruhr-Universität: Bochum, Germany, 2002.

(188) Twaiq, F.; Nasser, M. S.; Onaizi, S. A. Effect of the Degree of Template Removal from Mesoporous Silicate Materials on Their Adsorption of Heavy Oil from Aqueous Solution. *Front. Chem. Sci. Eng.* **2014**, *8* (4), 488–497.

(189) Lang, N.; Tuel, A. A Fast and Efficient Ion-Exchange Procedure To Remove Surfactant Molecules from MCM-41 Materials. *Chem. Mater.* **2004**, *16* (10), 1961–1966.

(190) Möller, K.; Kobler, J.; Bein, T. Colloidal Suspensions of Nanometer-Sized Mesoporous Silica. *Adv. Funct. Mater.* **2007**, *17* (4), 605–612.

(191) *Colloid Stability: The Role of Surface Forces*; Tadros, T. F., Ed.; Colloids and interface science series; Wiley-VCH Verlag: Weinheim, 2007.

(192) Verwey, E. J. W.; Overbeek, J. T. G. *Theory of the Stability of Lyophobic Colloids*; Dover Publications: Mineola, N.Y, 1999.

(193) Bergman, L.; Rosenholm, J.; Öst, A.-B.; Duchanoy, A.; Kankaanpää, P.; Heino, J.; Lindén, M. On the Complexity of Electrostatic Suspension Stabilization of Functionalized Silica Nanoparticles for Biotargeting and Imaging Applications. *J. Nanomater.* **2008**, *2008*, 1–9.

(194) Metin, C. O.; Lake, L. W.; Miranda, C. R.; Nguyen, Q. P. Stability of Aqueous Silica Nanoparticle Dispersions. *J. Nanoparticle Res.* **2011**, *13* (2), 839–850.

(195) Graf, C.; Gao, Q.; Schütz, I.; Noufele, C. N.; Ruan, W.; Posselt, U.; Korotianskiy, E.; Nordmeyer, D.; Rancan, F.; Hadam, S.; Vogt, A.; Lademann, J.; Haucke, V.; Rühl, E. Surface Functionalization of Silica Nanoparticles Supports Colloidal Stability in Physiological Media and Facilitates Internalization in Cells. *Langmuir* **2012**, *28* (20), 7598–7613.

(196) Coasne, B.; Di Renzo, F.; Galarneau, A.; Pellenq, R. J. M. Adsorption of Simple Fluid on Silica Surface and Nanopore: Effect of Surface Chemistry and Pore Shape. *Langmuir* **2008**, *24* (14), 7285–7293.

(197) Zhuravlev, L. T. The Surface Chemistry of Amorphous Silica. Zhuravlev Model. *Colloids Surf. Physicochem. Eng. Asp.* **2000**, *173* (1–3), 1–38.

(198) Gu, J.; Fan, W.; Shimojima, A.; Okubo, T. Organic–Inorganic Mesoporous Nanocarriers Integrated with Biogenic Ligands. *Small* **2007**, *3* (10), 1740–1744.

(199) Ong, S.; Zhao, X.; Eisenthal, K. B. Polarization of Water Molecules at a Charged Interface: Second Harmonic Studies of the Silica/Water Interface. *Chem. Phys. Lett.* **1992**, *191* (3–4), 327–335.

(200) Jal, P. Chemical Modification of Silica Surface by Immobilization of Functional Groups for Extractive Concentration of Metal Ions. *Talanta* **2004**, *62* (5), 1005–1028.

(201) Mercier, L.; Pinnavaia, T. J. Heavy Metal Ion Adsorbents Formed by the Grafting of a Thiol Functionality to Mesoporous Silica Molecular Sieves: Factors Affecting Hg(II) Uptake. *Environ. Sci. Technol.* **1998**, *32* (18), 2749–2754.

(202) Potapov, V. V.; Zhuravlev, L. T. Temperature Dependence of the Concentration of Silanol Groups in Silica Precipitated from a Hydrothermal Solution. *Glass Phys. Chem.* **2005**, *31* (5), 661–670.

(203) Pham, A. L.-T.; Sedlak, D. L.; Doyle, F. M. Dissolution of Mesoporous Silica Supports in Aqueous Solutions: Implications for Mesoporous Silica-Based Water Treatment Processes. *Appl. Catal. B Environ.* **2012**, *126*, 258–264.

(204) Dove, P. M.; Han, N.; Wallace, A. F.; De Yoreo, J. J. Kinetics of Amorphous Silica Dissolution and the Paradox of the Silica Polymorphs. *Proc. Natl. Acad. Sci.* **2008**, *105* (29), 9903–9908.

(205) He, Q.; Shi, J.; Zhu, M.; Chen, Y.; Chen, F. The Three-Stage in Vitro Degradation Behavior of Mesoporous Silica in Simulated Body Fluid. *Microporous Mesoporous Mater.* **2010**, *131* (1–3), 314–320.

(206) Li, L. Synthesis and Hydrolytic Stability of Mesoporous Silica Nanoparticles. M.Sc.(Tech), Åbo Akademi University: Turku, Finland, 2010.

(207) Lin, Y.-S.; Haynes, C. L. Impacts of Mesoporous Silica Nanoparticle Size, Pore Ordering, and Pore Integrity on Hemolytic Activity. *J. Am. Chem. Soc.* **2010**, *132* (13), 4834–4842.

(208) Yamada, H.; Urata, C.; Aoyama, Y.; Osada, S.; Yamauchi, Y.; Kuroda, K. Preparation of Colloidal Mesoporous Silica Nanoparticles with Different Diameters and Their Unique Degradation Behavior in Static Aqueous Systems. *Chem. Mater.* **2012**, *24* (8), 1462–1471.

(209) Finsy, R. On the Critical Radius in Ostwald Ripening. *Langmuir ACS J. Surf. Colloids* **2004**, *20* (7), 2975–2976.

(210) Cauda, V.; Argyo, C.; Bein, T. Impact of Different PEGylation Patterns on the Long-Term Bio-Stability of Colloidal Mesoporous Silica Nanoparticles. *J. Mater. Chem.* **2010**, *20* (39), 8693–8699.

(211) Cauda, V.; Schlossbauer, A.; Bein, T. Bio-Degradation Study of Colloidal Mesoporous Silica Nanoparticles: Effect of Surface Functionalization with Organo-Silanes and Poly(ethylene Glycol). *Microporous Mesoporous Mater.* **2010**, *132* (1–2), 60–71.

(212) Etienne, M.; Walcarius, A. Analytical Investigation of the Chemical Reactivity and Stability of Aminopropyl-Grafted Silica in Aqueous Medium. *Talanta* **2003**, *59* (6), 1173–1188.

(213) Zhmud, B. V.; Sonnefeld, J. Aminopolysiloxane Gels: Production and Properties. *J. Non-Cryst. Solids* **1996**, *195* (1–2), 16–27.

(214) Asenath Smith, E.; Chen, W. How To Prevent the Loss of Surface Functionality Derived from Aminosilanes. *Langmuir* **2008**, *24* (21), 12405–12409.

(215) Salmio, H.; Brühwiler, D. Distribution of Amino Groups on a Mesoporous Silica Surface after Submonolayer Deposition of Aminopropylsilanes from an Anhydrous Liquid Phase. *J. Phys. Chem. C* **2007**, *111* (2), 923–929.

(216) Lin, Y.-S.; Wu, S.-H.; Hung, Y.; Chou, Y.-H.; Chang, C.; Lin, M.-L.; Tsai, C.-P.; Mou, C.-Y. Multifunctional Composite Nanomaterials: Magnetic, Luminescent, and Mesoporous. *Chem Mater* **2006**, *18*, 5170–5172.

(217) Roberts, M. J.; Bentley, M. D.; Harris, J. M. Chemistry for Peptide and Protein PEGylation. *Adv. Drug Deliv. Rev.* **2012**, *64*, 116–127.

(218) Rosenholm, J. M.; Duchanoy, A.; Lindén, M. Hyperbranching Surface Polymerization as a Tool for Preferential Functionalization of the Outer Surface of Mesoporous Silica †. *Chem. Mater.* **2008**, *20* (3), 1126–1133.

(219) Burkett, S. L.; Sims, S. D.; Mann, S. Synthesis of Hybrid Inorganic–organic Mesoporous Silica by Co-Condensation of Siloxane and Organosiloxane Precursors. *Chem Commun* **1996**, No. 11, 1367–1368.

(220) Mercier, L.; Pinnavaia, T. J. Direct Synthesis of Hybrid Organic-Inorganic Nanoporous Silica by a Neutral Amine Assembly Route: Structure-Function Control by Stoichiometric Incorporation of Organisiloxane Molecules. *Chem Mater* **2000**, *12* (1), 188–196.

(221) Burleigh, M. C.; Markowitz, M. A.; Spector, M. S.; Gaber, B. P. Direct Synthesis of Periodic Mesoporous Organosilicas: Functional Incorporation by Co-Condensation with Organosilanes. *J.Phys.Chem.B* **2001**, *105* (41), 9935–9942.

(222) Beaudet, L.; Hossain, K.-Z.; Mercier, L. Direct Synthesis of Hybrid Organic–Inorganic Nanoporous Silica Microspheres. 1. Effect of Temperature and Organosilane Loading on the Nano- and Micro-Structure of Mercaptopropyl-Functionalized MSU Silica. *Chem Mater* **2003**, *15* (1), 327–334.

(223) Huh, S.; Wiench, J. W.; Yoo, J.-C.; Pruski, M.; Lin, V. S.-Y. Organic Functionalization and Morphology Control of Mesoporous Silicas via a Co-Condensation Synthesis Method. *Chem Mater* **2003**, *15* (22), 4247–4256.

(224) Rosenholm, J. M.; Meinander, A.; Peuhu, E.; Niemi, R.; Eriksson, J. E.; Sahlgren, C.; Lindén, M. Targeting of Porous Hybrid Silica Nanoparticles to Cancer Cells. *ACS Nano* **2009**, *3* (1), 197–206.

(225) Liong, M.; Lu, J.; Kovochich, M.; Xia, T. Multifunctional Inorganic Nanoparticles for Imaging, Targeting, and Drug Delivery. *ACS Nano* **2008**, *2* (5), 889–896.

(226) Liu, D.; Lei, J.-H.; Guo, L.-P.; Du, X.-D.; Zeng, K. Ordered Thiol-Functionalized Mesoporous Silica with Macrostructure by True Liquid Crystal Templating Route. *Microporous Mesoporous Mater.* **2009**, *117* (1–2), 67–74.

(227) Hüsing, N.; Hartmann, S. Inorganic-Organic Hybrid Porous Materials. In *Hybrid nanocomposites for nanotechnology: electronic, optical, magnetic and biomedical applications*; Merhari, L., Ed.; Springer: New York, 2009; pp 131–172.

(228) Walcarius, A.; Etienne, M.; Lebeau, B. Rate of Access to the Binding Sites in Organically Modified Silicates. 2. Ordered Mesoporous Silicas Grafted with Amine or Thiol Groups. *Chem. Mater.* **2003**, *15* (11), 2161–2173.

(229) Kecht, J.; Schlossbauer, A.; Bein, T. Selective Functionalization of the Outer and Inner Surfaces in Mesoporous Silica Nanoparticles. *Chem. Mater.* **2008**, *20* (23), 7207–7214.

(230) Ritter, H.; Brühwiler, D. Accessibility of Amino Groups in Postsynthetically Modified Mesoporous Silica. *J Phys Chem C* **2009**, *113* (24), 10667–10674.

(231) Kim, C. O.; Cho, S. J.; Park, J. W. Hyperbranching Polymerization of Aziridine on Silica Solid Substrates Leading to a Surface of Highly Dense Reactive Amine Groups. *J. Colloid Interface Sci.* **2003**, *260* (2), 374–378.

(232) Gartmann, N.; Schütze, C.; Ritter, H.; Brühwiler, D. The Effect of Water on the Functionalization of Mesoporous Silica with 3-Aminopropyltriethoxysilane. *J. Phys. Chem. Lett.* **2010**, *1* (1), 379–382.

(233) Brühwiler, D. Postsynthetic Functionalization of Mesoporous Silica. *Nanoscale* **2010**, *2* (6), 887.

(234) He, C.-X.; Tabata, Y.; Gao, J.-Q. Non-Viral Gene Delivery Carrier and Its Three-Dimensional Transfection System. *Int. J. Pharm.* **2010**, *386* (1–2), 232–242.

(235) Zhang, S.; Xu, Y.; Wang, B.; Qiao, W.; Liu, D.; Li, Z. Cationic Compounds Used in Lipoplexes and Polyplexes for Gene Delivery. *J. Controlled Release* **2004**, *100* (2), 165–180.

(236) Kim, H. J.; Moon, J. H.; Park, J. W. A Hyperbranched Poly(ethyleneimine) Grown on Surfaces. *J. Colloid Interface Sci.* **2000**, *227* (1), 247–249.

(237) Xia, T.; Kovochich, M.; Liong, M.; Meng, H.; Kabehie, S.; George, S.; Zink, J. I.; Nel, A. E. Polyethyleneimine Coating Enhances the Cellular Uptake of Mesoporous Silica Nanoparticles and Allows Safe Delivery of siRNA and DNA Constructs. *ACS Nano* **2009**, *3* (10), 3273–3286.

(238) Zhao, Q.-Q.; Chen, J.-L.; Han, M.; Liang, W.-Q.; Tabata, Y.; Gao, J.-Q. Combination of Poly(ethylenimine) and Chitosan Induces High Gene Transfection Efficiency and Low Cytotoxicity. *J. Biosci. Bioeng.* **2008**, *105* (1), 65–68.

(239) Xia, T.; Kovochich, M.; Liong, M.; Zink, J. I.; Nel, A. E. Cationic Polystyrene Nanosphere Toxicity Depends on Cell-Specific Endocytic and Mitochondrial Injury Pathways. *ACS Nano* **2008**, *2* (1), 85–96.

(240) Lim, Y.; Kim, S.-M.; Lee, Y.; Lee, W.; Yang, T.; Lee, M.; Suh, H.; Park, J. Cationic Hyperbranched Poly(amino Ester): A Novel Class of DNA Condensing Molecule with Cationic Surface, Biodegradable Three-Dimensional Structure, and Tertiary Amine Groups in the Interior. *J. Am. Chem. Soc.* **2001**, *123* (10), 2460–2461.

(241) Fuller, J. E.; Zugates, G. T.; Ferreira, L. S.; Ow, H. S.; Nguyen, N. N.; Wiesner, U. B.; Langer, R. S. Intracellular Delivery of Core–shell Fluorescent Silica Nanoparticles. *Biomaterials* **2008**, *29* (10), 1526–1532.

(242) Behr, J.-P. The Proton Sponge: A Trick to Enter Cells the Viruses Did Not Exploit. *Chim. Interantional J. Chem.* **1997**, *51* (1–2), 34–36.

(243) Hillaireau, H.; Couvreur, P. Nanocarriers' Entry into the Cell: Relevance to Drug Delivery. *Cell. Mol. Life Sci.* **2009**, *66* (17), 2873–2896.

(244) Godbey, W. T.; Wu, K. K.; Mikos, A. G. Poly(ethylenimine) and Its Role in Gene Delivery. *J. Controlled Release* **1999**, *60* (2–3), 149–160.

(245) Creusat, G.; Rinaldi, A.-S.; Weiss, E.; Elbaghdadi, R.; Remy, J.-S.; Mulherkar, R.; Zuber, G. Proton Sponge Trick for pH-Sensitive Disassembly of Polyethylenimine-Based siRNA Delivery Systems. *Bioconjug. Chem.* **2010**, *21* (5), 994–1002.

(246) Bieber, T.; Meissner, W.; Kostin, S.; Niemann, A.; Elsasser, H.-P. Intracellular Route and Transcriptional Competence of Polyethylenimine-DNA Complexes. *J. Control. Release Off. J. Control. Release Soc.* **2002**, *82* (2–3), 441–454.

(247) Won, Y.-Y.; Sharma, R.; Konieczny, S. F. Missing Pieces in Understanding the Intracellular Trafficking of Polycation/DNA Complexes. *J. Controlled Release* **2009**, *139* (2), 88–93.

(248) Boussif, O.; Lezoualcc'h, F.; Zanta, M. A. A Versatile Vector for Gene and Oligonucleotide Transfer into Cells in Culture and in Vivo: Polyethylenimine. *Proc. Natl. Acad. Sci. U. S. Am.* **1995**, *92* (16), 7297–7301.

(249) Hong, S.; Leroueil, P. R.; Janus, E. K.; Peters, J. L.; Kober, M.-M.; Islam, M. T.; Orr, B. G.; Baker, J. R.; Banaszak Holl, M. M. Interaction of Polycationic Polymers with Supported Lipid Bilayers and Cells: Nanoscale Hole Formation and Enhanced Membrane Permeability. *Bioconjug. Chem.* **2006**, *17* (3), 728–734.

(250) Benjaminsen, R. V.; Mattebjerg, M. A.; Henriksen, J. R.; Moghimi, S. M.; Andresen, T. L. The Possible "Proton Sponge " Effect of Polyethylenimine (PEI) Does Not Include Change in Lysosomal pH. *Mol. Ther.* **2013**, *21* (1), 149–157.

(251) Nel, A. E.; Mädler, L.; Velegol, D.; Xia, T.; Hoek, E. M. V.; Somasundaran, P.; Klaessig, F.; Castranova, V.; Thompson, M. Understanding Biophysicochemical Interactions at the Nano–bio Interface. *Nat. Mater.* **2009**, *8* (7), 543–557.

(252) Zhu, M.; Nie, G.; Meng, H.; Xia, T.; Nel, A.; Zhao, Y. Physicochemical Properties Determine Nanomaterial Cellular Uptake, Transport, and Fate. *Acc. Chem. Res.* **2013**, *46* (3), 622–631.

(253) Parida, S. K.; Dash, S.; Patel, S.; Mishra, B. K. Adsorption of Organic Molecules on Silica Surface. *Adv. Colloid Interface Sci.* **2006**, *121* (1–3), 77–110.

(254) Zou, H.; Wu, S.; Shen, J. Polymer/Silica Nanocomposites: Preparation, Characterization, Properties, and Applications. *Chem. Rev.* **2008**, *108* (9), 3893–3957.

(255) Moussaif, N.; Irusta, S.; Yagüe, C.; Arruebo, M.; Meier, J. G.; Crespo, C.; Jimenez, M. A.; Santamaría, J. Mechanically Reinforced Biodegradable Nanocomposites. A Facile Synthesis Based on PEGylated Silica Nanoparticles. *Polymer* **2010**, *51* (26), 6132–6139.

(256) Howard, M. D.; Jay, M.; Dziubla, T. D.; Lu, X. PEGylation of Nanocarrier Drug Delivery Systems: State of the Art. *J. Biomed. Nanotechnol.* **2008**, *4* (2), 133–148.

(257) Walkey, C. D.; Chan, W. C. W. Understanding and Controlling the Interaction of Nanomaterials with Proteins in a Physiological Environment. *Chem Soc Rev* **2012**, *41* (7), 2780–2799.

(258) Owens III, D.; Peppas, N. Opsonization, Biodistribution, and Pharmacokinetics of Polymeric Nanoparticles. *Int. J. Pharm.* **2006**, *307* (1), 93–102.

(259) Mishra, S. PEGylation Significantly Affects Cellular Uptake and Intracellular Trafficking of Non-Viral Gene Delivery Particles. *Eur. J. Cell Biol.* **2004**, *83* (3), 97–111.

(260) Romberg, B.; Hennink, W. E.; Storm, G. Sheddable Coatings for Long-Circulating Nanoparticles. *Pharm. Res.* **2008**, *25* (1), 55–71.

(261) *Poly(ethylene Glycol) Chemistry: Biotechnical and Biomedical Applications*; Harris, J. M., Ed.; Springer US, 1992.

(262) Şen Karaman, D.; Gulin-Sarfraz, T.; Hedström, G.; Duchanoy, A.; Eklund, P.; Rosenholm, J. M. Rational Evaluation of the Utilization of PEG-PEI Copolymers for the Facilitation of Silica Nanoparticulate Systems in Biomedical Applications. *J. Colloid Interface Sci.* **2014**, *418*, 300–310.

(263) Ulasov, A. V.; Khramtsov, Y. V.; Trusov, G. A.; Rosenkranz, A. A.; Sverdlov, E. D.; Sobolev, A. S. Properties of PEI-Based Polyplex Nanoparticles That Correlate With Their Transfection Efficacy. *Mol. Ther.* **2011**, *19* (1), 103–112.

(264) Kreuter, J. Nanoparticles. In *Colloidal drug delivery systems*; Kreuter, J., Ed.; Drugs and the pharmaceutical sciences; Dekker: New York, 1994; pp 219–342.

(265) Xing, Y.; Zhao, J.; Conti, P. S.; Chen, K. Radiolabeled Nanoparticles for Multimodality Tumor Imaging. *Theranostics* **2014**, *4* (3), 290–306.

(266) Perrie, Y.; Rades, T. *Pharmaceutics: Drug Delivery and Targeting*, 2. ed.; FASTtrack; Pharmaceutical Press: London, 2012.

(267) Srinivasan, M.; Rajabi, M.; Mousa, S. Multifunctional Nanomaterials and Their Applications in Drug Delivery and Cancer Therapy. *Nanomaterials* **2015**, *5* (4), 1690–1703.

(268) Allouche, J. Synthesis of Organic and Bioorganic Nanoparticles: An Overview of the Preparation Methods. In *Nanomaterials: A Danger or a Promise?*; Brayner, R., Fiévet, F., Coradin, T., Eds.; Springer London: London, 2013; pp 27–74.

(269) Faraji, A. H.; Wipf, P. Nanoparticles in Cellular Drug Delivery. *Bioorg. Med. Chem.* **2009**, *17* (8), 2950–2962.

(270) Debuigne, F.; Jeunieau, L.; Wiame, M.; B.Nagy, J. Synthesis of Organic Nanoparticles in Different W/O Microemulsions. *Langmuir* **2000**, *16* (20), 7605–7611.

(271) Kumari, A.; Yadav, S. K.; Yadav, S. C. Biodegradable Polymeric Nanoparticles Based Drug Delivery Systems. *Colloids Surf. B Biointerfaces* **2010**, *75* (1), 1–18.

(272) Li, X.; Anton, N.; Arpagaus, C.; Belleteix, F.; Vandamme, T. F. Nanoparticles by Spray Drying Using Innovative New Technology: The Büchi Nano Spray Dryer B-90. *J. Controlled Release* **2010**, *147* (2), 304–310.

(273) Rao, J. P.; Geckeler, K. E. Polymer Nanoparticles: Preparation Techniques and Size-Control Parameters. *Prog. Polym. Sci.* **2011**, *36* (7), 887–913.

(274) Wright, I. K.; Higginbotham, A.; Baker, S. M.; Donnelly, T. D. Generation of Nanoparticles of Controlled Size Using Ultrasonic Piezoelectric Oscillators in Solution. *ACS Appl. Mater. Interfaces* **2010**, *2* (8), 2360–2364.

(275) Janssen, M.; Mihov, G.; Welting, T.; Thies, J.; Emans, P. Drugs and Polymers for Delivery Systems in OA Joints: Clinical Needs and Opportunities. *Polymers* **2014**, *6* (3), 799–819.

(276) Mishra, P.; Nayak, B.; Dey, R. K. PEGylation in Anti-Cancer Therapy: An Overview. *Asian J. Pharm. Sci.* **2016**, *11* (3), 337–348.

(277) Wang, L.; Liu, Y.; Zhang, W.; Chen, X.; Yang, T.; Ma, G. Microspheres and Microcapsules for Protein Delivery: Strategies of Drug Activity Retention. *Curr. Pharm. Des.* **2013**, *19* (35), 6340–6352.

(278) Sun, X.; Li, F.; Wang, Y.; Liang, W. Cellular Uptake and Elimination of Lipophilic Drug Delivered by Nanocarriers. *Pharm.* **2010**, *65* (10), 737–742.

(279) Evangelatov, A.; Skrobanska, R.; Mladenov, N.; Petkova, M.; Yordanov, G.; Pankov, R. Epirubicin Loading in Poly(butyl Cyanoacrylate) Nanoparticles Manifests via Altered Intracellular Localization and Cellular Response in Cervical Carcinoma (HeLa) Cells. *Drug Deliv.* **2014**, 1–10.

(280) Delplace, V.; Nicolas, J. Degradable Vinyl Polymers for Biomedical Applications. *Nat. Chem.* **2015**, *7* (10), 771–784.

(281) Koo, H.; Young Yhee, J. Polymeric Nanoparticles in Cancer Therapy. In *Nanobiomaterials: Development and Applications*; Yi, D. K., Papaefthymiou, G. C., Eds.; CRC, Taylor & Francis: Boca Raton, FL, USA, 2014; pp 109–150.

(282) Lohcharoenkal, W.; Wang, L.; Chen, Y. C.; Rojanasakul, Y. Protein Nanoparticles as Drug Delivery Carriers for Cancer Therapy. *BioMed Res. Int.* **2014**, *2014*, 1–12.

(283) Mitra, S.; Gaur, U.; Ghosh, P. .; Maitra, A. . Tumour Targeted Delivery of Encapsulated Dextran–doxorubicin Conjugate Using Chitosan Nanoparticles as Carrier. *J. Controlled Release* **2001**, *74* (1–3), 317–323.

(284) Nam, H. Y.; Kwon, S. M.; Chung, H.; Lee, S.-Y.; Kwon, S.-H.; Jeon, H.; Kim, Y.; Park, J. H.; Kim, J.; Her, S.; Oh, Y.-K.; Kwon, I. C.; Kim, K.; Jeong, S. Y. Cellular Uptake Mechanism and Intracellular Fate of Hydrophobically Modified Glycol Chitosan Nanoparticles. *J. Controlled Release* **2009**, *135* (3), 259–267.

(285) Ghaz-Jahanian, M. A.; Abbaspour-Aghdam, F.; Anarjan, N.; Berenjian, A.; Jafarizadeh-Malmiri, H. Application of Chitosan-Based Nanocarriers in Tumor-Targeted Drug Delivery. *Mol. Biotechnol.* **2015**, *57* (3), 201–218.

(286) Senthilkumar, R.; Karaman, D. Ş.; Paul, P.; Björk, E. M.; Odén, M.; Eriksson, J. E.; Rosenholm, J. M. Targeted Delivery of a Novel Anticancer Compound Anisomelic Acid Using Chitosan-Coated Porous Silica Nanorods for Enhancing the Apoptotic Effect. *Biomater Sci* **2015**, *3* (1), 103–111.

(287) Panyam, J.; Labhasetwar, V. Sustained Cytoplasmic Delivery of Drugs with Intracellular Receptors Using Biodegradable Nanoparticles. *Mol. Pharm.* **2004**, *1* (1), 77–84.

(288) King, M. E.; Kinney, A. Y. Tissue Adhesives: A New Method of Wound Repair: *Nurse Pract.* **1999**, *24* (10), 66–75.

(289) Pollak, J. S.; White, R. I. The Use of Cyanoacrylate Adhesives in Peripheral Embolization. *J. Vasc. Interv. Radiol.* **2001**, *12* (8), 907–913.

(290) Singer, A. J.; Quinn, J. V.; Hollander, J. E. The Cyanoacrylate Topical Skin Adhesives. *Am. J. Emerg. Med.* **2008**, *26* (4), 490–496.

(291) Leggat, P. A.; Smith, D. R.; Kedjarune, U. Surgical Applications of Cyanoacrylate Adhesives: A Review of Toxicity. *ANZ J. Surg.* **2007**, *77* (4), 209–213.

(292) Couvreur, P.; Kante, B.; Roland, M.; Guiot, P.; Bauduin, P.; Speiser, P. Polycyanoacrylate Nanocapsules as Potential Lysosomotropic Carriers: Preparation, Morphological and Sorptive Properties. *J. Pharm. Pharmacol.* **1979**, *31* (5), 331–332.

(293) Couvreur, P.; Gref, R.; Andrieux, K.; Malvy, C. Nanotechnologies for Drug Delivery: Application to Cancer and Autoimmune Diseases. *Prog. Solid State Chem.* **2006**, *34* (2–4), 231–235.

(294) Couvreur, P.; Vauthier, C. Nanotechnology: Intelligent Design to Treat Complex Disease. *Pharm. Res.* **2006**, *23* (7), 1417–1450.

(295) Garcia-Garcia, E.; Andrieux, K.; Gil, S.; Couvreur, P. Colloidal Carriers and Blood–brain Barrier (BBB) Translocation: A Way to Deliver Drugs to the Brain? *Int. J. Pharm.* **2005**, *298* (2), 274–292.

(296) Vauthier, C.; Dubernet, C.; Fattal, E.; Pinto-Alphandary, H.; Couvreur, P. Poly(alkylcyanoacrylates) as Biodegradable Materials for Biomedical Applications. *Adv. Drug Deliv. Rev.* **2003**, *55* (4), 519–548.

(297) Vauthier, C.; Labarre, D.; Ponchel, G. Design Aspects of Poly(alkylcyanoacrylate) Nanoparticles for Drug Delivery. *J. Drug Target.* **2007**, *15* (10), 641–663.

(298) Chern, C.-S. *Principles and Applications of Emulsion Polymerization*; Wiley: Hoboken, N.J, 2008.

(299) Liu, Z.; Lammers, T.; Ehling, J.; Fokong, S.; Bornemann, J.; Kiessling, F.; Gätjens, J. Iron Oxide Nanoparticle-Containing Microbubble Composites as Contrast Agents for MR and Ultrasound Dual-Modality Imaging. *Biomaterials* **2011**, *32* (26), 6155–6163.

(300) Kiessling, F.; Fokong, S.; Bzyl, J.; Lederle, W.; Palmowski, M.; Lammers, T. Recent Advances in Molecular, Multimodal and Theranostic Ultrasound Imaging. *Adv. Drug Deliv. Rev.* **2014**, *72*, 15–27.

(301) Vauthier, C.; Bouchemal, K. Methods for the Preparation and Manufacture of Polymeric Nanoparticles. *Pharm. Res.* **2009**, *26* (5), 1025–1058.

(302) Ramge, P.; Unger, R. E.; Oltrogge, J. B.; Zenker, D.; Begley, D.; Kreuter, J.; Von Briesen, H. Polysorbate-80 Coating Enhances Uptake of Polybutylcyanoacrylate (PBCA)-Nanoparticles by Human and Bovine Primary Brain Capillary Endothelial Cells: Uptake of Nanoparticles by Brain Endothelial Cells. *Eur. J. Neurosci.* **2000**, *12* (6), 1931–1940.

(303) Mørch, Ý.; Hansen, R.; Berg, S.; Åslund, A. K. O.; Glomm, W. R.; Eggen, S.; Schmid, R.; Johnsen, H.; Kubowicz, S.; Snipstad, S.; Sulheim, E.; Hak, S.; Singh, G.; McDonagh, B. H.; Blom, H.; de Lange Davies, C.; Stenstad, P. M. Nanoparticle-Stabilized Microbubbles for Multimodal Imaging and Drug Delivery: NP-Stabilized Microbubbles for Multimodal Imaging and Drug Delivery. *Contrast Media Mol. Imaging* **2015**, *10* (5), 356–366.

(304) Dasgupta, A.; Liu, M.; Ojha, T.; Storm, G.; Kiessling, F.; Lammers, T. Ultrasound-Mediated Drug Delivery to the Brain: Principles, Progress and Prospects. *Drug Discov. Today Technol.* **2016**.

(305) Nicolas, J.; Couvreur, P. Synthesis of Poly(alkyl Cyanoacrylate)-Based Colloidal Nanomedicines. *Wiley Interdiscip. Rev. Nanomed. Nanobiotechnol.* **2009**, *1* (1), 111–127.

(306) Costantino, L.; Tosi, G.; Ruozi, B.; Bondioli, L.; Vandelli, M. A.; Forni, F. Colloidal Systems for CNS Drug Delivery. In *Nanoneuroscience and Nanoneuropharmacology*; Sharma, H. S., Ed.; Elsevier: Oxford, UK, 2009; pp 35–72.

(307) Müller, R. H.; Lherm, C.; Herbort, J.; Couvreur, P. In Vitro Model for the Degradation of Alkylcyanoacrylate Nanoparticles. *Biomaterials* **1990**, *11* (8), 590–595.

(308) Scherer, D.; Robinson, J. R.; Kreuter, J. Influence of Enzymes on the Stability of Polybutylcyanoacrylate Nanoparticles. *Int. J. Pharm.* **1994**, *101* (1–2), 165–168.

(309) Lherm, C.; Müller, R. H.; Puisieux, F.; Couvreur, P. Alkylcyanoacrylate Drug Carriers: II. Cytotoxicity of Cyanoacrylate Nanoparticles with Different Alkyl Chain Length. *Int. J. Pharm.* **1992**, *84* (1), 13–22.

(310) Yordanov, G. Poly (Alkyl Cyanoacrylate) Nanoparticles as Drug Carriers: 33 Years Later 1.2 (2012): 61-72. *Bulg. J. Chem.* **2012**, *1.2*, 61–72.

(311) Snipstad, S.; Westrøm, S.; Mørch, Y.; Afadzi, M.; Åslund, A. K.; de Lange Davies, C. Contact-Mediated Intracellular Delivery of Hydrophobic Drugs from Polymeric Nanoparticles. *Cancer Nanotechnol.* **2014**, *5* (1).

(312) Torchilin, V. P. Multifunctional, Stimuli-Sensitive Nanoparticulate Systems for Drug Delivery. *Nat. Rev. Drug Discov.* **2014**, *13* (11), 813–827.

(313) Jain, K. Nanodiagnostics: Application of Nanotechnology in Molecular Diagnostics. *Expert Rev. Mol. Diagn.* **2003**, *3* (2), 153–161.

(314) *Drug Delivery Systems*; Jain, K. K., Ed.; Methods in molecular biology; Humana: Totowa, NJ, 2008.

(315) Kayser, O.; Lemke, A.; Hernández-Trejo, N. The Impact of Nanobiotechnology on the Development of New Drug Delivery Systems. *Curr. Pharm. Biotechnol.* **2005**, *6* (1), 3–5.

(316) Ambrogio, M. W.; Thomas, C. R.; Zhao, Y.-L.; Zink, J. I.; Stoddart, J. F. Mechanized Silica Nanoparticles: A New Frontier in Theranostic Nanomedicine. *Acc. Chem. Res.* **2011**, *44* (10), 903–913.

(317) Bae, S. W.; Tan, W.; Hong, J.-I. Fluorescent Dye-Doped Silica Nanoparticles: New Tools for Bioapplications. *Chem. Commun.* **2012**, *48* (17), 2270.

(318) Jiang, S.; Gnanasammandhan, M. K.; Zhang, Y. Optical Imaging-Guided Cancer Therapy with Fluorescent Nanoparticles. *J. R. Soc. Interface* **2010**, *7* (42), 3–18.

(319) Rehor, I.; Slegerova, J.; Kucka, J.; Proks, V.; Petrakova, V.; Adam, M.-P.; Treussart, F.; Turner, S.; Bals, S.; Sacha, P.; Ledvina, M.; Wen, A. M.; Steinmetz, N. F.; Cigler, P. Fluorescent Nanodiamonds Embedded in Biocompatible Translucent Shells. *Small* **2014**, *10* (6), 1106–1115.

(320) Lee, S. B.; Kim, H. L.; Jeong, H.-J.; Lim, S. T.; Sohn, M.-H.; Kim, D. W. Mesoporous Silica Nanoparticle Pretargeting for PET Imaging Based on a Rapid Bioorthogonal Reaction in a Living Body. *Angew. Chem. Int. Ed.* **2013**, *52* (40), 10549–10552.

(321) Chen, F.; Hong, H.; Zhang, Y.; Valdovinos, H. F.; Shi, S.; Kwon, G. S.; Theuer, C. P.; Barnhart, T. E.; Cai, W. *In Vivo* Tumor Targeting and Image-Guided Drug Delivery with Antibody-Conjugated, Radiolabeled Mesoporous Silica Nanoparticles. *ACS Nano* **2013**, *7* (10), 9027–9039.

(322) Taylor, K. M. L.; Kim, J. S.; Rieter, W. J.; An, H.; Lin, W.; Lin, W. Mesoporous Silica Nanospheres as Highly Efficient MRI Contrast Agents. *J. Am. Chem. Soc.* **2008**, *130* (7), 2154–2155.

(323) Şen Karaman, D.; Desai, D.; Zhang, J.; Tadayon, S.; Unal, G.; Teuho, J.; Sarfraz, J.; Smått, J.-H.; Gu, H.; Näreoja, T.; Rosenholm, J. M. Modulation of the Structural Properties of Mesoporous Silica Nanoparticles to Enhance the T_1-Weighted MR Imaging Capability. *J Mater Chem B* **2016**, *4* (9), 1720–1732.

(324) Morelli, C.; Maris, P.; Sisci, D.; Perrotta, E.; Brunelli, E.; Perrotta, I.; Panno, M. L.; Tagarelli, A.; Versace, C.; Casula, M. F.; Testa, F.; Andò, S.; Nagy, J. B.; Pasqua, L. PEG-Templated Mesoporous Silica Nanoparticles Exclusively Target Cancer Cells. *Nanoscale* **2011**, *3* (8), 3198.

(325) Rosenholm, J. M.; Peuhu, E.; Eriksson, J. E.; Sahlgren, C.; Lindén, M. Targeted Intracellular Delivery of Hydrophobic Agents Using Mesoporous Hybrid Silica Nanoparticles as Carrier Systems. *Nano Lett.* **2009**, *9* (9), 3308–3311.

(326) Benezra, M.; Penate-Medina, O.; Zanzonico, P. B.; Schaer, D.; Ow, H.; Burns, A.; DeStanchina, E.; Longo, V.; Herz, E.; Iyer, S.; Wolchok, J.; Larson, S. M.; Wiesner, U.; Bradbury, M. S. Multimodal Silica Nanoparticles Are Effective Cancer-Targeted Probes in a Model of Human Melanoma. *J. Clin. Invest.* **2011**, *121* (7), 2768–2780.

(327) Zhang, Q.; Wang, X.; Li, P.-Z.; Nguyen, K. T.; Wang, X.-J.; Luo, Z.; Zhang, H.; Tan, N. S.; Zhao, Y. Biocompatible, Uniform, and Redispersible Mesoporous Silica Nanoparticles for Cancer-Targeted Drug Delivery In Vivo. *Adv. Funct. Mater.* **2014**, *24* (17), 2450–2461.

(328) Chan, M.-H.; Lin, H.-M. Preparation and Identification of Multifunctional Mesoporous Silica Nanoparticles for in Vitro and in Vivo Dual-Mode Imaging, Theranostics, and Targeted Tracking. *Biomaterials* **2015**, *46*, 149–158.

(329) Chen, F.; Hong, H.; Shi, S.; Goel, S.; Valdovinos, H. F.; Hernandez, R.; Theuer, C. P.; Barnhart, T. E.; Cai, W. Engineering of Hollow Mesoporous Silica Nanoparticles for Remarkably Enhanced Tumor Active Targeting Efficacy. *Sci. Rep.* **2014**, *4*.

(330) Luk, B. T.; Zhang, L. Current Advances in Polymer-Based Nanotheranostics for Cancer Treatment and Diagnosis. *ACS Appl. Mater. Interfaces* **2014**, *6* (24), 21859–21873.

(331) Fokong, S.; Fragoso, A.; Rix, A.; Curaj, A.; Wu, Z.; Lederle, W.; Iranzo, O.; Gätjens, J.; Kiessling, F.; Palmowski, M. Ultrasound Molecular Imaging of E-Selectin in Tumor Vessels Using Poly N-Butyl Cyanoacrylate Microbubbles Covalently Coupled to a Short Targeting Peptide: *Invest. Radiol.* **2013**, *48* (12), 843–850.

(332) Fokong, S.; Theek, B.; Wu, Z.; Koczera, P.; Appold, L.; Jorge, S.; Resch-Genger, U.; van Zandvoort, M.; Storm, G.; Kiessling, F.; Lammers, T. Image-Guided, Targeted and Triggered Drug Delivery to Tumors Using Polymer-Based Microbubbles. *J. Controlled Release* **2012**, *163* (1), 75–81.

(333) Arruebo, M. Drug Delivery from Structured Porous Inorganic Materials. *Wiley Interdiscip. Rev. Nanomed. Nanobiotechnol.* **2012**, *4* (1), 16–30.

(334) Vallet-Regi, M.; Rámila, A.; del Real, R. P.; Pérez-Pariente, J. A New Property of MCM-41: Drug Delivery System. *Chem. Mater.* **2001**, *13* (2), 308–311.

(335) *Controlled Drug Delivery: Fundamentals and Applications*, 2nd ed., and expanded.; Robinson, J. R., Lee, V. H. L., Eds.; Drugs and the pharmaceutical sciences; Dekker: New York, 1987.

(336) Pasqua, L.; Cundari, S.; Ceresa, C.; Cavaletti, G. Recent Development, Applications, and Perspectives of Mesoporous Silica Particles in Medicine and Biotechnology. *Curr. Med. Chem.* **2009**, *16* (23), 3054–3063.

(337) Olivier, J.-C. Drug Transport to Brain with Targeted Nanoparticles. *NeuroRX* **2005**, *2* (1), 108–119.

(338) Zhang, Y.; Zhi, Z.; Jiang, T.; Zhang, J.; Wang, Z.; Wang, S. Spherical Mesoporous Silica Nanoparticles for Loading and Release of the Poorly Water-Soluble Drug Telmisartan. *J. Controlled Release* **2010**, *145* (3), 257–263.

(339) Wang, Y.; Sun, Y.; Wang, J.; Yang, Y.; Li, Y.; Yuan, Y.; Liu, C. Charge-Reversal APTES-Modified Mesoporous Silica Nanoparticles with High Drug Loading and Release Controllability. *ACS Appl. Mater. Interfaces* **2016**, *8* (27), 17166–17175.

(340) Graf, A.; McDowell, A.; Rades, T. Poly(alkycyanoacrylate) Nanoparticles for Enhanced Delivery of Therapeutics – Is There Real Potential? *Expert Opin. Drug Deliv.* **2009**, *6* (4), 371–387.

(341) Aryal, S.; Hu, C.-M. J.; Zhang, L. Polymeric Nanoparticles with Precise Ratiometric Control over Drug Loading for Combination Therapy. *Mol. Pharm.* **2011**, *8* (4), 1401–1407.

(342) Azaïs, T.; Tourné-Péteilh, C.; Aussenac, F.; Baccile, N.; Coelho, C.; Devoisselle, J.-M.; Babonneau, F. Solid-State NMR Study of Ibuprofen Confined in MCM-41 Material. *Chem. Mater.* **2006**, *18* (26), 6382–6390.

(343) Rámila, A.; Munoz, B.; Pérez-Pariente, J.; Vallet-Regi, M. Mesoporous MCM-41 as Drug Host System. *J. Sol-Gel Sci. Technol.* **2003**, *26* (1), 1199–1202.

(344) Song, S.-W.; Hidajat, K.; Kawi, S. Functionalized SBA-15 Materials as Carriers for Controlled Drug Delivery: Influence of Surface Properties on Matrix−Drug Interactions. *Langmuir* **2005**, *21* (21), 9568–9575.

(345) Wang, G.; Otuonye, A. N.; Blair, E. A.; Denton, K.; Tao, Z.; Asefa, T. Functionalized Mesoporous Materials for Adsorption and Release of Different Drug Molecules: A Comparative Study. *J. Solid State Chem.* **2009**, *182* (7), 1649–1660.

(346) Higuchi, T. Mechanism of Sustained-action Medication. Theoretical Analysis of Rate of Release of Solid Drugs Dispersed in Solid Matrices. *J. Pharm. Sci.* **1963**, *52* (12), 1145–1149.

(347) Costa, P.; Sousa Lobo, J. M. Modeling and Comparison of Dissolution Profiles. *Eur. J. Pharm. Sci. Off. J. Eur. Fed. Pharm. Sci.* **2001**, *13* (2), 123–133.

(348) Müller, R. H.; Lherm, C.; Herbort, J.; Blunk, T.; Couvreur, P. Alkylcyanoacrylate Drug Carriers: I. Physicochemical Characterization of Nanoparticles with Different Alkyl Chain Length. *Int. J. Pharm.* **1992**, *84* (1), 1–11.

(349) Huang, C.-Y.; Lee, Y.-D. Core-Shell Type of Nanoparticles Composed of Poly[(n-Butyl Cyanoacrylate)-Co-(2-Octyl Cyanoacrylate)] Copolymers for Drug Delivery Application: Synthesis, Characterization and in Vitro Degradation. *Int. J. Pharm.* **2006**, *325* (1–2), 132–139.

(350) Kapoor, S.; Hegde, R.; Bhattacharyya, A. J. Influence of Surface Chemistry of Mesoporous Alumina with Wide Pore Distribution on Controlled Drug Release. *J. Controlled Release* **2009**, *140* (1), 34–39.

(351) Salonen, J.; Laitinen, L.; Kaukonen, A. M.; Tuura, J.; Björkqvist, M.; Heikkilä, T.; Vähä-Heikkilä, K.; Hirvonen, J.; Lehto, V.-P. Mesoporous Silicon Microparticles for Oral Drug Delivery: Loading and Release of Five Model Drugs. *J. Controlled Release* **2005**, *108* (2–3), 362–374.

(352) Heikkila, T.; Salonen, J.; Tuura, J.; Hamdy, M.; Mul, G.; Kumar, N.; Salmi, T.; Murzin, D.; Laitinen, L.; Kaukonen, A. Mesoporous Silica Material TUD-1 as a Drug Delivery System. *Int. J. Pharm.* **2007**, *331* (1), 133–138.

(353) Tourné-Péteilh, C.; Brunel, D.; Bégu, S.; Chiche, B.; Fajula, F.; Lerner, D. A.; Devoisselle, J.-M. Synthesis and Characterisation of Ibuprofen-Anchored MCM-41 Silica and Silica Gel. *New J Chem* **2003**, *27* (10), 1415–1418.

(354) Mortera, R.; Vivero-Escoto, J.; Slowing, I. I.; Garrone, E.; Onida, B.; Lin, V. S.-Y. Cell-Induced Intracellular Controlled Release of Membrane Impermeable Cysteine from a Mesoporous Silica Nanoparticle-Based Drug Delivery System. *Chem. Commun.* **2009**, No. 22, 3219.

(355) Panyam, J.; Labhasetwar, V. Biodegradable Nanoparticles for Drug and Gene Delivery to Cells and Tissue. *Adv. Drug Deliv. Rev.* **2003**, *55* (3), 329–347.

(356) Mura, S.; Nicolas, J.; Couvreur, P. Stimuli-Responsive Nanocarriers for Drug Delivery. *Nat. Mater.* **2013**, *12* (11), 991–1003.

(357) Yan, E.; Ding, Y.; Chen, C.; Li, R.; Hu, Y.; Jiang, X. Polymer/Silica Hybrid Hollow Nanospheres with pH-Sensitive Drug Release in Physiological and Intracellular Environments. *Chem. Commun.* **2009**, No. 19, 2718.

(358) Sebastián Alberti. Gated Supramolecular Chemistry in Hybrid Mesoporous Silica Nanoarchitectures: Controlled Delivery and Molecular Transport in Response to Chemical, Physical and Biological Stimuli. *Chem.Commun.* **2015**, *51*, 6050–6075.

(359) Huynh, C. T.; Lee, D. S. Controlled Release. In *Encyclopedia of Polymeric Nanomaterials*; Kobayashi, S., Müllen, K., Eds.; Springer Berlin Heidelberg: Berlin, Heidelberg, 2014; pp 439–449.

(360) Bhutia, S. K.; Maiti, T. K. Targeting Tumors with Peptides from Natural Sources. *Trends Biotechnol.* **2008**, *26* (4), 210–217.

(361) Niemelä, E.; Desai, D.; Nkizinkiko, Y.; Eriksson, J. E.; Rosenholm, J. M. Sugar-Decorated Mesoporous Silica Nanoparticles as Delivery Vehicles for the Poorly Soluble Drug Celastrol Enables Targeted Induction of Apoptosis in Cancer Cells. *Eur. J. Pharm. Biopharm.* **2015**, *96*, 11–21.

(362) Gullotti, E.; Yeo, Y. Extracellularly Activated Nanocarriers: A New Paradigm of Tumor Targeted Drug Delivery. *Mol. Pharm.* **2009**, *6* (4), 1041–1051.

(363) Singh, R.; Lillard, J. W. Nanoparticle-Based Targeted Drug Delivery. *Exp. Mol. Pathol.* **2009**, *86* (3), 215–223.

(364) *Nanotechnology for Cancer Therapy*; Amiji, M. M., Ed.; CRC/Taylor & Francis: Boca Raton, 2007.

(365) Davis, S. S. Biomédical Applications of Nanotechnology — Implications for Drug Targeting and Gene Therapy. *Trends Biotechnol.* **1997**, *15* (6), 217–224.

(366) Paolino, D.; Sinha, P.; Fresta, M.; Ferrari, M. Drug Delivery Systems. In *Encyclopedia of Medical Devices and Instrumentation*; Webster, J. G., Ed.; John Wiley & Sons, Inc.: Hoboken, NJ, USA, 2006.

(367) Rejman, J.; Oberle, V.; Zuhorn, I. S.; Hoekstra, D. Size-Dependent Internalization of Particles via the Pathways of Clathrin- and Caveolae-Mediated Endocytosis. *Biochem. J.* **2004**, *377* (1), 159–169.

(368) Amiji, M. *Nanotechnology-Improving Drug Delivery*; Drug Delivery; 17; Touch Briefings: London, UK, 2007; pp 53–56.

(369) Brigger, I.; Dubernet, C.; Couvreur, P. Nanoparticles in Cancer Therapy and Diagnosis. *Adv. Drug Deliv. Rev.* **2002**, *54* (5), 631–651.

(370) Pozzi, D.; Colapicchioni, V.; Caracciolo, G.; Piovesana, S.; Capriotti, A. L.; Palchetti, S.; De Grossi, S.; Riccioli, A.; Amenitsch, H.; Laganà, A. Effect of Polyethyleneglycol (PEG) Chain Length on the Bio–nano-Interactions between PEGylated Lipid Nanoparticles and Biological Fluids: From Nanostructure to Uptake in Cancer Cells. *Nanoscale* **2014**, *6* (5), 2782.

(371) Torchilin, V. Targeted Pharmaceutical Nanocarriers for Cancer Therapy and Imaging. *AAPS J.* **2007**, *9* (2), E128–E147.

(372) Owensiii, D.; Peppas, N. Opsonization, Biodistribution, and Pharmacokinetics of Polymeric Nanoparticles. *Int. J. Pharm.* **2006**, *307* (1), 93–102.

(373) Peracchia, M. T.; Vauthier, C.; Desmaele, D.; Gulik, A.; Dedieu, J.-C.; Demoy, M.; d'Angelo, J.; Couvreur, P. Pegylated Nanoparticles from a Novel Methoxypolyethylene Glycol Cyanoacrylate-Hexadecyl Cyanoacrylate Amphiphilic Copolymer. *Pharm. Res.* **1998**, *15* (4), 550–556.

(374) Hirsjarvi, S.; Passirani, C.; Benoit, J.-P. Passive and Active Tumour Targeting with Nanocarriers. *Curr. Drug Discov. Technol.* **2011**, *8* (3), 188–196.

(375) Allen, T. M. Drug Delivery Systems: Entering the Mainstream. *Science* **2004**, *303* (5665), 1818–1822.

(376) Iyer, A. K.; Khaled, G.; Fang, J.; Maeda, H. Exploiting the Enhanced Permeability and Retention Effect for Tumor Targeting. *Drug Discov. Today* **2006**, *11* (17–18), 812–818.

(377) Chouly, C.; Pouliquen, D.; Lucet, I.; Jeune, J. J.; Jallet, P. Development of Superparamagnetic Nanoparticles for MRI: Effect of Particle Size, Charge and Surface Nature on Biodistribution. *J. Microencapsul.* **1996**, *13* (3), 245–255.

(378) Xu, Z. P.; Zeng, Q. H.; Lu, G. Q.; Yu, A. B. Inorganic Nanoparticles as Carriers for Efficient Cellular Delivery. *Chem. Eng. Sci.* **2006**, *61* (3), 1027–1040.

(379) Lim, Y.; Kim, S.-M.; Lee, Y.; Lee, W.; Yang, T.; Lee, M.; Suh, H.; Park, J. Cationic Hyperbranched Poly(amino Ester): A Novel Class of DNA Condensing Molecule with Cationic Surface, Biodegradable Three-Dimensional Structure, and Tertiary Amine Groups in the Interior. *J. Am. Chem. Soc.* **2001**, *123* (10), 2460–2461.

(380) Chithrani, B. D.; Chan, W. C. W. Elucidating the Mechanism of Cellular Uptake and Removal of Protein-Coated Gold Nanoparticles of Different Sizes and Shapes. *Nano Lett.* **2007**, *7* (6), 1542–1550.

(381) Jin, H.; Heller, D. A.; Sharma, R.; Strano, M. S. Size-Dependent Cellular Uptake and Expulsion of Single-Walled Carbon Nanotubes: Single Particle Tracking and a Generic Uptake Model for Nanoparticles. *ACS Nano* **2009**, *3* (1), 149–158.

(382) Porter, C. J. H.; Moghimi, S. M.; Illum, L.; Davis, S. S. The Polyoxyethylene/Polyoxypropylene Block Co-Polymer Poloxamer-407 Selectively Redirects Intravenously Injected Microspheres to Sinusoidal Endothelial Cells of Rabbit Bone Marrow. *FEBS Lett.* **1992**, *305* (1), 62–66.

(383) Mao, Z.; Zhou, X.; Gao, C. Influence of Structure and Properties of Colloidal Biomaterials on Cellular Uptake and Cell Functions. *Biomater. Sci.* **2013**, *1* (9), 896.

(384) Huang, M.; Ma, Z.; Khor, E.; Lim, L.-Y. Uptake of FITC-Chitosan Nanoparticles by A549 Cells. *Pharm. Res.* **2002**, *19* (10), 1488–1494.

(385) Sulheim, E.; Baghirov, H.; von Haartman, E.; Bøe, A.; Åslund, A. K. O.; Mørch, Y.; Davies, C. de L. Cellular Uptake and Intracellular Degradation of Poly(alkyl Cyanoacrylate) Nanoparticles. *J. Nanobiotechnology* **2016**, *14* (1).

(386) *Handbook of Surfaces and Interfaces of Materials*; Nalwa, H. S., Ed.; Academic Press: San Diego, 2001; Vol. 5.

(387) Huang, X.; Teng, X.; Chen, D.; Tang, F.; He, J. The Effect of the Shape of Mesoporous Silica Nanoparticles on Cellular Uptake and Cell Function. *Biomaterials* **2010**, *31* (3), 438–448.

(388) *Molecular Cell Biology*, 6th ed.; Lodish, H. F., Ed.; W.H. Freeman: New York, 2008.

(389) Wang, L. H.; Rothberg, K. G.; Anderson, R. G. Mis-Assembly of Clathrin Lattices on Endosomes Reveals a Regulatory Switch for Coated Pit Formation. *J. Cell Biol.* **1993**, *123* (5), 1107–1117.

(390) Pelkmans, L. Local Actin Polymerization and Dynamin Recruitment in SV40-Induced Internalization of Caveolae. *Science* **2002**, *296* (5567), 535–539.

(391) Hayer, A.; Stoeber, M.; Ritz, D.; Engel, S.; Meyer, H. H.; Helenius, A. Caveolin-1 Is Ubiquitinated and Targeted to Intralumenal Vesicles in Endolysosomes for Degradation. *J. Cell Biol.* **2010**, *191* (3), 615–629.

(392) Scita, G.; Di Fiore, P. P. The Endocytic Matrix. *Nature* **2010**, *463* (7280), 464–473.

(393) Parton, R. G. Caveolae Meet Endosomes: A Stable Relationship? *Dev. Cell* **2004**, *7* (4), 458–460.

(394) von Haartman, E.; Lindberg, D.; Prabhakar, N.; Rosenholm, J. M. On the Intracellular Release Mechanism of Hydrophobic Cargo and Its Relation to the Biodegradation Behavior of Mesoporous Silica Nanocarriers. *Eur. J. Pharm. Sci.* **2016**, *95*, 17–26.

(395) Hu, Y.; Litwin, T.; Nagaraja, A. R.; Kwong, B.; Katz, J.; Watson, N.; Irvine, D. J. Cytosolic Delivery of Membrane-Impermeable Molecules in Dendritic Cells Using pH-Responsive Core−Shell Nanoparticles. *Nano Lett.* **2007**, *7* (10), 3056–3064.

(396) Zetasizer Nano user manual (MAN0485-1-1) http://www.malvern.com/Assets/Zetasizer-Nano-user-manual-English-MAN0485-1-1.pdf (accessed Sep 3, 2016).

(397) Berne, B. J.; Pecora, R. *Dynamic Light Scattering: With Applications to Chemistry, Biology, and Physics*, Dover ed.; Dover Publications: Mineola, N.Y, 2000.

(398) Shaw, D. J. *Introduction to Colloid and Surface Chemistry*, 4th ed.; Butterworth-Heinemann: Oxford ; Boston, 1992.

(399) Ford, Jr., N. C. Light Scattering Apparatus. In *Dynamic Light Scattering Applications of Photon Correlation Spectroscopy*; Pecora, R., Ed.; 1985; pp 7–58.

(400) Zeta potential - An introduction in 30 minutes, Technical Note www.malvern.com (accessed Mar 18, 2016).

(401) Hunter, R. J. *Zeta Potential in Colloid Science: Principles and Applications*; Colloid science; Academic Press: London ; New York, 1981.

(402) Zeta potential (AN011) Electrophoresis www.escubed.co.uk (accessed Mar 18, 2016).

(403) Bragg, W. L. Diffraction of Short Electromagnetic Waves by a Crystal. *Proc. Camb. Philos. Soc.* **1913**, *17*, 43–57.

(404) Cullity, B. D. Diffraction I: The Directions of Diffracted Beams. In *Elements of x-ray diffraction*; Addison-Wesley series in metallurgy and materials; Addison-Wesley: Reading, Mass., 1978; pp 78–103.

(405) Barton, T. J.; Bull, L. M.; Klemperer, W. G.; Loy, D. A.; McEnaney, B.; Misono, M.; Monson, P. A.; Pez, G.; Scherer, G. W.; Vartuli, J. C.; Yaghi, O. M. Tailored Porous Materials. *Chem. Mater.* **1999**, *11* (10), 2633–2656.

(406) Rouquerol, F.; Rouquerol, J.; Sing, K. S. W.; Llewellyn, P. L.; Maurin, G. *Adsorption by Powders and Porous Solids: Principles, Methodology and Applications*, Second edition.; Elsevier/AP: Amsterdam, 2014.

(407) Brunauer, S.; Emmett, P. H.; Teller, E. Adsorption of Gases in Multimolecular Layers. *J. Am. Chem. Soc.* **1938**, *60* (2), 309–319.

(408) Barrett, E. P.; Joyner, L. G.; Halenda, P. P. The Determination of Pore Volume and Area Distributions in Porous Substances. I. Computations from Nitrogen Isotherms. *J. Am. Chem. Soc.* **1951**, *73* (1), 373–380.

(409) Kruk, M.; Jaroniec, M.; Sakamoto, Y.; Terasaki, O.; Ryoo, R.; Ko, C. H. Determination of Pore Size and Pore Wall Structure of MCM-41 by Using Nitrogen Adsorption, Transmission Electron Microscopy, and X-Ray Diffraction. *J. Phys. Chem. B* **2000**, *104* (2), 292–301.

(410) Ravikovitch, P. I.; Domhnaill, S. C. O.; Neimark, A. V.; Schueth, F.; Unger, K. K. Capillary Hysteresis in Nanopores: Theoretical and Experimental Studies of Nitrogen Adsorption on MCM-41. *Langmuir* **1995**, *11* (12), 4765–4772.

(411) Tinoco, I.; Sauer, K.; Wang, J. C. *Physical Chemistry: Principles and Applications in Biological Sciences*, 3rd ed.; Prentice Hall: Englewood Cliffs, N.J, 1995.

(412) Thornburn Burns. Principles of Spectrophotometric Measurements with Particular Reference to the UV-Visible Region. In *UV spectroscopy: techniques, instrumentation, data handling*; Clark, B. J., Frost, T., Russell, M. A., Ultraviolet Spectrometry Group (Great

Britain), Eds.; Techniques in visible and ultraviolet spectrometry; Chapman & Hall: London ; New York, 1993.

(413) Parson, W. W. *Modern Optical Spectroscopy: With Exercises and Examples from Biophysics and Biochemistry*, Student ed.; Springer: Dordrecht ; New York, 2009.

(414) Bottom, R. Thermogravimetric Analysis. In *Principles and applications of thermal analysis*; Gabbott, P., Ed.; Blackwell Pub: Oxford ; Ames, Iowa, 2008; pp 87–118.

(415) Heal, G. R. Thermogravimetry and Derivative Thermogravimetry. In *Principles of Thermal Analysis and Calorimetry*; Haines, P. J., Ed.; RSC Paperbacks; Royal Society of Chemistry: Cambridge, UK, 2002.

(416) Reimer, L. *Scanning Electron Microscopy: Physics of Image Formation and Microanalysis*; 1998.

(417) Flegler, S. L.; Heckman, J. W.; Klomparens, K. L. *Scanning and Transmission Electron Microscopy: An Introduction*; Oxford University Press: New York, 1995.

(418) Mehta, R. Interactions, Imaging and Spectra in SEM. In *Scanning Electron Microscopy*; Kazmiruk, V., Ed.; InTech, 2012.

(419) Echlin, P. *Handbook of Sample Preparation for Scanning Electron Microscopy and X-Ray Microanalysis*; Springer: New York, NY, 2009.

(420) Goodhew, P. J.; Humphreys, F. J.; Beanland, R. *Electron Microscopy and Analysis*, 3rd ed.; Taylor & Francis: London ; New York, 2001.

(421) Williams, D. B.; Carter, C. B. *Transmission Electron Microscopy: A Textbook for Materials Science*, 2nd ed.; Springer: New York, 2008.

(422) *Transmission Electron Microscopy*; Amelinckx, S., van Dyck, D., van Landuyt, J., van Tendeloo, G., Eds.; VCH: Weinheim, 1997.

(423) Fultz, B.; Howe, J. M. *Transmission Electron Microscopy and Diffractometry of Materials*, 3rd ed.; Advanced texts in physics; Springer: Berlin ; New York, 2008.

(424) Givan, A. L. *Flow Cytometry: First Principles*, 2nd ed.; Wiley-Liss: New York, 2001.

(425) Watson, J. V. *Introduction to Flow Cytometry*; Cambridge Univ. Pr: Cambridge, 1991.

(426) *Flow Cytometry: A Practical Approach*, 3rd ed.; Ormerod, M. G., Ed.; The practical approach series; Oxford University Press: Oxford [England] ; New York, 2000.

(427) Greve, B.; Kelsch, R.; Spaniol, K.; Eich, H. T.; Götte, M. Flow Cytometry in Cancer Stem Cell Analysis and Separation. *Cytometry A* **2012**, *81A* (4), 284–293.

(428) Shapiro, H. M. *Practical Flow Cytometry*, 4th ed.; Wiley-Liss: New York, 2003.

(429) *Handbook of Biological Confocal Microscopy*, 3rd ed.; Pawley, J. B., Ed.; Springer: New York, NY, 2006.

(430) Zhang, S.; Li, L.; Kumar, A. Laser Confocal Fluorescence Microscopy. In *Materials characterization techniques*; CRC Press: Boca Raton, 2009; pp 295–318.

(431) Claxton, N. S.; Fellers, T. J.; Davidson, M. W. *Laser Scanning Confocal Microscopy*; Department od Optical microscopy and Digital Imaging: The Florida State University, Talahassee, USA.

(432) Hell, S. W. Toward Fluorescence Nanoscopy. *Nat. Biotechnol.* **2003**, *21* (11), 1347–1355.

(433) Dailey, M. E.; Manders, E.; Soll, D. R.; Terasaki, M. Confocal Microscopy of Living Cells. In *Handbook of biological confocal microscopy*; Pawley, J. B., Ed.; Springer: New York, NY, 2006; pp 381–403.

(434) Gravier, J.; Sancey, L.; Hirsjärvi, S.; Rustique, E.; Passirani, C.; Benoît, J.-P.; Coll, J.-L.; Texier, I. FRET Imaging Approaches for *in Vitro* and *in Vivo* Characterization of Synthetic Lipid Nanoparticles. *Mol. Pharm.* **2014**, *11* (9), 3133–3144.

(435) Klonis, N.; Rug, M.; Harper, I.; Wickham, M.; Cowman, A.; Tilley, L. Fluorescence Photobleaching Analysis for the Study of Cellular Dynamics. *Eur. Biophys. J. EBJ* **2002**, *31* (1), 36–51.

(436) Lippincott-Schwartz, J.; Altan-Bonnet, N.; Patterson, G. H. Photobleaching and Photoactivation: Following Protein Dynamics in Living Cells. *Nat. Cell Biol.* **2003**, *Suppl*, S7-14.

(437) Lind, A.; Andersson, J.; Karlsson, S.; Lindén, M.; Rosenholm, J. B. Solubilization of Benzene Derivatives in Silicate-Surfactant Systems. *Colloids Surf. Physicochem. Eng. Asp.* **2001**, *183–185*, 415–422.

(438) Wittig, R.; Rosenholm, J. M.; von Haartman, E.; Hemming, J.; Genze, F.; Bergman, L.; Simmet, T.; Lindén, M.; Sahlgren, C. Active Targeting of Mesoporous Silica Drug Carriers Enhances γ-Secretase Inhibitor Efficacy in an *in Vivo* Model for Breast Cancer. *Nanomed.* **2014**, *9* (7), 971–987.

(439) Molecular Probes Inc. Lipophilic Tracers — DiI, DiO, DiD, DiA and DiR. ThermoFisher Scientific Inc. 2008.

(440) Rosenholm, J. M.; Lindén, M. Towards Establishing Structure–activity Relationships for Mesoporous Silica in Drug Delivery Applications. *J. Controlled Release* **2008**, *128* (2), 157–164.

(441) Chen, K.; Zhang, J.; Gu, H. Dissolution from inside: A Unique Degradation Behaviour of Core–shell Magnetic Mesoporous Silica Nanoparticles and the Effect of Polyethyleneimine Coating. *J. Mater. Chem.* **2012**, *22* (41), 22005–22012.

(442) Li, L. Synthesis and Hydrolytic Stability of Mesoporous Silica Nanoparticles. M.Sc.(Tech), Åbo Akademi University, 2010.

(443) Keyes, J. T.; Simon, B. R.; Vande Geest, J. P. Location-Dependent Coronary Artery Diffusive and Convective Mass Transport Properties of a Lipophilic Drug Surrogate Measured Using Nonlinear Microscopy. *Pharm. Res.* **2013**, *30* (4), 1147–1160.

(444) Gravier, J.; Navarro, F. P.; Delmas, T.; Mittler, F.; Couffin, A.-C.; Vinet, F.; Texier, I. Lipidots: Competitive Organic Alternative to Quantum Dots for in Vivo Fluorescence Imaging. *J. Biomed. Opt.* **2011**, *16* (9), 096013.

(445) Klausner, R. D.; Wolf, D. E. Selectivity of Fluorescent Lipid Analogues for Lipid Domains. *Biochemistry (Mosc.)* **1980**, *19* (26), 6199–6203.

(446) Desai, D.; Prabhakar, N.; Mamaeva, V.; Sen Karaman, D.; Lähdeniemi, I.; Sahlgren, C.; Rosenholm, J.; Toivola, D. Targeted Modulation of Cell Differentiation in Distinct Regions of the Gastrointestinal Tract via Oral Administration of Differently PEG-PEI Functionalized Mesoporous Silica Nanoparticles. *Int. J. Nanomedicine* **2016**, 299–313.

(447) Chandler, D. Interfaces and the Driving Force of Hydrophobic Assembly. *Nature* **2005**, *437* (7059), 640–647.

(448) Wade, C. W. R.; Leonard, F. Degradation of Poly(methyl 2-Cyanoacrylates). *J. Biomed. Mater. Res.* **1972**, *6* (3), 215–220.

(449) Fattal, E.; Vauthier, C.; Aynie, I.; Nakada, Y.; Lambert, G.; Malvy, C.; Couvreur, P. Biodegradable Polyalkylcyanoacrylate Nanoparticles for the Delivery of Oligonucleotides. *J. Controlled Release* **1998**, *53* (1–3), 137–143.

(450) Panyam, J. Rapid Endo-Lysosomal Escape of poly(DL-Lactide-Co-Glycolide) Nanoparticles: Implications for Drug and Gene Delivery. *FASEB J.* **2002**, *16* (10), 1217–1226.

(451) Yordanov, G.; Evangelatov, A.; Skrobanska, R. Epirubicin Loaded to Pre-Polymerized Poly(butyl Cyanoacrylate) Nanoparticles: Preparation and in Vitro Evaluation in Human Lung Adenocarcinoma Cells. *Colloids Surf. B Biointerfaces* **2013**, *107*, 115–123.

(452) dos Santos, T.; Varela, J.; Lynch, I.; Salvati, A.; Dawson, K. A. Quantitative Assessment of the Comparative Nanoparticle-Uptake Efficiency of a Range of Cell Lines. *Small* **2011**, *7* (23), 3341–3349.

(453) Iversen, T.-G.; Skotland, T.; Sandvig, K. Endocytosis and Intracellular Transport of Nanoparticles: Present Knowledge and Need for Future Studies. *Nano Today* **2011**, *6* (2), 176–185.

(454) You, J.-O.; Auguste, D. T. Feedback-Regulated Paclitaxel Delivery Based on poly(N,N-Dimethylaminoethyl Methacrylate-Co-2-Hydroxyethyl Methacrylate) Nanoparticles. *Biomaterials* **2008**, *29* (12), 1950–1957.

(455) Mahmoudi, M.; Lynch, I.; Ejtehadi, M. R.; Monopoli, M. P.; Bombelli, F. B.; Laurent, S. Protein−Nanoparticle Interactions: Opportunities and Challenges. *Chem. Rev.* **2011**, *111* (9), 5610–5637.

(456) Mochalin, V. N.; Shenderova, O.; Ho, D.; Gogotsi, Y. The Properties and Applications of Nanodiamonds. *Nat. Nanotechnol.* **2011**, *7* (1), 11–23.

(457) Kim, J. H.; Yoon, S. B.; Kim, J.-Y.; Chae, Y. B.; Yu, J.-S. Synthesis of Monodisperse Silica Spheres with Solid Core and Mesoporous Shell: Morphological Control of Mesopores. *Colloids Surf. Physicochem. Eng. Asp.* **2008**, *313–314*, 77–81.

(458) Lu, Y.; Yin, Y.; Mayers, B. T.; Xia, Y. Modifying the Surface Properties of Superparamagnetic Iron Oxide Nanoparticles through A Sol−Gel Approach. *Nano Lett.* **2002**, *2* (3), 183–186.

(459) Zhao, W.; Gu, J.; Zhang, L.; Chen, H.; Shi, J. Fabrication of Uniform Magnetic Nanocomposite Spheres with a Magnetic Core/Mesoporous Silica Shell Structure. *J. Am. Chem. Soc.* **2005**, *127* (25), 8916–8917.

(460) Chow, E. K.; Zhang, X.-Q.; Chen, M.; Lam, R.; Robinson, E.; Huang, H.; Schaffer, D.; Osawa, E.; Goga, A.; Ho, D. Nanodiamond Therapeutic Delivery Agents Mediate Enhanced Chemoresistant Tumor Treatment. *Sci. Transl. Med.* **2011**, *3* (73), 73ra21-73ra21.

(461) Merkel, T. J.; DeSimone, J. M. Dodging Drug-Resistant Cancer with Diamonds. *Sci. Transl. Med.* **2011**, *3* (73), 73ps8-73ps8.

(462) Burleson, T.; Yusuf, N.; Stanishevsky, A. Surface Modification of Nanodiamonds for Biomedical Application and Analysis by Infrared Spectroscopy. *J. Achiev. Mater. Manuf. Eng.* **2009**, *37* (2), 258–263.

(463) Treussart, F.; Jacques, V.; Wu, E.; Gacoin, T.; Grangier, P.; Roch, J.-F. Photoluminescence of Single Colour Defects in 50nm Diamond Nanocrystals. *Phys. B Condens. Matter* **2006**, *376–377*, 926–929.

(464) Cheng, C.-Y.; Perevedentseva, E.; Tu, J.-S.; Chung, P.-H.; Cheng, C.-L.; Liu, K.-K.; Chao, J.-I.; Chen, P.-H.; Chang, C.-C. Direct and in Vitro Observation of Growth Hormone Receptor Molecules in A549 Human Lung Epithelial Cells by Nanodiamond Labeling. *Appl. Phys. Lett.* **2007**, *90* (16), 163903.

(465) Vaijayanthimala, V.; Tzeng, Y.-K.; Chang, H.-C.; Li, C.-L. The Biocompatibility of Fluorescent Nanodiamonds and Their Mechanism of Cellular Uptake. *Nanotechnology* **2009**, *20* (42), 425103.

(466) Fang, C.-Y.; Vaijayanthimala, V.; Cheng, C.-A.; Yeh, S.-H.; Chang, C.-F.; Li, C.-L.; Chang, H.-C. The Exocytosis of Fluorescent Nanodiamond and Its Use as a Long-Term Cell Tracker. *Small* **2011**, *7* (23), 3363–3370.

(467) Chu, Z.; Zhang, S.; Zhang, B.; Zhang, C.; Fang, C.-Y.; Rehor, I.; Cigler, P.; Chang, H.-C.; Lin, G.; Liu, R.; Li, Q. Unambiguous Observation of Shape Effects on Cellular Fate of Nanoparticles. *Sci. Rep.* **2014**, *4*.

(468) Rojas, S.; Gispert, J. D.; Martín, R.; Abad, S.; Menchón, C.; Pareto, D.; Víctor, V. M.; Álvaro, M.; García, H.; Herance, J. R. Biodistribution of Amino-Functionalized Diamond Nanoparticles. *In Vivo* Studies Based on ^{18}F Radionuclide Emission. *ACS Nano* **2011**, *5* (7), 5552–5559.

(469) Zhu, Y.; Li, J.; Li, W.; Zhang, Y.; Yang, X.; Chen, N.; Sun, Y.; Zhao, Y.; Fan, C.; Huang, Q. The Biocompatibility of Nanodiamonds and Their Application in Drug Delivery Systems. *Theranostics* **2012**, *2* (3), 302–312.

(470) Wilhelm, S.; Tavares, A. J.; Dai, Q.; Ohta, S.; Audet, J.; Dvorak, H. F.; Chan, W. C. W. Analysis of Nanoparticle Delivery to Tumours. *Nat. Rev. Mater.* **2016**, *1* (5), 16014.

ISBN 978-952-12-3507-8